

Global and Local Topological Crystalline Markers for Rotation-Symmetric Insulators

Saavanth Velury,^{*} Yoonseok Hwang, and Taylor L. Hughes
*Department of Physics and Anthony J. Leggett Institute for Condensed Matter Theory,
University of Illinois at Urbana-Champaign, Urbana, Illinois 61801-3080, USA*

Crystalline symmetry can be used to predict bulk and surface properties of topological phases. For non-interacting cases, symmetry-eigenvalue analysis of Bloch states at high symmetry points in the Brillouin zone simplifies the calculation of topological quantities. However, when open boundaries are present, and only the point group part of the symmetry group remains, it is unclear how to utilize crystalline symmetries to diagnose band topology. In this work, we introduce topological crystalline markers to characterize bulk topology in C_n -symmetric ($n = 2, 3, 4, 6$) crystalline insulators and superconductors with and without translation symmetry. These markers are expressed using a crystalline symmetry operator and the ground state projector, and are defined locally in position space. First, we provide a general method to calculate topological markers in periodic systems with an arbitrary number of unit cells. This includes cases where momentum quantization does not span all necessary high-symmetry points for computing the topological quantities, which we address using twisted boundary conditions. Second, we map these markers to the Chern number, bulk polarization, and sector charge for two-dimensional C_n -symmetric insulators in symmetry classes A, AI, AII, and superconductors in class D. Finally, we show how to numerically calculate the markers in finite-size systems with translation-symmetry (and even rotation-symmetry) breaking defects, and how to diagnose the bulk topology from the marker. Our results demonstrate how to compute bulk topological crystalline invariants locally in position space, thereby providing broader scope to diagnosing bulk crystalline topology that works even in inhomogeneous systems where there is no global rotation symmetry.

I. INTRODUCTION

Recently, the classification of non-interacting topological crystalline insulators has been established for the 230 nonmagnetic, and 1651 magnetic, space groups [1–30]. For the efficient diagnosis of such insulators, lattice translation symmetry plays an essential role. In fact, symmetry indicator methods and topological quantum chemistry use the irreducible, crystalline-symmetry representations of the electronic bands at high symmetry momenta within the Brillouin zone [1–3, 9, 10]. For example, for an inversion and time-reversal symmetric insulator in two dimensions, the number of occupied, odd-parity at each high symmetry momentum (modulo 2) indicates the \mathbb{Z}_2 topological invariant [16]. We call such information *momentum-space data*. Momentum-space data is also useful for predicting the boundary signatures of crystalline insulators, e.g., the appearance of edge or corner states, or fractional boundary charge [31–47].

Given the success of these classification approaches that leverage momentum-space data to determine position-space, e.g., boundary, properties, one natural question is whether it is possible to characterize the topological properties of the ground state of an insulating phase *solely* in position-space. This is an important question because determining momentum space data requires translation symmetry, and translation symmetry can be broken in many cases. For example, a given system can be confined within a domain, have open boundary conditions, or be subjected to crystal defects such as vacan-

cies or dislocations. Even with periodic boundary conditions and perfect translation symmetry, there are cases where one cannot access enough momentum-space data to compute the symmetry indicators for finite-sized systems. For example, the momentum quantization grid for finite systems depends on the linear sizes of the system, and hence some high-symmetry points may not be defined for particular system sizes.

Considering these challenges, we plan to develop a position-based method that can classify crystalline topology and connect to boundary signatures. There have been several approaches in this direction. For two-dimensional Chern insulators, the real-space Chern marker can determine the Chern number by computing the local Chern number in each unit cell [48–50]. Another approach is the spectral localizer technique [51–55], which can predict the appearance of topological surface states [55]. However, these techniques do not address, or fully exploit, the crystalline symmetries. Furthermore, it is unclear how other bulk topological quantities protected by crystalline symmetry can be determined using these methods.

In this work, we instead formulate bulk topological crystalline invariants in terms of basis-independent, operator-based quantities known as *topological crystalline markers*. As the name suggests, topological crystalline markers [56] are topological markers, which locally measure bulk topological invariants on the position-space lattice. The focus of this work will be to construct topological markers that incorporate the crystalline symmetry, namely the C_n rotation symmetry for $n = 2, 3, 4$ and 6, for gapped phases with spinless or spin-1/2 fermions, with or without time-reversal symmetry

^{*} svelury2@illinois.edu

or particle-hole symmetry (i.e., Altland-Zirnbauer (AZ) symmetry classes A, AI, AII, and D [57, 58]).

The topological crystalline markers we discuss in this work are constructed from projected symmetry operators, i.e., crystalline symmetry operators projected onto the subspace of occupied energy states (i.e., the full ground state) of a given system. By expressing the polarization and sector charge of obstructed atomic insulators, and, separately, the Chern number in Chern insulators and topological crystalline superconductors in terms of these projected symmetry operators, we are able to spatially resolve these quantities on the crystalline lattice, and show that their support is localized at the symmetry centers of the lattice. Importantly, compared to the existing Chern markers [48–50] that can diagnose the exact Chern number, our crystalline markers can efficiently determine the polarization, corner charge, etc., but can determine the Chern number only modulo n for C_n symmetry. So, while our method has advantages over previous spatially-resolved topological markers (which we will discuss in more detail within), we sacrifice precision in the determination of the Chern number. Remarkably, we will see that our method also provides a new way of understanding previously established results. Indeed, our method is applicable to systems that do not have translational symmetry, and even cases that are not globally point-group symmetric.

This work is organized as follows. First, in Sec. II, we layout the notation used in this article for the rotation operators and topological crystalline markers. Then we discuss the properties of C_n -symmetric lattices and Brillouin zones. In Sec. III, we define the topological crystalline markers and detail their basis-independent properties. We first demonstrate how the markers can be decomposed in terms of momentum-space based topological invariants when translation symmetry is present (e.g., irreducible representation multiplicities of the Bloch states, and rotation invariants). We then describe how to spatially resolve these quantities on the position-space lattice. Following this, in Sec. IV, we construct a mapping between bulk quantities and the topological crystalline markers for lattices having periodic boundary conditions and a number of unit cells that allows for the maximal number of high-symmetry momenta to exist in the Brillouin zone. In Sec. V, we generalize this mapping to lattices which have no restriction on the number of unit cells in each lattice direction, and thus could have quantized-momentum grids that miss high symmetry momenta. For such lattices, the traditional diagnosis of bulk crystalline topology via momentum-space based symmetry indicators does not hold. However, we show that the marker formalism we develop can still be applied to any lattice by considering twisted boundary conditions in addition to untwisted periodic boundary conditions. Next, in Sec. VI, we consider some applications of the topological crystalline markers to tight-binding models realizing phases having Chern number quantized by C_2 symmetry, as well as obstructed atomic limit phases that have well-

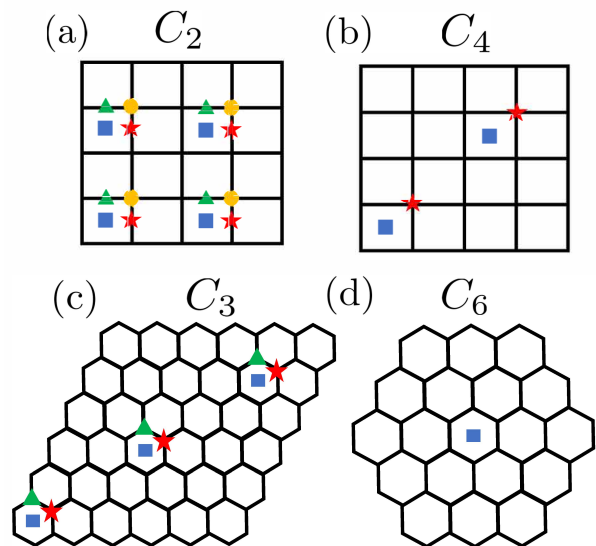


FIG. 1. Illustration of (a) C_2 -symmetric, (b) C_4 -symmetric, (c) C_3 -symmetric, and (d) C_6 -symmetric lattices and the corresponding sets of invariant positions $\mathcal{X}[c_n(\mathbf{r}_0)]$ given by Eq. (1) for lattices with dimensions $N_1 \times N_2$ specified by Eq. (3). The set of invariant positions $\mathcal{X}[c_n(\mathbf{r}_0)]$ for each C_n -symmetric lattice is determined with respect to the unit cell at $\mathbf{R} = \mathbf{0}$ located at the lower left corner for the C_2 , C_3 , and C_4 lattices shown in (a)-(c) respectively, while the unit cell at $\mathbf{R} = \mathbf{0}$ is located at the center of the C_6 -symmetric lattice in (d). For each lattice depicted in (a)-(d), the invariant positions correspond to WPs of multiplicity 1, and when the dimensions $N_1 \times N_2$ satisfy Eq. (3), the set $\mathcal{X}[c_n(\mathbf{r}_0)]$ is formed from Wyckoff positions of the same symbol (i.e., same shape and color) as per Eq. (1). The different choices of \mathbf{r}_0 correspond to different symbols.

defined bulk polarization. Importantly, we show how the markers can be used to diagnose bulk crystalline topology in systems hosting spatial inhomogeneities such as domain walls separating regions having different bulk topological properties. This is an exciting application since it allows us to treat systems that are not globally crystalline symmetric, but which have a sense of crystalline symmetry only locally. Finally, in Sec. VII, we conclude this work by reviewing our results, as well as mentioning possible applications of topological crystalline markers to strongly interacting systems and other phases such as amorphous systems and quasicrystals.

II. OVERVIEW OF NOTATION AND PROPERTIES OF C_n -SYMMETRIC LATTICES AND BRILLOUIN ZONE

We begin by reviewing some properties of lattices that have rotational symmetry, and the notation that will be used throughout this work. For now we will focus on 2D lattices of finite-size that are C_n -symmetric ($n = 2, 3, 4, 6$) and have periodic boundary conditions.

Figure 1 illustrates the different C_n -symmetric lattices. The lattices shown in Fig. 1 are spanned by a choice of lattice vectors \mathbf{a}_1 and \mathbf{a}_2 . The location of any unit cell on the position-space lattice is specified by a Bravais lattice vector $\mathbf{R} = n_1\mathbf{a}_1 + n_2\mathbf{a}_2$ where $n_{1,2}$ are non-negative integers. The dimensions N_1, N_2 of the lattice are specified by the number of unit cells along each direction spanned by the primitive lattice vectors \mathbf{a}_1 and \mathbf{a}_2 respectively. The Wyckoff positions (WPs) within each unit cell will play an important role in our discussion and are shown in Fig. 2.

For a given C_n -symmetric lattice having periodic boundary conditions along the directions spanned by $\mathbf{a}_{1,2}$, there is a set of positions that are invariant under the C_n rotation as shown in Fig. 1. To define the set of invariant positions, let us consider a C_n rotation axis located at \mathbf{r}_o , and denote the rotation operation as $c_n(\mathbf{r}_o)$. The position \mathbf{r}_o which specifies the location of a C_n rotation axis is always given by a multiplicity 1 WP, hence there are multiple, inequivalent choices marked with different symbols/colors in Fig. 1. Because of periodic boundary conditions, there can be more than one fixed point of the lattice under rotation, as shown by the matching symbols near different unit cells in Fig. 1. The set of invariant positions corresponding to $n = 2, 3, 4$ and 6 C_n -symmetric lattices respectively, is given by:

$$\begin{aligned} \mathcal{X}[c_2(\mathbf{r}_o)] &= \left\{ \mathbf{r}_o, \frac{N_1}{2}\mathbf{a}_1 + \mathbf{r}_o, \frac{N_2}{2}\mathbf{a}_2 + \mathbf{r}_o, \right. \\ &\quad \left. \frac{N_1}{2}\mathbf{a}_1 + \frac{N_2}{2}\mathbf{a}_2 + \mathbf{r}_o \right\}, \\ \mathcal{X}[c_3(\mathbf{r}_o)] &= \left\{ \mathbf{r}_o, \frac{N}{3}(\mathbf{a}_1 + \mathbf{a}_2) + \mathbf{r}_o, \frac{2N}{3}(\mathbf{a}_1 + \mathbf{a}_2) + \mathbf{r}_o \right\}, \\ \mathcal{X}[c_4(\mathbf{r}_o)] &= \left\{ \mathbf{r}_o, \frac{N}{2}(\mathbf{a}_1 + \mathbf{a}_2) + \mathbf{r}_o \right\}, \\ \mathcal{X}[c_6(\mathbf{r}_o)] &= \{\mathbf{r}_o\}, \end{aligned} \quad (1)$$

where we assumed $N_1 = N_2 = N$ for $C_{3,4,6}$.

As a simple example to demonstrate how the sets of invariant positions can be determined, we briefly explain how to determine $\mathcal{X}[c_2(\mathbf{r}_o)]$. Under the action of $c_2(\mathbf{r}_o)$, a position \mathbf{r} on the lattice is mapped to $-\mathbf{r} + 2\mathbf{r}_o$. The fixed points \mathbf{r}_* comprising the set of invariant positions are determined from the condition $\mathbf{r}_* = -\mathbf{r}_* + 2\mathbf{r}_o$. Solving this equation for a C_2 -symmetric lattice having periodic boundary conditions along both directions yields the set of four positions specified by $\mathcal{X}[c_2(\mathbf{r}_o)]$. Similar reasoning holds for determining $\mathcal{X}[c_n(\mathbf{r}_o)]$ for $n = 3, 4, 6$. Noting that \mathbf{r}_o always denotes the location of a multiplicity 1 WP, one can determine the allowed values of \mathbf{r}_o for each C_n -symmetric lattice. When restricted to a unit cell at $\mathbf{R} = \mathbf{0}$, the allowed \mathbf{r}_o for each C_n -symmetric lattice are

$$\begin{aligned} C_2 : \mathbf{r}_o &\in \{\mathbf{x}_{1a}, \mathbf{x}_{1b}, \mathbf{x}_{1c}, \mathbf{x}_{1d}\}, \\ C_3 : \mathbf{r}_o &\in \{\mathbf{x}_{1a}, \mathbf{x}_{1b}, \mathbf{x}_{1c}\}, \\ C_4 : \mathbf{r}_o &\in \{\mathbf{x}_{1a}, \mathbf{x}_{1b}\}, \end{aligned}$$

$$C_6 : \mathbf{r}_o \in \{\mathbf{x}_{1a}\}, \quad (2)$$

where \mathbf{x}_W with $W = 1a, 1b, 1c, \dots$ are the position offsets for the multiplicity 1 WPs as illustrated in, and detailed in the caption of, Fig. 2. Note that from Fig. 2, we use the standard convention that the $1a$ WP is the origin of the unit cell, i.e., $\mathbf{x}_{1a} = \mathbf{0}$.

Although the set of invariant positions given in Eq. (1) is determined with respect to the unit cell located at $\mathbf{R} = \mathbf{0}$, it is possible to determine an equivalent set of invariant positions with respect to a unit cell located at any \mathbf{R} on the periodic lattice. In general, for a rotation axis located at $\mathbf{R} + \mathbf{r}_o$, the corresponding rotation operator is denoted by $c_n(\mathbf{R} + \mathbf{r}_o)$, and the set of invariant positions is denoted by $\mathcal{X}[c_n(\mathbf{R} + \mathbf{r}_o)]$. This detail will be important for the discussion in Sec. VIB. However, for the majority of this work, $\mathcal{X}[c_n(\mathbf{r}_o)]$ will be specified with respect to $\mathbf{R} = \mathbf{0}$.

It is also important to note that the positions forming $\mathcal{X}[c_n(\mathbf{r}_o)]$ in Eq. (1) depend on the number of unit cells, $N_{1,2}$ and N . For example, for C_2 -symmetric lattices with $N_{1,2} \in 2\mathbb{Z}$, all four positions in $\mathcal{X}[c_2(\mathbf{r}_o)]$ correspond to the same WP \mathbf{r}_o up to a Bravais lattice translation. However, when $N_{1,2} \in 2\mathbb{Z} + 1$, $\mathcal{X}[c_2(\mathbf{r}_o)]$ is composed of four different WPs, $1a, 1b, 1c,$ and $1d$. Until Sec. V, we will consider only the simplest case where all invariant positions of rotation axis $c_n(\mathbf{r}_o)$, i.e., all elements of $\mathcal{X}[c_n(\mathbf{r}_o)]$, represent the same WPs (but within different unit cells). Hence, we impose the following conditions for each lattice:

$$\begin{aligned} C_2 : (N_1, N_2) &= (0, 0) \pmod{2} \\ C_4 : N &= 0 \pmod{2} \\ C_{n=3,6} : N &= 0 \pmod{n}. \end{aligned} \quad (3)$$

In Sec. V, we will generalize our results to lattices that have unit cell numbers that do not satisfy the constraint given by Eq. (3).

Before proceeding to the next section it will be useful to connect our position-space discussion to momentum-space. In conventional studies of topological crystalline insulators based on momentum-space symmetry eigenvalues/indicators, the constraints on the lattice dimensions are crucial, but often implicitly assumed to obey the constraints in Eq. (3). Indeed, satisfying these constraints allows for the maximal number of high-symmetry points to exist in the Brillouin zone. This is important, because it is at these points where one can efficiently compute topological crystalline invariants from symmetry eigenvalues of Bloch states. However, the existence of the high symmetry points depends on the dimensions of the lattice, because the crystalline momentum wavevector \mathbf{k} is quantized as:

$$\mathbf{k} = \frac{n_1}{N_1}\mathbf{b}_1 + \frac{n_2}{N_2}\mathbf{b}_2, \quad (4)$$

for suitable reciprocal lattice basis vectors $\mathbf{b}_{1,2}$ such that $\mathbf{b}_i \cdot \mathbf{a}_j = 2\pi\delta_{ij}$, and $n_i \in \{0, \dots, N_i - 1\}$ for $i, j = 1, 2$. The high symmetry momenta \mathbf{k} are defined to be the

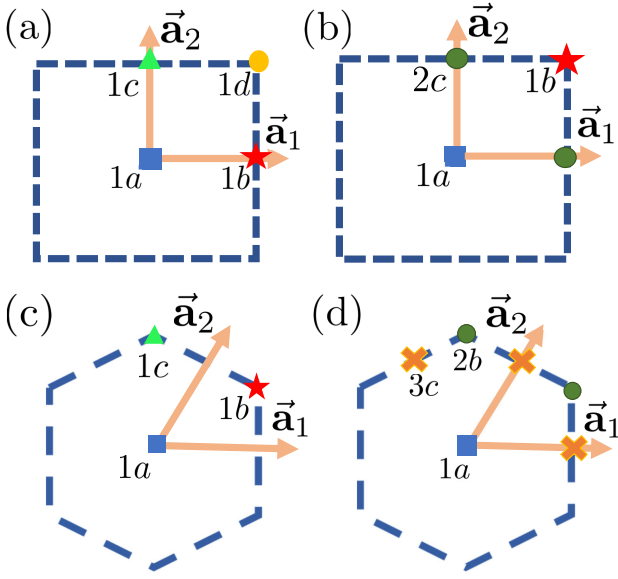


FIG. 2. Illustration of a unit cell for each C_n -symmetric lattice and the corresponding Wyckoff positions (WPs). (a) C_2 symmetry. The WPs $1a, 1b, 1c, 1d$ are located at $\mathbf{x}_{1a} = \mathbf{0}$, $\mathbf{x}_{1b} = \frac{1}{2}\mathbf{a}_1$, $\mathbf{x}_{1c} = \frac{1}{2}\mathbf{a}_2$, and $\mathbf{x}_{1d} = \frac{1}{2}(\mathbf{a}_1 + \mathbf{a}_2)$, respectively. (b) C_4 symmetry. The WPs $1a$ and $1b$ are located at $\mathbf{x}_{1a} = \mathbf{0}$ and $\mathbf{x}_{1b} = \frac{1}{2}(\mathbf{a}_1 + \mathbf{a}_2)$, respectively. The WP $2c$ is composed of two C_4 -related positions, $\mathbf{x}_{2c,1} = \frac{1}{2}\mathbf{a}_1$ and $\mathbf{x}_{2c,2} = \frac{1}{2}\mathbf{a}_2$. (c) C_3 symmetry. The WPs $1a, 1b, 1c$ are located at $\mathbf{x}_{1a} = \mathbf{0}$, $\mathbf{x}_{1b} = \frac{1}{3}(\mathbf{a}_1 + \mathbf{a}_2)$, and $\mathbf{x}_{1c} = \frac{1}{3}(-\mathbf{a}_1 + 2\mathbf{a}_2)$, respectively. (d) C_6 symmetry. The WP $1a$ is located $\mathbf{x}_{1a} = \mathbf{0}$. The WP $2b$ is composed of $\mathbf{x}_{2b,1} = \frac{1}{3}(\mathbf{a}_1 + \mathbf{a}_2)$, $\mathbf{x}_{2b,2} = \frac{1}{3}(-\mathbf{a}_1 + 2\mathbf{a}_2)$. The WP $3c$ is composed of $\mathbf{x}_{3c,1} = \frac{1}{2}\mathbf{a}_1$, $\mathbf{x}_{3c,2} = \frac{1}{2}\mathbf{a}_2$, and $\mathbf{x}_{3c,3} = \frac{1}{2}(-\mathbf{a}_1 + \mathbf{a}_2)$. The primitive lattice vectors $\mathbf{a}_{1,2}$ are set as $\mathbf{a}_1 = (1, 0)$ and $\mathbf{a}_2 = (0, 1)$ for $C_{2,4}$, and $\mathbf{a}_1 = (1, 0)$ and $\mathbf{a}_2 = (\frac{1}{2}, \frac{\sqrt{3}}{2})$ for $C_{3,6}$.

momenta in the Brillouin zone (BZ) that are invariant under the C_n rotation (up to a reciprocal lattice vector). The maximal set of high symmetry points for each C_n -symmetric BZ is shown in Fig. 3, which require the dimensions given by Eq. (3). For lattices that do not satisfy this constraint, a subset of high symmetry points will be missing depending on the values of $N_{1,2}$ and N . As mentioned above, we will revisit this complication in Sec. V.

III. DEFINITION AND PROPERTIES OF TOPOLOGICAL CRYSTALLINE MARKERS

Having reviewed the properties of the C_n -symmetric lattices in position-space and their corresponding BZs in momentum-space, we now proceed to define the topological crystalline markers (TCMs) (as discussed in Ref. 56) and discuss their properties. In order to do so, we first set some conventions for the lattice Hamiltonians we consider. The single-particle Hamiltonian H can be ex-

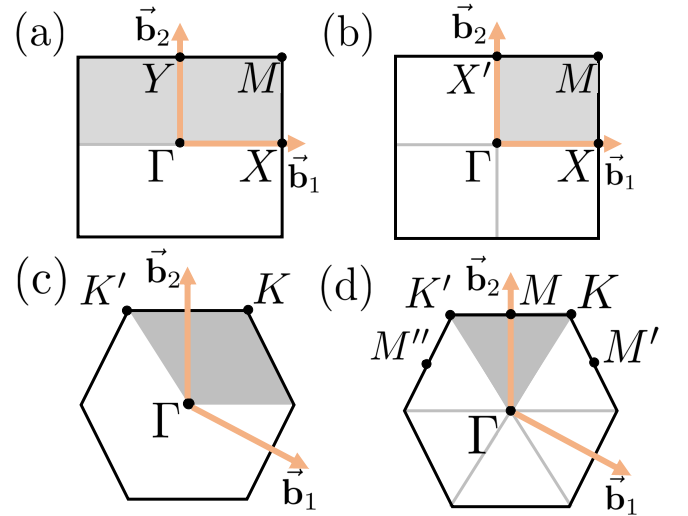


FIG. 3. Brillouin zones and their high symmetry momenta for the corresponding C_n -symmetric lattices shown in Fig. 1 with dimensions $N_1 \times N_2$ given by Eq. (3). (a) C_2 -symmetric BZ (b) C_4 -symmetric BZ (c) C_3 -symmetric BZ, and (d) C_6 -symmetric BZ. The reciprocal lattice vectors $\mathbf{b}_{1,2}$ that span each Brillouin zone are set as $\mathbf{b}_1 = (2\pi, 0)$ and $\mathbf{b}_2 = (0, 2\pi)$ for $C_{2,4}$, and $\mathbf{b}_1 = \frac{2\pi}{\sqrt{3}}(\sqrt{3}, -1)$ and $\mathbf{b}_2 = \frac{4\pi}{\sqrt{3}}(0, 1)$ for $C_{3,6}$. Shaded regions indicate the domains that generate the entire Brillouin zone upon rotation around the fixed point at the center Γ of the Brillouin zones.

pressed as

$$H = \sum_{\mathbf{R}, \mathbf{R}'} \sum_{\alpha, \beta} t_{(\mathbf{R}, \alpha), (\mathbf{R}', \beta)} |\mathbf{R}, \alpha\rangle \langle \mathbf{R}', \beta|, \quad (5)$$

where $|\mathbf{R}, \alpha\rangle$ is the orthonormal position-space basis, and $t_{(\mathbf{R}, \alpha), (\mathbf{R}', \beta)}$ are the hopping amplitudes. Also, α denotes internal degrees of freedom, such as spin, orbital, sublattice, etc., defined within a unit cell \mathbf{R} . To construct a TCM we will need the ground-state projector P_{GS} , which is a sum of projectors over occupied single-particle states. The TCM is then given by the product of P_{GS} and $c_n(\mathbf{r}_o)$ measured by the position-space basis $|\mathbf{R}, \alpha\rangle$:

$$\langle c_n(\mathbf{r}_o) \rangle_{\mathbf{R}} = \sum_{\alpha} \langle \mathbf{R}, \alpha | c_n(\mathbf{r}_o) P_{GS} | \mathbf{R}, \alpha \rangle. \quad (6)$$

From this definition, the TCM is a function of the unit cell position \mathbf{R} for a fixed choice of rotation center \mathbf{r}_o . It was shown in Ref. 56 that for gapped and non-interacting systems, the TCM is sharply localized around the invariant points $\mathcal{X}[c_n(\mathbf{r}_o)]$ of the position-space lattice. The sharpness of the localization is controlled by the correlation length ζ , which is determined by the inverse of the gap in the single-particle energy spectrum. As such, the ground-state projector for a gapped, rotation-symmetric ground state exhibits a short-range correlation behavior:

$$\sum_{\alpha} \langle \mathbf{R}', \alpha | P_{GS} | \mathbf{R}, \alpha \rangle \sim \mathcal{O}\left(e^{-|\mathbf{R}' - \mathbf{R}|/\zeta}\right), \quad (7)$$

for $|\mathbf{R}' - \mathbf{R}| \gg \zeta$. After a short calculation one observes that this leads to the exponential localization of the TCMs around the invariant points $\mathbf{r} \in \mathcal{X}[c_n(\mathbf{r}_o)]$ as defined in Eq. (1) [56]. That is,

$$\langle c_n(\mathbf{r}_o) \rangle_{\mathbf{R}} \sim \sum_{\mathbf{r} \in \mathcal{X}[c_n(\mathbf{r}_o)]} \mathcal{O}\left(e^{-2|\sin \frac{\pi}{n}| |\mathbf{r} - \mathbf{R}| / \zeta}\right). \quad (8)$$

Since the TCM exhibits exponential localization around rotation-invariant positions $\mathbf{r} \in \mathcal{X}[c_n(\mathbf{r}_o)]$ (c.f. Fig. 7), we can compute the weight of the distribution of the TCM in some region \mathcal{S} near \mathbf{r} . For this, we define a *traced TCM* for a given support \mathcal{S} ,

$$\langle c_n(\mathbf{r}_o) \rangle_{\mathcal{S}} = \sum_{\mathbf{R} \in \mathcal{S}} \langle c_n(\mathbf{r}_o) \rangle_{\mathbf{R}}. \quad (9)$$

For the special case when the support \mathcal{S} covers the entire periodic lattice, then the traced TCMs become basis-independent quantities expressed solely in terms of operators, P_{GS} and $c_n(\mathbf{r}_o)$. In that case, we define the *global, fully traced TCM*

$$\langle c_n(\mathbf{r}_o) \rangle_F = \text{Tr}[c_n(\mathbf{r}_o) P_{GS}]. \quad (10)$$

By noticing that $P_{GS} = \sum_{a \in \text{occ}} |\psi_a\rangle \langle \psi_a|$ and

$$\langle c_n(\mathbf{r}_o) \rangle_F = \sum_{a \in \text{occ}} \langle \psi_a | c_n(\mathbf{r}_o) | \psi_a \rangle, \quad (11)$$

for the wave functions $|\psi_a\rangle$ comprising the occupied states, the fully traced TCM $\langle c_n(\mathbf{r}_o) \rangle_F$ yields the group-theory character of a ground state for the rotation symmetry $c_n(\mathbf{r}_o)$.

While it is not apparent at this stage, we will show in Secs. IV and V that topological invariants such as the Chern number and bulk polarization can be determined using the fully traced TCMs. Furthermore, using the developments of Ref. 56, we explicitly demonstrate how the TCMs that are not fully traced can be used to spatially resolve topological properties of inhomogeneous systems in Sec. VI. This application can be anticipated from Eq. (8). That is, since the TCMs are exponentially localized around $\mathcal{X}[c_n(\mathbf{r}_o)]$, the fully traced TCMs for periodic boundary conditions are approximately the sum of partially traced TCMs around each of the individual invariant positions,

$$\langle c_n(\mathbf{r}_o) \rangle_F = \sum_{\mathbf{r} \in \mathcal{X}[c_n(\mathbf{r}_o)]} \langle c_n(\mathbf{r}_o) \rangle_{\mathcal{S}(\mathbf{r})} + O(e^{-\xi_S/\zeta}), \quad (12)$$

if the linear size ξ_S of the support $\mathcal{S}(\mathbf{r})$ around the rotation-invariant position \mathbf{r} is sufficiently larger than the correlation length ζ . The result simplifies for open boundary conditions since the sum receives contributions from only the neighborhood near the unique rotation center \mathbf{r}_o . Hence, by scanning the choice of rotation center \mathbf{r}_o , we can form a mesh of invariants defined across the entire lattice that will allow us to spatially resolve topological properties. We will demonstrate this approach in much more detail in Sec. VIB.

TABLE I. Character table for C_2 . The rows and columns denote the irreps and symmetry operations respectively. E , \bar{E} are the trivial element and 2π spin rotation. Note that $(C_2)^2 = \bar{E}$. The irreps with positive (negative) \bar{E} character correspond to spinless (spin-1/2) electrons.

	E	C_2	\bar{E}	$\bar{E}C_2$
A	1	1	1	1
B	1	-1	1	-1
${}^1\bar{E}$	1	i	-1	$-i$
${}^2\bar{E}$	1	$-i$	-1	i

As a complementary picture to our position-space discussion, we now consider the decomposition of the fully traced TCMs in the momentum-space eigenstate basis. This is not just a formal exercise. Indeed, in the next section we will use this decomposition to map previous results for momentum-space symmetry indicators to the fully traced TCMs. To begin, let us consider a C_n -symmetric lattice having periodic boundary conditions and lattice dimensions given by the constraint in Eq. (3). Starting with a lattice Hamiltonian expanded in momentum-space, we denote the Bloch Hamiltonian as $H(\mathbf{k})$, and the momentum-space representation of the rotation operator with origin at a WP \mathbf{r}_o as $c_n(\mathbf{r}_o, \mathbf{k})$.

Now, suppose that a high symmetry momentum (HSM) $\bar{\mathbf{k}}$ is left invariant under C_n rotation (modulo reciprocal lattice vectors), i.e.,

$$c_n(\mathbf{r}_o, \bar{\mathbf{k}}) : \bar{\mathbf{k}} \rightarrow C_n \bar{\mathbf{k}} = \bar{\mathbf{k}} + \mathbf{b}, \quad (13)$$

regardless of \mathbf{r}_o . Then, $H(\bar{\mathbf{k}})$ commutes with $c_n(\mathbf{r}_o, \bar{\mathbf{k}})$, and we can define simultaneous eigenstates for $H(\bar{\mathbf{k}})$ and $c_n(\mathbf{r}_o, \bar{\mathbf{k}})$.

Since $(C_n)^n$ is identical to a 2π spin rotation for generic C_n rotations, the eigenvalues with respect to $c_n(\mathbf{r}_o, \bar{\mathbf{k}})$ (i.e., the rotation eigenvalues) are quantized as $\exp(\frac{2\pi i}{n}\mathbb{Z})$ for spinless electrons and $\exp(\frac{2\pi i}{n}(\mathbb{Z} + \frac{1}{2}))$ for spin-1/2 electrons. Hence, we can label an energy eigenstate at a C_n -invariant HSM $\bar{\mathbf{k}}$ with an irreducible representation (irrep) $\bar{\mathbf{k}}_p$ ($p = 1, 2, \dots, n$) of, say, $c_n(\mathbf{x}_{1a} = \mathbf{0}, \mathbf{k})$. Where our choice of $\mathbf{r}_o = \mathbf{x}_{1a}$ will serve as a reference for labeling the irreps at HSM. We define an irrep $\bar{\mathbf{k}}_p$ at the HSM $\bar{\mathbf{k}}$ if it carries the rotation eigenvalue of $c_n(\mathbf{0}, \bar{\mathbf{k}})$ equal to $e^{\frac{2\pi i}{n}\ell}$. Here, ℓ is the orbital angular momentum of irrep $\bar{\mathbf{k}}_p$, which is defined by $\ell = p - 1$ for spinless electrons and $\ell = p - 1/2$ for spin-1/2 electrons. As an example, Table I shows the spinless and spin-1/2 representations for C_2 rotations. So, for instance, when a band in a spinless C_2 -symmetric lattice corresponds to irrep A (B) at Γ , we label it as Γ_1 (Γ_2).

In some cases we will need to know the irrep multiplicities for more than one rotation center. When needed, we can infer the rotation eigenvalue of irrep $\bar{\mathbf{k}}_p$ with respect

to $c_n(\mathbf{r}_o, \bar{\mathbf{k}})$ from the relation between $c_n(\mathbf{r}_o)$ and $c_n(\mathbf{0})$:

$$\begin{aligned} c_n(\mathbf{r}_o) &= T(\mathbf{r}_o)c_n(\mathbf{0})T(\mathbf{r}_o)^{-1} \\ &= c_n(\mathbf{0})T(c_n(\mathbf{0})^{-1}\mathbf{r}_o - \mathbf{r}_o), \end{aligned} \quad (14)$$

where $T(\mathbf{x})$ is a translation operator mapping \mathbf{r} to $\mathbf{r} + \mathbf{x}$. For example, $c_2(\mathbf{x}_{1b})\mathbf{r} = -\mathbf{r} + 2\mathbf{x}_{1b} = -\mathbf{r} + (\mathbf{x}_{1b} - (-\mathbf{x}_{1b}))$, i.e., $c_2(\mathbf{x}_{1b}) = c_2(\mathbf{0})T(c_2(\mathbf{0})^{-1}\mathbf{x}_{1b} - \mathbf{x}_{1b})$ because $c_2(\mathbf{0})$ acts on real-space coordinate as $-\mathbb{1}_{2 \times 2}$. Thus, we find the relation between momentum-space representation of rotation operators,

$$c_n(\mathbf{r}_o, \mathbf{k}) = c_n(\mathbf{0}, \mathbf{k}) \exp(-i\mathbf{k} \cdot (c_n(\mathbf{0})^{-1}\mathbf{r}_o - \mathbf{r}_o)). \quad (15)$$

Here, we utilized the momentum-space representation of the translation operator, $t(\mathbf{x}) = e^{-i\mathbf{k} \cdot \mathbf{x}}$ at momentum \mathbf{k} . Thus, the irrep $\bar{\mathbf{k}}_p$ carries the rotation eigenvalue of $c_n(\mathbf{r}_o, \bar{\mathbf{k}})$,

$$\begin{aligned} e^{i\phi_{n,p}(\mathbf{r}_o, \bar{\mathbf{k}})} &= \exp\left(\frac{2\pi i}{n}\ell - i\bar{\mathbf{k}} \cdot (c_n(\mathbf{0})^{-1}\mathbf{r}_o - \mathbf{r}_o)\right) \\ &= \exp\left(\frac{2\pi i}{n}\ell - i(C_n\bar{\mathbf{k}} - \bar{\mathbf{k}}) \cdot \mathbf{r}_o\right), \end{aligned} \quad (16)$$

where in the last step we used the transpose property of orthogonal rotation matrices with respect to the dot product.

For insulators, the irrep multiplicities $m(\bar{\mathbf{k}}_p) \in \mathbb{N}_0^1$, i.e., the number of each representation comprising the ground state, are well-defined and are topological crystalline invariants. Crucially, we find a relationship between the fully-traced TCMs and the irrep multiplicities $m(\bar{\mathbf{k}}_p)$, which shows that the traced TCMs encode bulk topological data. By expanding the ground-state projector P_{GS} , and the rotation operator $c_n(\mathbf{r}_o)$, in terms of momentum-space eigenstates, the fully traced TCM becomes

$$\langle c_n(\mathbf{r}_o) \rangle_F = \sum_{\bar{\mathbf{k}} \in \text{HSM}_n} \sum_{p=1}^n e^{i\phi_{n,p}(\mathbf{r}_o, \bar{\mathbf{k}})} m(\bar{\mathbf{k}}_p) \quad (17)$$

where HSM_n is the set of momenta in the first BZ that are left invariant under C_n rotation. Thus, the fully traced TCM can be decomposed into the irrep multiplicities in momentum space. While this is not difficult to derive (see Supplemental Material [59] for details), this result is the essential element to connect the fully traced TCMs to bulk topological invariants.

At this point, we have considered only periodic boundary conditions, and in the next section, we will detail the mapping between the TCMs, bulk topological invariants, and physical observables for periodic lattices that have dimensions $N_1 \times N_2$ which satisfy Eq. (3). However, in

Sec. V, we will extend our discussion to lattices whose dimensions do not satisfy Eq. (3), where one must consider lattices with *twisted* periodic boundary conditions. Consequently, it is useful to extend the TCMs discussed above to lattices with twisted boundary conditions. Denoting $\boldsymbol{\theta} = \theta_1\mathbf{a}_1 + \theta_2\mathbf{a}_2 \equiv (\theta_1, \theta_2)$ as the parameters of the boundary condition, we introduce the following modified notation for the TCM when twisted boundary conditions are present:

$$\langle c_n(\mathbf{r}_o) \rangle_{\mathbf{R}}^{\boldsymbol{\theta}} = \sum_{\alpha} \langle \mathbf{R}, \alpha | c_n(\mathbf{r}_o) P_{GS}^{\boldsymbol{\theta}} | \mathbf{R}, \alpha \rangle. \quad (18)$$

This modified notation extends in a similar manner to the traced TCM (e.g., $\langle c_n(\mathbf{r}_o) \rangle_{\mathcal{S}}^{\boldsymbol{\theta}}$) and the fully traced TCM (e.g., $\langle c_n(\mathbf{r}_o) \rangle_F^{\boldsymbol{\theta}}$). Throughout this work, when the superscript $\boldsymbol{\theta}$ is omitted from the TCM, it can be assumed that the TCM is applied to a lattice having untwisted periodic or open boundaries.

IV. MAPPING TOPOLOGICAL CRYSTALLINE MARKERS TO BULK TOPOLOGICAL INVARIANTS AND PHYSICAL OBSERVABLES

In the previous section, we exemplified the basis-independent properties of the fully traced TCMs by explicitly decomposing them in both momentum-space and position-space. In this section, we will use these results to show how the Chern number in C_n -symmetric Chern insulators, and the bulk polarization and sector charge for C_n -symmetric atomic insulators, can be expressed in terms of the markers, starting with the momentum-space decomposition of the fully traced TCMs. For this section, we restrict our focus to C_n -symmetric lattices with constraints on the dimensions given by Eq. (3); these lattices contain the maximal set of high symmetry momentum points in the BZ. The other types of lattices will be discussed in Sec. V.

A. Chern number and mapping procedure

First, we discuss the mapping between the fully traced TCMs and the Chern number \mathcal{C} for C_n -symmetric Chern insulators in Altland-Zirnbauer (AZ) class A [57]. Then, we will proceed to lay out the general procedure for mapping the fully traced TCMs to the momentum-space symmetry data for each AZ symmetry class. From Ref. 20, the Chern number can be expressed as follows for each C_n symmetry

$$\begin{aligned} C_2 : \mathcal{C} &= [X_1] + [Y_1] + [M_1] \pmod{2}, \\ C_3 : \mathcal{C} &= [K_1] + 2[K_2] + [K'_1] + 2[K'_2] \pmod{3}, \\ C_4 : \mathcal{C} &= [M_1] + 2[M_2] + 3[M_3] + 2[X_1] \pmod{4}, \\ C_6 : \mathcal{C} &= 2[K_1] - 2[K_2] + 3[M_1] \pmod{6}, \end{aligned} \quad (19)$$

where we have introduced the notation for momentum-space rotation invariants $[k_p]$ at each HSM given by $\bar{\mathbf{k}}$.

¹ Here \mathbb{N}_0 is the set of natural numbers including zero, while \mathbb{N} is the set of natural numbers.

The rotation invariants are defined as follows,

$$\begin{aligned}
C_2 : [\bar{\mathbf{k}}_{p=1,2}] &= m(\bar{\mathbf{k}}_p) - m(\Gamma_p) \text{ for } \bar{\mathbf{k}} \in \{X, Y, M\}, \\
C_3 : [\bar{\mathbf{k}}_{p=1,2,3}] &= m(\bar{\mathbf{k}}_p) - m(\Gamma_p) \text{ for } \bar{\mathbf{k}} \in \{K, K'\}, \\
C_4 : [M_{p=1,2,3,4}] &= m(M_p) - m(\Gamma_p), \\
[X_{p=1,2}] &= m(X_p) - m(\Gamma_p) - m(\Gamma_{p+2}), \\
C_6 : [K_{p=1,2,3}] &= m(K_p) - m(\Gamma_p) - m(\Gamma_{p+3}), \\
[M_{p=1,2}] &= m(M_p) - m(\Gamma_p) - m(\Gamma_{p+2}) - m(\Gamma_{p+4}).
\end{aligned} \tag{20}$$

Using these momentum-space rotation invariants, one can re-express the decomposition of the fully traced TCM in momentum-space in Eq. (17). For example, we can rewrite Eq. (17) as

$$\begin{aligned}
\langle c_2(\mathbf{0}) \rangle_F &= \sum_{\bar{\mathbf{k}} \in \text{HSM}_2} \sum_{p=1,2} e^{i\phi_{n,p}(\mathbf{r}_0, \bar{\mathbf{k}})} m(\bar{\mathbf{k}}_p) \\
&= \sum_{\bar{\mathbf{k}} \in \text{HSM}_2} (m(\bar{\mathbf{k}}_1) - m(\bar{\mathbf{k}}_2)) \\
&= [X_1] + [Y_1] + [M_1] - [X_2] - [Y_2] - [M_2] \\
&\quad + 4m(\Gamma_1) - 4m(\Gamma_2),
\end{aligned} \tag{21}$$

where $\text{HSM}_2 = \{\Gamma, X, Y, M\}$ is the set of HSM for C_2 symmetry. Thus, we can express the fully traced C_2 TCM with rotation center at the $1a$ WP ($\mathbf{r}_o = \mathbf{x}_{1a} = \mathbf{0}$) using a combination of rotation invariants $[\bar{\mathbf{k}}_p]$ and Γ -point irrep multiplicities $m(\Gamma_p)$. We gain additional data from the fully traced C_2 TCMs obtained for the $1b$, $1c$, and $1d$ WPs, and this generalizes straightforwardly to the other symmetry groups and corresponding WPs.

Our goal of expressing the Chern number formulae in Eq. (19) in terms of the fully traced TCMs involves mapping the fully traced TCMs to a combination of momentum-space rotation invariants and irrep multiplicities at the Γ -point. As illustrated in the example above, this will require multiple applications of the decomposition given by Eq. (17). To construct the mapping, we must first determine both the set of independent, fully traced TCMs, and the independent momentum-space symmetry data. The latter consists of the set of independent momentum-space rotation invariants and irrep multiplicities at Γ . The procedure to determine these sets can be summarized in three steps:

- Step 1: For a given wallpaper ($d = 2$) or space ($d = 3$) group, list the WPs W and their onsite symmetry group G_W . The onsite symmetry group G_W is composed of symmetries that leave the location \mathbf{x}_W of WP W invariant, i.e., $g_W \mathbf{x}_W = \mathbf{x}_W$ for all $g_W \in G_W$. When a WP W is composed of multiple positions, $\mathbf{x}_{W,1}, \mathbf{x}_{W,2}, \dots$, we consider the onsite symmetry group of one representative position, say $\mathbf{x}_{W,1}$. (The reason for this is explained below.) A set of all elements in the *unitary subset* of $G_{\text{TCM}} = \cup_W G_W$ are considered operators for defining the TCMs. Note that it is not necessary

to consider a generic WP which has a trivial onsite symmetry group since the trivial group is always a subgroup of G_W and will be included in G_{TCM} . If $g \in G_{\text{TCM}}$ is antiunitary, then the corresponding TCM $\langle g \rangle_F$ is not invariant under a basis transformation of the orbitals comprising the ground state.

- Step 2: Construct a set of fully traced TCMs for the group elements in G_{TCM} defined in Step 1. One can further identify certain relations between the TCMs of some group elements. For example, for g and its inverse g^{-1} , the corresponding fully traced TCMs are complex conjugates of each other, i.e., $\langle g^{-1} \rangle_F = \langle g \rangle_F^*$. This means that when we consider a C_n -symmetric system and compute the fully traced TCM of $c_{m \leq n}(\mathbf{r}_o)$, $\langle c_m(\mathbf{r}_o) \rangle_F^* = \langle c_m(\mathbf{r}_o)^{-1} \rangle_F$.
- Step 3: Utilize symmetries of the Hamiltonian (e.g., charge conservation and/or time-reversal symmetry and/or particle-hole symmetry) to determine an independent set of momentum-space irrep multiplicities. This set can be translated into the set of independent momentum-space rotation invariants and irrep multiplicities at Γ . Then, we construct the mapping between this momentum-space symmetry data and the set of fully traced TCMs constructed in Step 2, based on Eq. (17).

To demonstrate the first two steps of constructing the fully traced TCMs for a particular C_n -symmetry group, we consider the specific example of a C_6 -symmetric system. Let $\mathbf{a}_1, \mathbf{a}_2$ be defined as in Fig. 2. For Step 1, let us first list the WPs having nontrivial onsite symmetry groups. As shown in Fig. 2, a C_6 -symmetric unit cell has three sets of maximal WPs distinguished by the labels $1a$, $2b$, and $3c$. The $1a$ WP is the origin of the unit cell given by $\mathbf{x}_{1a} = \mathbf{0}$, the $2b$ WPs are given by $\mathbf{x}_{2b,1} = (\mathbf{a}_1 + \mathbf{a}_2)/3$ and $\mathbf{x}_{2b,2} = (-\mathbf{a}_1 + 2\mathbf{a}_2)/3$, and the $3c$ WPs are given by $\mathbf{x}_{3c,1} = \mathbf{a}_1/2$, $\mathbf{x}_{3c,2} = \mathbf{a}_2/2$, and $\mathbf{x}_{3c,3} = (-\mathbf{a}_1 + \mathbf{a}_2)/2$. Now we consider the various unitary symmetries that are elements of onsite symmetry groups of the $1a$, $2b$, $3c$ WPs. The onsite symmetry group of the $1a$ WP, G_{1a} , is point group C_6 , which is generated by $c_6(\mathbf{x}_{1a})$. Similarly, we define the onsite symmetry groups $G_{2b,i=1,2}$, $G_{3c,j=1,2,3}$ for the WP positions $\mathbf{x}_{2b,i}$ and $\mathbf{x}_{3c,j}$. Then, $G_{2b,i}$ is generated by C_3 rotation $c_3(\mathbf{x}_{2b,i})$, and $G_{3c,j}$ by C_2 rotation $c_2(\mathbf{x}_{3c,j})$. In this way, we define $G_{\text{TCM}} = G_{1a} \cup G_{2b,1} \cup G_{3c,1}$.

As an aside, note that we do not include $G_{2b,2}$, $G_{3c,2}$, $G_{3c,3}$ in G_{TCM} . Indeed, for a WP with multiplicity greater than 1, the fully traced TCMs evaluated at the positions composing the WP give the same result. This means that, for example, in a C_6 -symmetric lattice, evaluating the fully traced TCM for the C_3 rotation operator with origin at either $\mathbf{x}_{2b,1}$ or $\mathbf{x}_{2b,2}$ is equivalent. This also holds true for the fully traced TCMs for the C_2 rotation operators with origin at $\mathbf{x}_{3c,1}$, $\mathbf{x}_{3c,2}$, or $\mathbf{x}_{3c,3}$. To see this, let us consider the relation between $G_{2b,1}$ and $G_{2b,2}$. First, note that $\mathbf{x}_{2b,2} = c_6(\mathbf{x}_{1a})\mathbf{x}_{2b,1}$. By

TABLE II. Chern number for class A spinless and spin-1/2 C_n -symmetric insulators and class D crystalline superconductors expressed in terms of fully traced TCMs $\langle c_n(\mathbf{x}_W) \rangle_F$ evaluated over multiplicity 1 WPs W . These labels are given as $W \in \{1a, 1b, 1c, 1d\}$ for C_2 , $W \in \{1a, 1b, 1c\}$ for C_3 , $W \in \{1a, 1b\}$ for C_4 , and it is simply the $1a$ WP for C_6 . The Chern number for $C_{4,6}$ -symmetric insulators has other expressions in terms of TCMs (see Supplemental Material [59]). For class D superconductors we assume that the particle-hole and the rotation operator in its BdG form commute, which includes a wide class of models.

	A and D (spinless)	A and D (spin-1/2)
C_2	$\frac{1}{2}\langle c_2(\mathbf{x}_W) \rangle_F \bmod 2$	$-\frac{i}{2}\langle c_2(\mathbf{x}_W) \rangle_F \bmod 2$
C_3	$\frac{2}{\sqrt{3}}\text{Im}\langle c_3(\mathbf{x}_W) \rangle_F \bmod 3$	$-\frac{2}{\sqrt{3}}\text{Im}\langle c_3(\mathbf{x}_W) \rangle_F \bmod 3$
C_4	$\pm\sqrt{2}\text{Re}[e^{-\frac{i\pi}{4}}\langle c_4(\mathbf{x}_W) \rangle_F] - \frac{1}{2}\langle c_2(\mathbf{x}_W) \rangle_F \bmod 4$	$\pm\sqrt{2}\text{Re}\langle c_4(\mathbf{x}_W) \rangle_F - \frac{i}{2}\langle c_2(\mathbf{x}_W) \rangle_F \bmod 4$
C_6	$-\frac{4}{\sqrt{3}}\text{Im}\langle c_3(\mathbf{x}_W) \rangle_F + \frac{3}{2}\langle c_2(\mathbf{x}_W) \rangle_F \bmod 6$	$\frac{4}{\sqrt{3}}\text{Im}\langle c_3(\mathbf{x}_W) \rangle_F + \frac{3i}{2}\langle c_2(\mathbf{x}_W) \rangle_F \bmod 6$

definition, $g\mathbf{x}_{2b,1} = \mathbf{x}_{2b,1}$ for any $g \in G_{2b,1}$, and thus $hgh^{-1}\mathbf{x}_{2b,2} = \mathbf{x}_{2b,2}$ where $h = c_6(\mathbf{x}_{1a})$. In other words, $G_{2b,2} = \{g' = hgh^{-1} | \forall g \in G_{2b,1}\}$. In this case, the fully traced TCM of g' must be same as the one for g since $\langle g' \rangle_F = \text{Tr}[g'P_{SG}] = \text{Tr}[hgh^{-1}P_{GS}] = \text{Tr}[gP_{GS}] = \langle g \rangle_F$. Here, we use the fact that the ground state is symmetric under h , i.e. $hP_{GS} = P_{GS}h$.

For Step 2, we compute the TCMs for the elements in $G_{\text{TCM}} = G_{1a} \cup G_{2b,1} \cup G_{3c,1}$. There are 8 group elements of G_{TCM} besides the trivial group element. They are $c_{2,3,6}(\mathbf{x}_{1a})$, $c_3(\mathbf{x}_{2b,1})$, $c_2(\mathbf{x}_{3c,1})$, and the (independent) inverses $c_{3,6}(\mathbf{x}_{1a})^{-1}$ and $c_3(\mathbf{x}_{2b,1})^{-1}$. (Note that the inverse of C_2 is C_2 up to a 2π spin rotation.) Thus, we find that the complete set of fully traced TCMs for a C_6 -symmetric system is given as $\langle c_{2,3,6}(\mathbf{x}_{1a}) \rangle_F$, $\langle c_3(\mathbf{x}_{2b}) \rangle_F$, $\langle c_2(\mathbf{x}_{3c}) \rangle_F$ and their complex conjugations, which represent the inverses of the rotation operators. (Note that $\langle g^{-1} \rangle_F = \text{Tr}[g^{-1}P_{GS}] = \text{Tr}[(P_{GS}g)^\dagger] = \langle g \rangle_F^*$ from the properties of trace and the Hermiticity of P_{GS} .) Therefore, for a C_6 -symmetric system, there are a total of 8 independent fully traced TCMs that can be constructed (or 9 independent fully traced TCMs if one includes a fully traced TCM for the trivial group element, which is associated to the particle number and filling factor).

For Step 3, we need to identify both the minimal set of momentum-space rotation invariants and irrep multiplicities at the Γ -point (denoted as $m(\Gamma_p)$) that must be considered. To achieve this we must take into account the internal symmetries of the Hamiltonian. The internal symmetries of the Hamiltonian (e.g., charge conservation, time-reversal, particle-hole, chiral) impose constraints on the momentum-space rotation invariants and the $m(\Gamma_p)$.

The most fundamental symmetry we consider is charge conservation, which allows one to define a filling constraint. The filling constraint implies that the total number of occupied Bloch states is equal to a filling ν . Hence, at each HSM, the irrep multiplicities must satisfy a filling constraint sum rule, because the total number of occupied Bloch states is fixed throughout the BZ for a gapped system. To illustrate the filling constraint, suppose that Γ and some HSM $\bar{\mathbf{k}}$ are C_n - and $C_{m \leq n}$ -invariant points

respectively. Then, we can set

$$\nu = \sum_{p=1}^m m(\bar{\mathbf{k}}_p) = \sum_{p=1}^n m(\Gamma_p) \rightarrow \sum_{p=1}^m [\bar{\mathbf{k}}_p] = 0. \quad (22)$$

In the last line, we used the definition of the rotation invariant $[\bar{\mathbf{k}}_p]$ in Eq. (20). For instance, in a C_2 -symmetric system, $\nu = m(\Gamma_1) + m(\Gamma_2) = m(X_1) + m(X_2)$ implies $[X_1] + [X_2] = m(X_1) - m(\Gamma_1) + m(X_2) - m(\Gamma_2) = 0$.

Other internal symmetries, such as time-reversal symmetry for class AI and AII insulators, can introduce additional constraints between the rotation invariants. A rotation eigenvalue $e^{\frac{2\pi i}{n}\ell}$ is determined by the angular momentum ℓ , which can be expressed either as $\ell = p - 1$ for spinless electrons, or $\ell = p - 1/2$ for spin-1/2 electrons, where $p \in \{1, \dots, n\}$. Time-reversal symmetry maps the rotation eigenvalue $e^{\frac{2\pi i}{n}\ell}$ of an occupied Bloch state at an HSM $\bar{\mathbf{k}}$ to its complex conjugate $e^{-\frac{2\pi i}{n}\ell}$ of an occupied Bloch state at $-\bar{\mathbf{k}}$. This imposes the constraint that the total number of occupied Bloch states at an HSM $\bar{\mathbf{k}}$ with rotation eigenvalue $e^{\frac{2\pi i}{n}\ell}$ must equal the total number of occupied Bloch states at $-\bar{\mathbf{k}}$ with the corresponding complex conjugated rotation eigenvalue. For example, for class AII systems having time-reversal symmetry and $\ell = p - 1/2$, i.e., the spin-1/2 case, the rotation invariants are constrained to obey:

$$\begin{aligned} C_2 : [\bar{\mathbf{k}}_p] &= [\bar{\mathbf{k}}_{3-p}] \text{ for } \bar{\mathbf{k}} \in \{X, Y, M\} \text{ and } p \in \{1, 2\}, \\ C_3 : [K_p] &= [K'_{4-p}] \text{ for } p \in \{1, 2, 3\}, \\ C_4 : [M_p] &= [M_{5-p}] \text{ for } p \in \{1, 2, 3, 4\}, \\ &[X_p] = [X_{3-p}] \text{ for } p \in \{1, 2\}, \\ C_6 : [K_p] &= [K_{4-p}] \text{ for } p \in \{1, 2, 3\}, \\ &[M_p] = [M_{3-p}] \text{ for } p \in \{1, 2\}. \end{aligned} \quad (23)$$

In addition to time-reversal symmetry, one can consider constraints induced by the particle-hole symmetry for class D superconductors, described using the Bogoliubov-de Gennes (BdG) formalism. For such BdG Hamiltonians the viability of symmetry indicators, such as rotation invariants, to diagnose the bulk topological properties of superconductors depends on the pairing

symmetry [60–62]. For the results shown in Table II, we study spinless and spin-1/2 superconductors where the particle-hole and C_n rotation operators commute (e.g., as in Ref. 25). (For a discussion of pairing symmetry possibilities, see the Supplemental Material [59].)

Finally, rotational symmetry can also impose a constraint between rotation invariants; specifically for C_4 and C_6 -symmetric systems. As shown in Fig. 3, the C_4 -symmetric BZ has two C_2 -symmetric HSMs labeled by X and X' that are related to each other via a C_4 rotation. The rotation invariants for these points are equal to each other (e.g., $[X_p] = [X'_p]$ for $p = 1, 2$). Similarly, for the C_6 -symmetric BZ, it is clear that $[K_p] = [K'_p]$ for $p = 1, 2, 3$ and $[M_p] = [M'_p] = [M''_p]$ for $p = 1, 2$.

To illustrate how the symmetry constraints can be applied, let us return to the example of the C_6 -symmetric system and consider the symmetries of class A for spinless fermions. For a class A insulator the relevant symmetries that impose constraints between the momentum-space rotation invariants and Γ point irrep multiplicities are only charge conservation and rotation symmetry. The filling constraint leads to the following relations,

$$\begin{aligned} \nu &= \sum_{p=1}^6 m(\Gamma_p), \quad \sum_{p=1}^3 [K_p] = \sum_{p=1}^3 [K'_p] = 0, \\ \sum_{p=1}^2 [M_p] &= \sum_{p=1}^2 [M'_p] = \sum_{p=1}^2 [M''_p] = 0. \end{aligned} \quad (24)$$

Additionally, rotational symmetry imposes the equivalence of the rotation invariants at the K and K' points, and likewise for the M , M' , and M'' points.

Taking these constraints into account, we find that the minimal set of rotation invariants and Γ irrep multiplicities one needs to consider is given by $m(\Gamma_1)$, $m(\Gamma_2)$, $m(\Gamma_3)$, $m(\Gamma_4)$, $m(\Gamma_5)$, $[K_1]$, $[K_2]$, and $[M_1]$, for a total of 8 momentum-space quantities, or equivalently, 9 momentum-space quantities if one chooses to include either the filling ν (or alternatively $m(\Gamma_6)$). Thus, for a class A C_6 -symmetric insulator, this indicates there can be a bijective map between the fully traced TCMs and the momentum-space symmetry data. Indeed, we expect this to be these case since Eq. (17) is a linear map and the number of independent, fully-traced TCMs matches the number of independent momentum-space invariants. To confirm this intuition we found that the map between the fully traced TCMs and momentum-space data is invertible for every C_n -symmetry group. The computational details of all such mappings are provided in the Supplemental Material [59].

As a result of the mapping, we find that the Chern number modulo n can be expressed *solely* in terms of the fully traced TCMs. The results for class A C_n -symmetric insulators, for both spinless and spin-1/2 fermions, as well as class D crystalline superconductors with trivial pairing symmetry, are shown in Table II. These results reveal that for any C_n -symmetric Chern insulator ($n = 2, 3, 4, 6$), the bulk Chern number can be deter-

TABLE III. Representation of bands induced from Wannier orbitals for a C_2 -symmetric lattice with spinless electrons. Each Wannier orbital type is labeled by a maximal WP, $W = 1a, 1b, 1c, 1d$, and an angular momentum $l = 0$ or 1. The 2-5th columns denote the C_2 eigenvalues of bands at high-symmetry points in momentum space. The 6-8th columns represent the rotation invariants.

(l, W)	Γ	X	Y	M	$[X_1]$	$[Y_1]$	$[M_1]$
$(0, 1a)$	+1	+1	+1	+1	0	0	0
$(1, 1a)$	-1	-1	-1	-1	0	0	0
$(0, 1b)$	+1	-1	+1	-1	-1	0	-1
$(1, 1b)$	-1	+1	-1	+1	+1	0	+1
$(0, 1c)$	+1	+1	-1	-1	0	-1	-1
$(1, 1c)$	-1	-1	+1	+1	0	+1	+1
$(0, 1d)$	+1	-1	-1	+1	-1	-1	0
$(1, 1d)$	-1	+1	+1	-1	+1	+1	0

mined modulo n by evaluating the TCMs of the rotation operators with an origin at *any* multiplicity 1 WP. Particularly for C_2 , C_3 , and C_4 -symmetric Chern insulators, the Chern number can be *equally* determined at any multiplicity 1 WP, which demonstrates that the Chern number does not depend on the origin of the rotation operator. Equivalently, this result demonstrates that in the bulk, redefining the unit cell origin does not change the Chern number, which corroborates with the Chern number being a strong topological invariant.

B. Bulk polarization and sector charge

In atomic insulators, the Chern number is always zero and therefore, it is possible to construct exponentially localized Wannier functions. The Wannier functions allow for an efficient position-space description in terms of the Wannier-orbital configuration on the position-space lattice. For point-group symmetric insulators, the symmetry representation and multiplicity of each Wannier orbital is well defined. Furthermore, with this knowledge, one can determine topological quantities that characterize atomic insulators in position-space. Here, let us focus on the polarization and sector charge [35] as representative examples.

1. Electronic polarization

For each C_n symmetry, it is possible to determine the bulk polarization by considering the number of Wannier orbitals localized at maximal WPs away from the $1a$ position. For class A systems, these are given as follows,

$$\begin{aligned} C_2 : \mathbf{P} &= \frac{e}{2} [(n_{1b} + n_{1d}) \mathbf{a}_1 + (n_{1c} + n_{1d}) \mathbf{a}_2], \\ C_3 : \mathbf{P} &= \frac{e}{3} (n_{1b} - n_{1c})(\mathbf{a}_1 + \mathbf{a}_2), \end{aligned}$$

$$\begin{aligned} C_4 : \mathbf{P} &= \frac{e}{2}(n_{1b} + n_{2c})(\mathbf{a}_1 + \mathbf{a}_2), \\ C_6 : \mathbf{P} &= \mathbf{0}, \end{aligned} \quad (25)$$

where we have used the convention $e = -|e|$ for the electron charge. Each component of the polarization $\mathbf{P} = p_1\mathbf{a}_1 + p_2\mathbf{a}_2$ is defined modulo e , and n_W refers to the total number of Wannier orbitals at Wyckoff position W .

Equation (25) can be understood as follows. Without loss of generality, we can assume that all Wannier orbitals are localized at maximal WPs. Indeed, any Wannier orbital on non-maximal WPs can be adiabatically moved to maximal WPs while preserving all the symmetries of the system. At each maximal WP each Wannier orbital carries rotation eigenvalue $e^{\frac{2\pi i}{n}\ell}$, where ℓ is their angular momenta². Thus, we can define $n_W^{(\ell)}$, the multiplicity of each Wannier orbital type at maximal position W . Note that the total number of Wannier orbitals at W is given by

$$n_W = \sum_{\ell} n_W^{(\ell)}. \quad (26)$$

Note that \sum_{ℓ} means $\sum_{\ell=0}^{n-1}$ for spinless electrons and $\sum_{\ell=1/2}^{n-1/2}$ for spin-1/2 electrons. Since the polarization is the sum of Wannier centers of occupied electrons [63], we set

$$\mathbf{P} = e \sum_W n_W \mathbf{x}_W, \quad (27)$$

which yields Eq. (25). For example, in a C_2 -symmetric system, there are four maximal WPs $W = 1a, 1b, 1c, 1d$ having positions $\mathbf{x}_{1a} = (0, 0)$, $\mathbf{x}_{1b} = 1/2\mathbf{a}_1$, $\mathbf{x}_{1c} = 1/2\mathbf{a}_2$, and $\mathbf{x}_{1d} = 1/2(\mathbf{a}_1 + \mathbf{a}_2)$. Substituting these quantities into Eq. (27) directly leads to the first line in Eq. (25).

In this context we will now show that Eq. (25) can be obtained by computing the fully traced TCMs in position space, instead of using the usual momentum-space data. First, a linear combination of Wannier orbital multiplicities can be mapped to momentum-space data, using the induced band representation [1–3]. Second, Eq. (17) implies the fully traced TCM can be represented in terms of momentum-space data including the rotation-invariants and Γ irrep multiplicities. Combining these two, we construct a mapping from the set of fully traced TCMs to the Wannier orbital multiplicities for each C_n symmetry and symmetry class A, AI, and AII.

To demonstrate how this mapping is carried out with a simple example, consider a C_2 -symmetric, spinless, class A atomic insulator. Table III lists the HSM C_2 eigenvalue data of the band representations induced from Wannier orbitals at maximal WPs [1–3]. From Table III, and the

definition of the rotation invariants $[\bar{\mathbf{k}}_p]$ ($p = 1, 2$) in Eq. (20), we find

$$\begin{aligned} [X_1] &= -[X_2] = n_{1b}^{(1)} - n_{1b}^{(0)} + n_{1d}^{(1)} - n_{1d}^{(0)}, \\ [Y_1] &= -[Y_2] = n_{1c}^{(1)} - n_{1c}^{(0)} + n_{1d}^{(1)} - n_{1d}^{(0)}, \\ [M_1] &= -[M_2] = n_{1b}^{(1)} - n_{1b}^{(0)} + n_{1c}^{(1)} - n_{1c}^{(0)}, \\ m(\Gamma_p) &= \sum_{W \in \text{WP}_2} n_W^{(p-1)}, \end{aligned} \quad (28)$$

where $\text{WP}_2 = \{1a, 1b, 1c, 1d\}$ is the list of maximal WPs for a C_2 -symmetric lattice. These relations are the outcome of the first step.

For the second step we use Eq. (17), which is the mapping between the fully traced TCMs for each WP and a combination of momentum-space rotation invariants and the Γ irrep multiplicities. Noting that the fully traced TCM for the $1a$ WP is already given by Eq. (21), we can use Eqs. (16) and (17) to find

$$\begin{aligned} \langle c_2(\mathbf{x}_{1a}) \rangle_F &= 2([X_1] + [Y_1] + [M_1]) + 4(m(\Gamma_1) - m(\Gamma_2)), \\ \langle c_2(\mathbf{x}_{1b}) \rangle_F &= 2(-[X_1] + [Y_1] - [M_1]), \\ \langle c_2(\mathbf{x}_{1c}) \rangle_F &= 2([X_1] - [Y_1] - [M_1]), \\ \langle c_2(\mathbf{x}_{1d}) \rangle_F &= 2(-[X_1] - [Y_1] + [M_1]). \end{aligned} \quad (29)$$

With the second step complete we can combine the mappings in Eqs. (28) and (29) to yield the following mapping between the fully traced TCMs and the Wannier orbital irrep multiplicities:

$$\langle c_2(\mathbf{x}_W) \rangle_F = 4(n_W^{(0)} - n_W^{(1)}), \quad (30)$$

for $W \in \text{WP}_2 = \{1a, 1b, 1c, 1d\}$.

This is an important result, and we can derive it from an alternative perspective. For a generic C_n -symmetric atomic insulator, the Wannier-orbital multiplicity at each WP is well defined. Then, the fully traced TCM in Eq. (10) can be computed with the position-space Wannier orbital basis. In this case, we have

$$\langle c_n(\mathbf{r}_o) \rangle_F = \sum_{W^* \in \mathcal{X}[c_n(\mathbf{r}_o)]} e^{2\pi i \ell / n} n_W^{(\ell)}. \quad (31)$$

In the previous example of C_2 -symmetric insulators with unit-cell constraint $(N_1, N_2) = (0, 0) \bmod 2$ [Eq. (3)], all four C_2 -invariant positions in $\mathcal{X}[c_2(\mathbf{r}_o)]$ correspond to same WP type, say W . This explains the factor 4 in Eq. (30). Also, at the WP W , Wannier orbital types having angular momentum $\ell = 0, 1$ are defined. Thus, their multiplicities $n_W^{(\ell)}$ and angular momentum factor $e^{2\pi i \ell / n}$ contribute to Eq. (30) as $e^{i0} n_W^{(0)} + e^{i\pi} n_W^{(1)}$. So, in this way, the fully traced TCM is related to the momentum-space data and the position space data contained in the Wannier orbital multiplicities of atomic insulators.

With the mapping between the fully traced TCMs and Wannier-orbital multiplicities in hand, we can express the bulk polarization in Eq. (25) solely in terms of the fully

² Recall that $\ell = p - 1$ ($p - 1/2$) for spinless (spin-1/2) cases for $p = 1, \dots, n$.

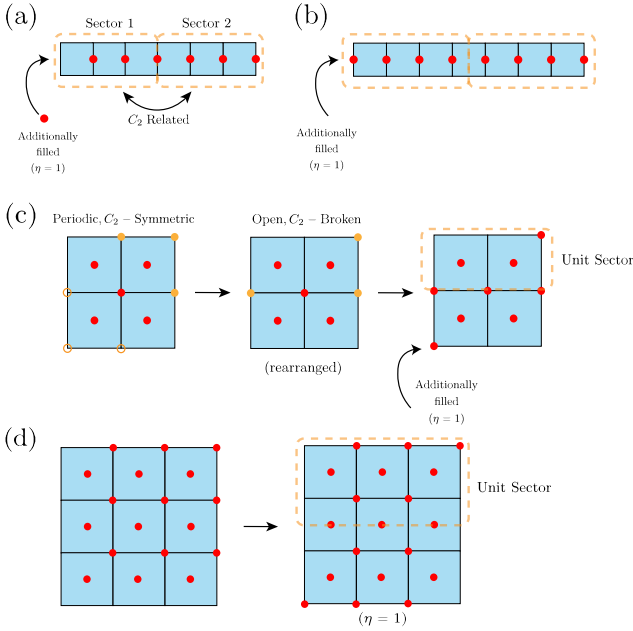


FIG. 4. Illustration of the filling anomaly in a 1D obstructed atomic insulator (e.g., SSH model) with (a) an even number of unit cells ($N = 6$), (b) an odd number of unit cells ($N = 7$), and a 2D C_2 obstructed atomic insulator with (c) an even number of unit cells ($N_1 = N_2 = 2$), and (d) an odd number of unit cells ($N_1 = N_2 = 3$). The yellow dashed lines in all the figures indicate a fundamental unit C_2 sector. In (a) and (b), the 1D obstructed atomic insulator has a filling anomaly of $\eta = 1$ since an additional electron must be filled to restore the C_2 symmetry, at the expense of losing charge neutrality. Similar reasoning holds for (c) and (d), in which the 2D C_2 obstructed atomic insulator has a filling anomaly of $\eta = 1 \pmod{2}$. In open boundary conditions, the neutral configuration of localized electrons cannot satisfy the C_2 symmetry even if the boundary electrons are rearranged. This can also be seen from the fact that the number of electrons on the boundary is an odd integer, however, C_2 symmetry requires an even number of boundary electrons. To respect C_2 symmetry, we must deviate from neutrality, i.e., a filling anomaly must occur.

traced TCMs. For example, we can combine Eqs. (25) and (30) to express the polarization for C_2 -symmetric, spinless, class A atomic insulators in terms of the fully traced TCMs. Since the polarization is defined modulo e , and $n_W^{(\ell)} \in \mathbb{Z}$ for atomic insulators, the polarization along the \mathbf{a}_1 direction [Eq. (25)] is equivalent to $(\mathbf{P})_x = \frac{e}{2}[(-n_{1b}^{(0)} + n_{1b}^{(1)}) + (-n_{1d}^{(0)} + n_{1d}^{(1)})]$. By combining this and Eq. (30), we find $(\mathbf{P})_x = -\frac{e}{8}(\langle c_2(\mathbf{x}_{1b}) \rangle_F + \langle c_2(\mathbf{x}_{1d}) \rangle_F)$, and a similar result for $(\mathbf{P})_y$. We can generalize these results to other symmetry classes, and we summarize the results for C_n -symmetric insulators in classes A, AI, and AII in Tables IV and V.

2. Fractional sector charge and filling anomaly

In addition to the bulk polarization, another important property of atomic insulators is the sector charge. The sector charge is essentially the fractional charge in a $2\pi/n$ sector of a C_n -symmetric, finite lattice having open boundaries [35, 64]. It is a property that generalizes the notion of fractional corner charge when rotation symmetry is present, but perhaps not translation symmetry.

To compute the sector charge, a unit sector must be defined first. To illustrate how the unit sector is defined, let us consider the 1D Su-Schrieffer-Heeger (SSH) model [65] having C_2 symmetry. Figure 4(a) illustrates a finite-length SSH chain having an even number of unit cells ($N_{\text{cells}} \in 2\mathbb{N}$). This system has C_2 rotation which flips the sign of 1D coordinate x , i.e., $C_2 : x \rightarrow -x$. Using the C_2 rotation center, $x = 0$, as a reference point, the system can be divided into two sectors: one sector is the region where $x \geq 0$, and the other one where $x \leq 0$ [see Fig. 4(a)]. Note that these sectors are related to each other by C_2 , they do not have any overlapping area, and together they cover the whole system.

Analogously, we can define C_n -related sectors in C_n -symmetric systems in any spatial dimension. For example, a sector of a C_n -symmetric lattice is the region subtended by an angle of $2\pi/n$ radians around a fixed (unique for open boundaries) rotation center. The other $(n-1)$ sectors can be identified with C_n -rotated copies of the first sector. Figures 4(c)-(d) illustrate how C_2 -related sectors are defined in a 2D C_2 -symmetric lattice.

Once a C_n -symmetric lattice has a clear division into its n sectors, the sector charge Q_{sector} is defined as follows. The total system has charge Q_{tot} . Because n sectors are related by C_n without overlapping area, the sector charge is

$$Q_{\text{sector}} = \frac{Q_{\text{tot}}}{n}. \quad (32)$$

For a system having periodic boundary conditions, the total charge is simply defined by the filling per unit cell ν , and the total number of unit cells N_{cells} : $Q_{\text{total}} = e\nu N_{\text{cells}}$. Thus $Q_{\text{sector}} = e\nu N_{\text{cells}}/n$ for periodic boundary conditions³.

However, the situation is more interesting when we apply open boundary conditions. In open boundary conditions, the filling νN_{cells} defined in periodic boundary conditions may not be compatible with keeping the crystalline symmetry of the system. In fact, this is the case in the obstructed atomic insulator phase of the SSH model, which has a quantized polarization $e/2$. In the obstructed phase, one electron is filled per unit cell ($\nu = 1$), and the Wannier functions are centered at the unit cell boundary ($x = 1/2 \pmod{1}$) as shown in Fig. 4(a). When periodic

³ Note that we are not considering ionic contributions to the total charge or the sector charge.

boundary conditions are applied, the electron configuration with total number of electrons $\nu N_{\text{cells}} = N_{\text{cells}}$ shown in Fig. 4 respects the C_2 rotation. (Note that the left and right edges should be identified in this case because of periodic boundary conditions.)

In contrast, a configuration of N_{cells} electrons in the obstructed phase must break C_2 rotation when open boundary conditions are implemented (see Ref. 35 for more detail). In our example shown in Fig. 4(a), one electron occupies the right edge, but the left edge is empty. While which edge is occupied and which is empty is a choice, the two ends will always be unbalanced at this filling. Crucially, the C_2 symmetry can be restored if we additionally fill one electron at the left edge or unfill one electron at the right edge. Now, the system respects the C_2 symmetry but the total number of electrons is changed by $\eta = \pm 1$ from the total number of electrons needed to make a symmetric, insulating configuration in periodic boundary conditions. This phenomena is called the filling anomaly [35]. Importantly, the filling anomaly is not present in the trivial atomic insulator phase of the SSH chain. This implies that the filling anomaly depends on the locations of the Wannier centers of the occupied bands. For some configurations of Wannier centers, a system having open boundary conditions cannot respect the crystal symmetry at the same filling required for a symmetric insulator in periodic boundary conditions. The filling anomaly occurs in other symmetry classes and higher-dimensional systems as well. For example, the filling anomaly in a 2D C_2 -symmetric insulator is illustrated in Figs. 4(c)-(d).

The point of reviewing the filling anomaly was to motivate contributions to the sector charge for rotation invariant insulators having open boundaries. As such, we find that, for open boundary conditions, the contribution from the filling anomaly must be considered when computing the total and sector charges. Let us denote the filling-anomaly as η . If $\eta > 0$ ($\eta < 0$) then, to keep the symmetry in an open boundary system, $|\eta|$ additional electrons must be filled (unfilled) with respect to the symmetric, insulating filling defined for a translation symmetric system having periodic boundary conditions. We note that $\eta = 0$ means there is no filling anomaly. The total charge for a system having open boundary conditions is now given by $Q_{\text{tot}} = e\nu N_{\text{cells}} + e\eta$, and thus the sector charge is

$$Q_{\text{sector}} = e\nu N_{\text{cells}}/n + e\eta/n. \quad (33)$$

Note that the sector charge depends on ν , N_{cells} and η .

As an example, in Fig. 4(a) the SSH model has an even number of unit cells, a periodic filling factor $\nu = 1$, and a filling anomaly factor $\eta = 1$. In this case, $Q_{\text{sector}} = e\nu N_{\text{cells}}/2 + e/2 = e\mathbb{N} + e/2$, and thus $Q_{\text{sector}} = e/2 \pmod{e}$. When the number of unit cells is odd, as shown in Fig. 4(b), the electronic contribution to the sector charge is computed as $Q_{\text{sector}} = eN_{\text{cells}}/2 + e/2 = e(\mathbb{N} + 1/2) + e/2$. Thus $Q_{\text{sector}} = 0 \pmod{e}$.

To find the mapping between the fully traced TCMs

and the sector charge, we need to find the relationship between the sector charge and Wannier-orbital multiplicities, which can then be subsequently related to the fully traced TCMs as we just carried out for the polarization. To achieve this, let us determine the total charge Q_{total} from a slightly different perspective [41]. Suppose that a ground state with Q_{tot} in Eq. (33) respects C_n symmetry. Note that the rotation center must coincide with a maximal WP X with C_n on-site symmetry. However, there is a subtlety we now point out. A C_2 -symmetric system having open boundary conditions has a unique C_2 center that depends on the linear sizes N_1, N_2 . The rotation center coincides with (i) the WP $1a$ if $(N_1, N_2) = (1, 1) \pmod{2}$, (ii) the WP $1b$ if $(N_1, N_2) = (0, 1) \pmod{2}$, (iii) the WP $1c$ if $(N_1, N_2) = (1, 0) \pmod{2}$, and (iv) the WP $1d$ if $(N_1, N_2) = (0, 0) \pmod{2}$. The cases (i) and (iv) are shown in Figs. 4(d) and (c) respectively. Note that although the center WP is determined by $(N_1, N_2) \pmod{2}$, the on-site symmetry of the rotation center is always C_2 in all four cases.

For atomic insulators where the electronic Wannier orbital functions are exponentially localized, the total charge is determined by two contributions, (i) the electrons localized at the rotation center X and (ii) those away from X . Fortunately, there is a simplification because the electrons away from X form C_n symmetric multiplet configurations, and thus their number is $n\mathbb{Z}$. For example, let us consider the SSH chain with an even number of unit cells shown in Fig. 4(a). There is a single electron at the C_2 center, which corresponds to the contribution (i). In addition to the electron at the center, there are 4 [6] other electrons in our diagram when the filling-anomaly factor η is -1 [1]. These electrons correspond to the contribution (ii). They respect the C_2 symmetry, and thus their number is $2\mathbb{Z}$ since they clearly come in C_2 -related pairs. Similar arguments hold for an SSH chain having an odd number of unit cells [Fig. 4(b)]. Furthermore, the arguments immediately apply to the 2D C_2 -symmetric insulators illustrated in Figs. 4(c)-(d), and any other C_n -symmetric atomic insulators.

With this in mind, we can immediately conclude that for generic C_n -symmetric atomic insulators, $Q_{\text{tot}} \pmod{ne}$ is solely determined by the number of electrons localized at the rotation center. This is simply expressed as

$$Q_{\text{tot}} = e \sum_{\ell} n_X^{(\ell)} \pmod{ne}. \quad (34)$$

Combining this and Eq. (33), we find the expression for the sector charge (modulo e) and the filling-anomaly factor (modulo n for C_n symmetry):

$$\begin{aligned} Q_{\text{sector}} &= \frac{e}{n} \sum_{\ell} n_X^{(\ell)} \pmod{e}, \\ \eta &= \sum_{\ell} n_X^{(\ell)} - \nu N_{\text{cells}} \pmod{n}. \end{aligned} \quad (35)$$

In general, both the sector charge and the filling-anomaly factor η depend on the values of $N_{1,2}$, the filling ν per unit

cell, and the orbital multiplicities $n_X^{(\ell)}$. Indeed, for the SSH chain example above we saw that the sector charge flipped from half-integer to integer when the number of unit cells flipped from even to odd. Note that the sector charge depends on $N_{1,2}$ implicitly, as the types of WPs X corresponding to the rotation centers are determined by $N_{1,2}$.

The final step is to connect the sector charge and filling-anomaly factor formulas in Eq. (35) to the fully traced TCMs. Even though the sector charge and filling-anomaly factor are defined under open boundary conditions, they are still determined by linear combinations of orbital multiplicities, as shown in Eq. (35). These linear combinations can be computed by evaluating the fully traced TCMs under periodic boundary conditions as follows. First, the factor νN_{cells} can be determined by $N_{1,2}$ and the fully traced TCM for the trivial symmetry operation $\mathbb{1}$; $N_{\text{cells}} = N_1 N_2$ and $\nu = \langle \mathbb{1} \rangle_F = \text{Tr}[P_{GS}]$. Second, Eq. (31) maps the fully traced TCM $\langle c_n(\mathbf{r}_o) \rangle_F$ to a linear combination of orbital multiplicities, $\sum_{W \in \mathcal{X}[c_n(\mathbf{r}_o)]} e^{2\pi i \ell / n} n_W^{(\ell)}$, at several WPs in $\mathcal{X}[c_n(\mathbf{r}_o)]$. Hence, under the constraint Eq. (3), the sector charge can be expressed solely in terms of the fully traced TCMs, as we can simply apply the mapping between the fully traced TCMs and Wannier orbital multiplicities. In this case, for a system having open boundaries, the rotation center X corresponds to a WP $1d$, (see Fig. 4(c)). Then the factor $\sum_{\ell=0}^{n-1} n_X^{(\ell)}$ in Eq. (35) becomes $n_{1d}^{(0)} + n_{1d}^{(1)}$, which is identical to $-n_{1d}^{(0)} + n_{1d}^{(1)}$ modulo 2, since $n_{1d}^{(\ell)} \in \mathbb{Z}$ for (obstructed) atomic insulators. Then, from Eq. (30), we obtain $\sum_{\ell=0}^{n-1} n_X^{(\ell)} = -\frac{1}{4} \langle c_2(\mathbf{x}_{1d}) \rangle_F \text{ mod } 2$. This implies that $Q_{\text{sector}} = -\frac{e}{8} \langle c_2(\mathbf{x}_{1d}) \rangle_F \text{ mod } e$ for a C_2 -symmetric system. Accordingly, the filling-anomaly factor η is given by $-\frac{1}{4} \langle c_2(\mathbf{x}_{1d}) \rangle_F \text{ mod } 2$. (Note that the factor $\nu N_{\text{cell}} = \nu N_1 N_2$ in Eq. (35) becomes 0 mod 2 for any integer, periodic filling ν , when Eq. (3) is assumed.) We computed the TCM expressions of the sector charge for class A insulators (see Table VI), and for class AI and AII insulators (see Table VII) for each C_n .

Unfortunately, when Eq. (3) is not satisfied it is not immediately obvious how to carry out this mapping for a generic lattice type with arbitrary $N_{1,2}$. This is because when Eq. (3) is not satisfied, $\mathcal{X}[c_n(\mathbf{r}_o)]$ is composed of different WPs, while, e.g., the right-hand side of the sector charge formula in Eq. (35) requires summing the orbital multiplicities $n_X^{(\ell)}$ at the same WP X . We will treat this case separately in Sec. V. (See also the comments in Sec. IV C for the case without satisfying Eq. (3).)

Now, let us comment further on the sector charge Q_{sector} and the filling-anomaly factor η . First, when Eq. (3) is satisfied, Q_{sector} and η are simply proportional to each other:

$$Q_{\text{sector}} = \frac{e}{n} \eta \pmod{e}. \quad (36)$$

We can see this because the factor νN_{cell} in Eq. (35) becomes $n\mathbb{Z}$ when the constraint Eq. (3) is satisfied for a

C_n -symmetric insulator. Second, for class AII insulators, when only the electronic charges are considered, Q_{sector} (η) can be defined modulo $2e$ ($2n$) because of Kramers theorem. However, this is not true if the contribution from the ions is carefully studied [66]. Specifically, time-reversal symmetry allows an ion with an integer spin and odd charge, i.e., $e \text{ mod } 2e$. When such ions are added in a C_n -symmetric manner, the total charge of the system is only well defined modulo ne instead of $2ne$, meaning that the sector charge is well defined modulo e . Thus, even when we consider only the electronic contribution for a simpler discussion, we still define Q_{sector} modulo e and η modulo n for the classes A, AI, and AII, as in Refs. 41 and 66. Moreover, defining Q_{sector} modulo e offers an advantage. In this case, Q_{sector} can be determined by the fully traced TCMs as we have shown. Note that Q_{sector} (similarly, the corner charges) mod $2e$ is not symmetry-indicated such that the momentum-space data does not determine Q_{sector} uniquely [36, 67].

C. Some comments on the Chern number, polarization, and sector charge

Interestingly, the expressions for the bulk polarization, sector charge, and Chern number in terms of the fully traced TCMs elucidate fundamental differences in these topological responses in position-space, such as the dependence on unit cell origin, that are otherwise not apparent when each of these quantities are expressed solely in terms of momentum-space irrep multiplicities. Although it was previously known, our results make manifest that the polarization depends on the unit-cell origin, and the sector charge depends on the rotation center. Indeed, one must specify the unit-cell origin and rotation center (or linear system sizes $N_{1,2}$ since for open boundaries the rotation symmetry is uniquely determined by the linear dimensions) to define the polarization and the sector charge. Our results in Tables IV-V are specifically for a crystal where the unit cell origin is located at the $1a$ WP. Redefining the unit cell origin to another WP would change which Wannier orbital multiplicities contribute to the bulk polarization. Hence, the polarization and sector charge differ from the Chern number, whose value (and manifest expression in terms of TCMs) is unit cell origin-independent, and linear dimension-independent, owing to the strong topological nature of the Chern insulator. This precisely reflects the differing character of obstructed atomic insulators (which may have polarization and/or sector charge) and topological insulators (which may have Chern number).

Moreover, all of the topological quantities studied so far (which are the Chern number modulo n , polarization, sector charge, and filling-anomaly factor) are symmetry indicated, i.e., their values can be determined by momentum-space data. What we have shown here is that the fully traced TCMs can completely replace the momentum-space data to diagnose the topology. In other

TABLE IV. Bulk polarization for AZ class A (for both spinless and spin-1/2) C_n -symmetric atomic insulators expressed in terms of fully traced TCMs evaluated over maximal WPs. The bulk polarization for C_4 -symmetric atomic insulators has alternative expressions in terms of fully traced TCMs (see Supplemental Material [59]). Each component of the polarization is defined modulo e , i.e., $\mathbf{P} = p_1 \mathbf{a}_1 + p_2 \mathbf{a}_2$ with $p_{1,2} \pmod{e}$ where $e = -|e|$. For C_4 , $s_{1,2} \in \{-1, +1\}$.

	A (Spinless)	A (Spin-1/2)
C_2	$p_1 = -\frac{e}{8}(\langle c_2(\mathbf{x}_{1b}) \rangle_F + \langle c_2(\mathbf{x}_{1d}) \rangle_F)$ $p_2 = -\frac{e}{8}(\langle c_2(\mathbf{x}_{1c}) \rangle_F + \langle c_2(\mathbf{x}_{1d}) \rangle_F)$	$p_1 = i\frac{e}{8}(\langle c_2(\mathbf{x}_{1b}) \rangle_F + \langle c_2(\mathbf{x}_{1d}) \rangle_F)$ $p_2 = i\frac{e}{8}(\langle c_2(\mathbf{x}_{1c}) \rangle_F + \langle c_2(\mathbf{x}_{1d}) \rangle_F)$
C_3	$p_1 = p_2 = \frac{4e}{9}\text{Re}[\langle c_3(\mathbf{x}_{1b}) \rangle_F - \langle c_3(\mathbf{x}_{1c}) \rangle_F]$	$p_1 = p_2 = \frac{2e}{9}\text{Re}[\langle c_3(\mathbf{x}_{1b}) \rangle_F - \langle c_3(\mathbf{x}_{1c}) \rangle_F]$
C_4	$p_1 = p_2 = \frac{e}{8}(s_1 \langle c_2(\mathbf{x}_{1b}) \rangle_F + s_2 \langle c_2(\mathbf{x}_{2c}) \rangle_F)$	$p_1 = p_2 = i\frac{e}{8}(s_1 \langle c_2(\mathbf{x}_{1b}) \rangle_F + s_2 \langle c_2(\mathbf{x}_{2c}) \rangle_F)$
C_6	$p_1 = p_2 = 0$	$p_1 = p_2 = 0$

TABLE V. Bulk polarization for AZ classes AI and AII C_n -symmetric atomic insulators expressed in terms of fully traced TCMs evaluated over maximal WPs. The bulk polarization for C_4 -symmetric atomic insulators has other expressions in terms of fully traced TCMs (see Supplemental Material [59]). Each component of the polarization is defined modulo e , i.e., $\mathbf{P} = p_1 \mathbf{a}_1 + p_2 \mathbf{a}_2$ with $p_{1,2} \pmod{e}$ where $e = -|e|$. For C_4 , $s_{1,2} \in \{-1, +1\}$.

	AI	AII
C_2	$p_1 = -\frac{e}{8}(\langle c_2(\mathbf{x}_{1b}) \rangle_F + \langle c_2(\mathbf{x}_{1d}) \rangle_F)$ $p_2 = -\frac{e}{8}(\langle c_2(\mathbf{x}_{1c}) \rangle_F + \langle c_2(\mathbf{x}_{1d}) \rangle_F)$	$p_1 = p_2 = 0$
C_3	$p_1 = p_2 = \frac{e}{9}(\langle c_3(\mathbf{x}_{1b}) \rangle_F - \langle c_3(\mathbf{x}_{1c}) \rangle_F)$	$p_1 = p_2 = \frac{2e}{9}(\langle c_3(\mathbf{x}_{1b}) \rangle_F - \langle c_3(\mathbf{x}_{1c}) \rangle_F)$
C_4	$p_1 = p_2 = \frac{e}{8}(s_1 \langle c_2(\mathbf{x}_{1b}) \rangle_F + s_2 \langle c_2(\mathbf{x}_{2c}) \rangle_F)$	$p_1 = p_2 = 0$
C_6	$p_1 = p_2 = 0$	$p_1 = p_2 = 0$

TABLE VI. Sector charge for AZ class A (both spinless and spin-1/2) C_n -symmetric atomic insulators expressed in terms of fully traced TCMs evaluated over maximal WPs, for lattices with dimensions $N_1 \times N_2$ given by Eq. (3). The sector charge is defined modulo e where $e = -|e|$. While the sector charge measures the net charge in a $2\pi/n$ rad sector of an open boundary C_n -symmetric lattice, the expressions below are in terms of fully traced TCMs evaluated on C_n -symmetric lattices having periodic boundaries.

	A (Spinless)	A (Spin-1/2)
C_2	$-\frac{e}{8} \langle c_2(\mathbf{x}_{1d}) \rangle_F$	$i\frac{e}{8} \langle c_2(\mathbf{x}_{1d}) \rangle_F$
C_3	$\frac{4e}{9} \text{Re}[\langle c_3(\mathbf{x}_{1a}) \rangle_F]$	$\frac{2e}{9} \text{Re}[\langle c_3(\mathbf{x}_{1a}) \rangle_F]$
C_4	$-\frac{e}{16}(\langle c_2(\mathbf{x}_{1b}) \rangle_F + 4\text{Re}\langle c_4(\mathbf{x}_{1b}) \rangle_F)$	$-\frac{e}{16}(i\langle c_2(\mathbf{x}_{1b}) \rangle_F + 4\text{Re}[e^{-\frac{i\pi}{4}} \langle c_4(\mathbf{x}_{1b}) \rangle_F])$
C_6	$-\frac{e}{72}(3\langle c_2(\mathbf{x}_{1a}) \rangle_F + 24\text{Re}\langle c_6(\mathbf{x}_{1a}) \rangle_F + 8\text{Re}\langle c_3(\mathbf{x}_{1a}) \rangle_F)$	$-\frac{e}{72}(3i\langle c_2(\mathbf{x}_{1a}) \rangle_F + 24\text{Im}[\langle c_6(\mathbf{x}_{1a}) \rangle_F] - 8\text{Re}[\langle c_3(\mathbf{x}_{1a}) \rangle_F])$

words, the TCMs play the role of position-space symmetry indicators. Furthermore, this also implies that using the TCMs, topological quantities such as the Chern number and the sector charge still can be defined robustly without momentum-space consideration.

Finally, anticipating what is to come in the next section, we briefly comment on cases where the system is either (i) periodic but not obeying the constraint Eq. (3), or (ii) has open boundaries. For (i), we need to introduce the TCMs with twisted boundary conditions as we will

demonstrate in Sec. V. There, we provide a definitive prescription for how the TCM formulas predicting the topological quantities, e.g., those shown in Tables IV-VII, change according to the choice of (N_1, N_2) . For (ii), we show instead that the traced TCMs around the local peak at the unique rotation center can diagnose the topological quantities, and we illustrate this with concrete tight-binding calculations in Sec. VI.

TABLE VII. Sector charge for AZ classes AI and AII C_n -symmetric atomic insulators expressed in terms of fully traced TCMs evaluated over maximal WPs, for lattices with dimensions $N_1 \times N_2$ given by Eq. (3). The sector charge is defined modulo e where $e = -|e|$. While the sector charge measures the net charge in a $2\pi/n$ rad sector of an open boundary C_n -symmetric lattice, the expressions below are in terms of fully traced TCMs evaluated on C_n -symmetric lattices having periodic boundaries.

	AI	AII
C_2	$-\frac{e}{8} \langle c_2(\mathbf{x}_{1d}) \rangle_F$	0
C_3	$\frac{e}{9} \langle c_3(\mathbf{x}_{1a}) \rangle_F$	$\frac{2e}{9} \langle c_3(\mathbf{x}_{1a}) \rangle_F$
C_4	$-\frac{e}{16} (\langle c_2(\mathbf{x}_{1b}) \rangle_F + 4 \langle c_4(\mathbf{x}_{1b}) \rangle_F)$	$-\frac{e}{4\sqrt{2}} \langle c_4(\mathbf{x}_{1b}) \rangle_F$
C_6	$-\frac{e}{72} (3 \langle c_2(\mathbf{x}_{1a}) \rangle_F + 24 \langle c_6(\mathbf{x}_{1a}) \rangle_F + 8 \langle c_3(\mathbf{x}_{1a}) \rangle_F)$	$\frac{e}{9} \langle c_3(\mathbf{x}_{1a}) \rangle_F$

V. FINITE-SIZE LATTICES AND TWISTING BOUNDARY CONDITIONS

In the previous section, we demonstrated how the Chern number, bulk polarization, and sector charge for C_n -symmetric Chern insulators and atomic insulators, respectively, could be reformulated in terms of basis-independent, fully traced TCMs which rely on only the rotation operators and the ground state. This removes the need to utilize symmetry data from the momentum-space band structure to characterize the bulk crystalline topology of C_n -symmetric insulators. Furthermore, the momentum-space based approach of classifying topological crystalline insulators implicitly relies on the assumption that the dimensions of the finite-size lattice allow for the existence of the maximal set of high symmetry momenta in the BZ. While it is true that in the thermodynamic limit (i.e., $N_{1,2} \rightarrow \infty$ such that the spacing between discrete momenta in the BZ vanishes) the maximal set of high symmetry momenta exists in the limit, this does not hold for every finite-size lattice. Explicitly, a lattice having dimensions $N_1 \times N_2$ and periodic boundary conditions will have a crystal momentum vector quantized as shown in Eq. (4). Thus, unless N_1 and N_2 satisfy the constraints laid out in Eq. (3), only a subset of all possible high symmetry momenta will exist in the BZ. Therefore, it remains an open question how to apply the symmetry-based diagnosis of crystalline topology to generic C_n -symmetric lattices having arbitrary linear dimensions N_1, N_2 . Here we systematically develop a method that accomplishes this challenge by building on earlier results in Refs. 68–70.

To overcome this issue, we will show that the mappings between the fully traced TCMs on one side, and the Chern number, bulk polarization, and sector charge on the other, can be modified by adjusting the boundary condition(s) of the lattice along the dimension(s) that do not satisfy the constraint in Eq. (3). We will demonstrate that this procedure extends the classification of C_n -symmetric Chern insulators and (obstructed) atomic insulators using TCMs to any finite-size lattice.

To begin, let us consider a C_n -symmetric lattice having arbitrary dimensions $N_1 \times N_2$, where N_1 and N_2 are

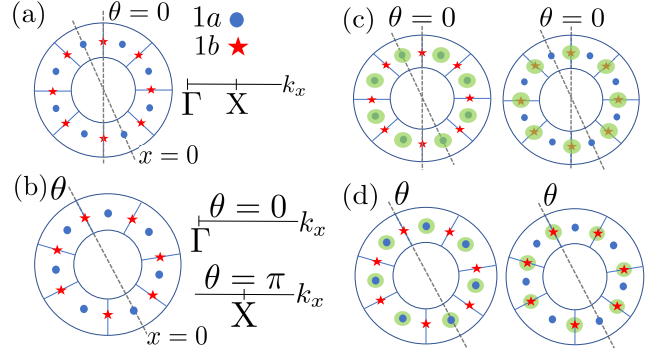


FIG. 5. Simplified illustration of a finite-size, 1D atomic insulator such as the SSH chain with C_2 symmetry on a periodic lattice shown using a circular geometry to emphasize the periodicity. Details of the inner structure of the unit cell, such as sublattice sites, have been omitted. The blue circles denote the $1a$ WPs, and the red stars denote the $1b$ WPs. The green circles indicate electronic Wannier orbital centers. The parameter θ indicates the boundary condition twist/flux at the C_2 rotation center ($\theta = 0$ periodic, $\theta = \pi$ anti-periodic). (a) An even number of unit cells and corresponding C_2 -invariant momenta in BZ. (b) An odd number of unit cells and the corresponding C_2 -invariant momenta for each boundary condition. In both (a) and (b), $x = 0$ denotes the coordinates of the unit cell serving as the origin of the lattice. Positions of electronic Wannier orbital centers in (c) even and (d) odd unit cell cases for both the trivial (left) and obstructed (right) atomic insulator phases. In order to distinguish the phases of the SSH chain in (d), $\theta = 0$ and $\theta = \pi$ must both be considered (i.e., periodic and anti-periodic boundary conditions).

such that the C_n symmetry is preserved (e.g., $N_1 \neq N_2$ in general for C_2 symmetry, but $N_1 = N_2 = N$ for C_3 , C_4 , and C_6 symmetry). We will now consider *twisting* the boundary conditions on the lattice, with twists parameterized by (θ_1, θ_2) , where θ_1 and θ_2 correspond to the flux through the cycles parallel to \mathbf{a}_1 and \mathbf{a}_2 respectively. The twisted boundary conditions can be formulated in terms of the position-space basis as

$$\begin{aligned} |\mathbf{R} + N_1 \mathbf{a}_1, \alpha\rangle &= e^{-i\theta_1} |\mathbf{R}, \alpha\rangle \\ |\mathbf{R} + N_2 \mathbf{a}_2, \alpha\rangle &= e^{-i\theta_2} |\mathbf{R}, \alpha\rangle. \end{aligned} \quad (37)$$

With twisted boundary conditions $\theta_{1,2}$, the quantization of crystalline momentum is modified as:

$$\mathbf{k} = \left(\frac{n_1}{N_1} - \frac{\theta_1}{2\pi N_1} \right) \mathbf{b}_1 + \left(\frac{n_2}{N_2} - \frac{\theta_2}{2\pi N_2} \right) \mathbf{b}_2. \quad (38)$$

Now, for arbitrary, finite N_1 and N_2 , when untwisted periodic boundary conditions are present ($\theta_1 = \theta_2 = 0 \pmod{2\pi}$), the set of discrete momenta given by Eq. (38) may contain only a subset of high symmetry momenta. In such cases it is possible to adjust θ_1 and θ_2 such that the set of discrete momenta given by Eq. (38) contains a different subset of high symmetry momenta. Therefore, for arbitrary finite N_1 and N_2 that do not satisfy Eq. (3), one can consider lattices having different boundary conditions parameterized by (θ_1, θ_2) such that the complete set of high symmetry momenta is obtained by considering a set of systems having different twists.

A. 1D example: SSH chain

To demonstrate the necessity of twisting boundary conditions, we first consider a simple model for a one-dimensional atomic insulator with C_2 symmetry, such as the Su-Schrieffer-Heeger (SSH) chain [65], as shown in Fig. 5. Each gapped phase of the SSH model admits a Wannier representation, and there is a clear distinction between the obstructed atomic insulator phase (i.e., Wannier orbitals are localized at WP $1b$), and the trivial atomic insulator phase (i.e., Wannier orbitals localized at WP $1a$). We know this distinction is captured by the momentum-space data of the occupied energy band at the Γ and X points [18, 71], and thus, we should be able to apply our methods to give an alternative characterization. Although we describe this procedure for a one-dimensional system for simplicity, this generalizes straightforwardly to two dimensions for any C_n symmetry.

In order to make the discussion presented in this subsection concrete, we introduce the following Hamiltonian for the SSH chain in the tight-binding position-space basis $|x, \sigma = A, B\rangle$,

$$H_{\text{SSH, PBC}} = \sum_{x=1}^N m(|x, B\rangle\langle x, A| + |x, A\rangle\langle x, B|) + \sum_{x=1}^N t(|x+1, A\rangle\langle x, B| + |x, B\rangle\langle x+1, A|). \quad (39)$$

where A, B are the sublattice degrees of freedom, and periodic boundary conditions are specified as $|x+N, \sigma\rangle = |x, \sigma\rangle$. For a periodic, translation invariant chain we can Fourier transform to arrive at the Bloch Hamiltonian

$$H_{\text{SSH}}(k_x) = (m + t \cos k_x) \sigma_1 + t \sin k_x \sigma_2, \quad (40)$$

where σ_i for $i \in \{1, 2, 3\}$ are the conventional Pauli matrices with respect to the two-atom sublattice basis in

each unit cell. This model is C_2 -symmetric, with the C_2 operator given by σ_1 , e.g., $\sigma_1 H_{\text{SSH}}(k_x) \sigma_1 = H_{\text{SSH}}(-k_x)$, as well as chiral-symmetric with the chiral operator given by σ_3 , e.g., $\sigma_3 H_{\text{SSH}}(k_x) \sigma_3 = -H_{\text{SSH}}(k_x)$. The two bulk bands of this model are therefore symmetric in energy around $E = 0$. Here, we take the ground state to be such that the Fermi level is tuned to $E_F = 0$ within the bulk gap so that the lower band is always occupied.

There are two phases of this model. The first is the so-called ‘‘obstructed atomic limit’’ phase which occurs for $|m| < |t|$. Here, the ground state is given by a periodic arrangement of electrons localized at the $1b$ WP of every unit cell, yielding a non-trivial bulk polarization of $\mathbf{P} = (e/2)\mathbf{a}_1 \pmod{e}$. The second phase is the ‘‘trivial atomic limit’’ phase, which occurs for $|m| > |t|$ where the ground state is given by a periodic arrangement of electrons localized at the $1a$ WP of every unit cell, resulting in a trivial bulk polarization $\mathbf{P} = \mathbf{0} \pmod{e}$.

Now let us study the properties of finite chains having an even or odd number of unit cells (the former satisfying the constraints Eq. (3), while the latter does not). First, we consider the conventional case of a periodic SSH chain having an even number of unit cells $N_1 = 2q$ where $q \in \mathbb{N}$. In this case, the momentum is simply given by $k_x = (2\pi/N_1)n_1$ for $n_1 \in \mathbb{Z}$. Since N_1 is even, this implies that both C_2 -invariant HSM $k_x = 0$ (the Γ -point) and $k_x = \pi$ (the X -point) are allowed as discrete momentum points in the BZ, i.e., $n_1 = 0$ and $n_1 = N_1/2$ respectively. Hence, in momentum space we have a set of two Γ -point irrep multiplicities and two rotation invariants given by $\{m(\Gamma_1), m(\Gamma_2), [X_1], [X_2]\}^4$.

Another consequence of having an even number of unit cells, is that the periodic SSH chain has two distinct C_2 rotation center choices given by either a pair of invariant $1a$ WPs or a pair of invariant $1b$ WPs. Thus, using the C_2 rotation operators at the $1a$ and the $1b$ WPs, one can construct a corresponding fully traced TCM for each. Hence, in position space we have two fully traced TCMs given by $\{\langle c_2(\mathbf{x}_{1a}) \rangle_F^{\theta=0}, \langle c_2(\mathbf{x}_{1b}) \rangle_F^{\theta=0}\}$. Given that a bulk gap exists, and the number of occupied bands is specified by the filling ν , the set of momentum space quantities can be further constrained to just two quantities, one at each C_2 -invariant momenta, e.g., $\{m(\Gamma_1), [X_1]\}$. Hence, for a one-dimensional atomic insulator having an even number of unit cells and C_2 symmetry, there exists a one-to-one mapping between the pair of fully traced TCMs and the reduced set of momentum-space irrep multiplicities and rotation invariants. Both sets of quantities can distinguish the trivial and obstructed phases without having to twist the boundary conditions.

Now we consider the SSH chain having an odd number of unit cells $N_1 = 2q + 1$. With periodic boundary conditions the momentum is still quantized as $k_x = (2\pi/N_1)n_1$

⁴ The lower indices 1 and 2 correspond to C_2 eigenvalues of +1 and -1, respectively, representing angular momentum 0 and 1 mod 2.

for $n_1 \in \mathbb{Z}$. However, since N_1 is odd, only one C_2 -invariant momentum is allowed as a discrete momentum point in the BZ, i.e., $n_1 = 0$ the Γ -point. The X point would require $n_1 = N_1/2 = q + 1/2 \notin \mathbb{Z}$. Hence, the momentum-space symmetry data consists of simply $\{m(\Gamma_1)_{\theta=0}, m(\Gamma_2)_{\theta=0}\}$, where we have specified the twisted boundary conditions parameterized by θ in the irrep multiplicity $m(\mathbf{k}_p)$. Furthermore, in position space, unlike the even unit cell case, where the $1a$ ($1b$) C_2 rotation center leaves two $1a$ ($1b$) WPs at antipodal points of the periodic lattice invariant under C_2 , this is not true for the odd unit cell case. In fact, as shown in Figs. 5(b) and (d), there is only one type of C_2 rotation center and it leaves invariant one $1a$ and one $1b$ WP at antipodal points of the periodic lattice. For such lattices, we will label the C_2 rotation center by the WP with respect to the unit cell located at the origin of the lattice. In this case, for the one-dimensional lattice shown in Figs. 5(b) and (d), the C_2 rotation center will be denoted by the $1a$ WP.

Unfortunately, neither the irrep multiplicities $m(\Gamma_{1,2})_{\theta=0}$ nor the fully traced TCM $\langle c_2(\mathbf{x}_{1a}) \rangle_F^{\theta=0}$ contain enough information to distinguish the trivial and obstructed phases of the SSH chain with odd number of unit cells. For example, if we consider the irrep multiplicities for the occupied band of Eq. (40), there is always one occupied Bloch state at Γ with a -1 C_2 eigenvalue, which means $m(\Gamma_1)_{\theta=0} = 0$ and $m(\Gamma_2)_{\theta=0} = 1$ in both phases. For comparison, in position space there is either an electronic Wannier orbital localized at the $1a$ WP on the C_2 rotation center (trivial phase) with C_2 eigenvalue -1 or one localized at the $1b$ WP (obstructed atomic limit) phase with C_2 eigenvalue of -1 . Hence, the fully traced TCM for an odd number of unit cells will receive equal contributions from both configurations and hence cannot distinguish the phases.

We can clearly illustrate the orbital configurations in the obstructed atomic limit (with $m = 0$ and $t \neq 0$) and the trivial atomic limit (with $m \neq 0$ and $t = 0$) of Eq. (40). In these limits, the single-particle eigenstates of the tight-binding Hamiltonian and the Wannier orbital states are identical. To be explicit, let the C_2 rotation center refer to the $c_2(\mathbf{x}_{1a})$ operator. Note that in position-space for $N_1 = 2q + 1$, $c_2(\mathbf{x}_{1a})$ maps $|x, A\rangle \rightarrow |N_1 - x, B\rangle$ and $|x, B\rangle \rightarrow |N_1 - x, A\rangle$. In the $m = 0, t \neq 0$ limit, the electronic Wannier orbital state localized at the C_2 rotation center is $|W_-(N_1/2)\rangle = \frac{1}{\sqrt{2}}(|(N_1 + 1)/2, A\rangle - |(N_1 - 1)/2, B\rangle)$, and it follows that $c_2(\mathbf{x}_{1a})|W_-(N_1/2)\rangle = -|W_-(N_1/2)\rangle$, implying that $|W_-(N_1/2)\rangle$ has a C_2 eigenvalue of -1 . Similarly, in the $m \neq 0, t = 0$ limit, the electronic Wannier orbital state localized at the C_2 rotation center located at the $1a$ WP is now given as $|W_-(0)\rangle = \frac{1}{\sqrt{2}}(|0, B\rangle - |0, A\rangle)$, which means $c_2(\mathbf{x}_{1a})|W_-(0)\rangle = -|W_-(0)\rangle$. For reference, in Fig. 5 (d), an illustration of the Wannier orbital centers is provided for the trivial and obstructed atomic limits for $N_1 = 7$ unit cells. This analysis extends to all pa-

TABLE VIII. TCMs for the 1D lattice having even ($N = 0 \bmod 2$) unit cells lattice corresponding to each C_2 center, i.e., for the $1a$ and $1b$ WPs, as shown in the first column. The fully traced TCMs for the even unit cell lattice can be mapped to the fully traced TCMs for the odd ($N = 1 \bmod 2$) unit cell lattice having different boundary conditions (periodic, $\theta = 0$ and anti-periodic, $\theta = \pi$), as shown in second column.

$N = 0 \bmod 2$	$N = 1 \bmod 2$
$\langle c_2(\mathbf{x}_{1a}) \rangle_F^{\theta=0}$	$\langle c_2(\mathbf{x}_{1a}) \rangle_F^{\theta=0} + \langle c_2(\mathbf{x}_{1a}) \rangle_F^{\theta=\pi}$
$\langle c_2(\mathbf{x}_{1b}) \rangle_F^{\theta=0}$	$\langle c_2(\mathbf{x}_{1a}) \rangle_F^{\theta=0} - \langle c_2(\mathbf{x}_{1a}) \rangle_F^{\theta=\pi}$

parameter choices within the obstructed atomic limit phase ($|m| < |t|$) and trivial atomic limit phase ($|m| > |t|$) since the limits $m = 0, t \neq 0$ and $m \neq 0, t = 0$ are adiabatically connected (while preserving C_2) to different parameter choices within each of their respective phases due to the existence of a bulk gap. This means $\langle c_2(\mathbf{x}_{1a}) \rangle_F^{\theta=0} = -1$ in both phases, and hence does not distinguish the phases.

The resolution to this issue is to introduce anti-periodic boundary conditions ($\theta = \pi$) at the C_2 rotation center, and to *jointly* consider the symmetry data obtained from *both* periodic and anti-periodic boundary conditions. The twisted boundary conditions are introduced by choosing a gauge where the full flux θ passes through a C_2 invariant bond, i.e., where the $1b$ WP is located as shown in Fig. 5.

For this discussion, we will focus on the tight-binding Hamiltonian with periodic boundary conditions in Eq. (40). To implement twisted boundary conditions we modify this Hamiltonian as follows,

$$\begin{aligned}
H_{\text{SSH,TBC}} &= \sum_x m(|x, B\rangle\langle x, A| + |x, A\rangle\langle x, B|) \\
&+ \sum_{x \neq \frac{N_1-1}{2}} t(|x+1, A\rangle\langle x, B| + |x, B\rangle\langle x+1, A|) \\
&+ t(e^{-i\theta}|(N_1+1)/2, A\rangle\langle (N_1-1)/2, B| \\
&+ e^{i\theta}|(N_1-1)/2, B\rangle\langle (N_1+1)/2, A|), \quad (41)
\end{aligned}$$

where a flux θ has been inserted on the hopping t between the unit cells located at $x = (N_1 - 1)/2$ and $x = (N_1 + 1)/2$ (referring to Fig. 5 (b) where $N_1 = 7$ unit cells, this would be between the unit cells located at $x = 3$ and $x = 4$).

The Hamiltonian $H_{\text{SSH,TBC}}$ given by Eq. (41) is invariant under $c_2(\mathbf{x}_{1a})$ which, as an operator, can be expanded in the position-space basis as:

$$\begin{aligned}
c_2(\mathbf{x}_{1a}) &= \sum_{x=0}^{(N_1-1)/2} [|N_1 - x, B\rangle\langle x, A| + |N_1 - x, A\rangle\langle x, B| \\
&+ |x, B\rangle\langle N_1 - x, A| + |x, A\rangle\langle N_1 - x, B|]. \quad (42)
\end{aligned}$$

It can be shown that $[H, c_2(\mathbf{x}_{1a})] = 0$. Note that the $H_{\text{SSH,TBC}}$ specified in Eq. (41) is invariant *only* under

$c_2(\mathbf{x}_{1a})$ given by Eq. (42), and not under any other $c_2(\mathbf{R}+\mathbf{x}_{1a})$ operator with $\mathbf{R} \neq \mathbf{0}$ unless the $c_2(\mathbf{R}+\mathbf{x}_{1a})$ is modified by an appropriate gauge transformation phase factor that accounts for moving the position of the flux line.

Introducing anti-periodic boundary conditions shifts the momentum quantization to $k_x = (2\pi/N_1)(n_1 - \frac{1}{2})$ where $n_1 \in \{1, \dots, N_1\}$. Note that only one C_2 -invariant momentum still exists, but it is no longer the Γ point, i.e., the X point is now allowed instead when $n_1 = (N_1 + 1)/2$ (see Fig. 5(b)). Hence, the momentum-space symmetry data is now $\{m(X_1)_{\theta=\pi}, m(X_2)_{\theta=\pi}\}$. We can now convert these data to momentum space invariants $\{[X_1], [X_2]\}$ by redefining the rotation invariants as $[X_p] = m(X_p)_{\theta=\pi} - m(\Gamma_p)_{\theta=0}$ for $p = 1, 2$. This redefinition emphasizes how we are combining the momentum-space symmetry data for lattices having both periodic and anti-periodic boundary conditions in order to generate both HSM.

In parallel, we have the fully traced TCMs for the C_2 rotation center, but now for anti-periodic boundary conditions, $\langle c_2(\mathbf{x}_{1a}) \rangle_F^{\theta=\pi}$. Taking into account the symmetry data from both the periodic and anti-periodic boundary conditions yields $\{\langle c_2(\mathbf{x}_{1a}) \rangle_F^{\theta=0}, \langle c_2(\mathbf{x}_{1a}) \rangle_F^{\theta=\pi}\}$ in position space and $\{m(\Gamma_1)_{\theta=0}, m(\Gamma_2)_{\theta=0}, [X_1], [X_2]\}$ for momentum space. Thus, we expect that we now have enough data to diagnose the trivial and obstructed phases of this model, as in the even unit cell case. Intuitively we can see this as follows. As shown in Fig. 5(d), both phases of the odd unit cell SSH model always have an electronic Wannier orbital localized at either the $1a$ or $1b$ WP of the C_2 rotation center. Introducing anti-periodic boundary conditions can flip the C_2 eigenvalue of the electronic Wannier orbital at the invariant $1b$ WP in the obstructed atomic limit phase localized from -1 to $+1$. This is enough to show that the trivial and obstructed limits will generate different fully traced TCMs if we include both twisted and untwisted boundary conditions.

More precisely, while we have seen that we can generate a pair of position space quantities by twisting boundary conditions, we have not shown that the twisted, fully traced TCMs capture the relevant symmetry data. To do this we need to construct the mapping between the twisted, fully traced TCMs and the momentum-space symmetry data. This can be made explicit by expanding the fully traced TCMs in momentum-space. First, we have $\langle c_2(\mathbf{x}_{1a}) \rangle_F^{\theta=0} = m(\Gamma_1)_{\theta=0} - m(\Gamma_2)_{\theta=0}$ and $\langle c_2(\mathbf{x}_{1a}) \rangle_F^{\theta=\pi} = m(X_1)_{\theta=\pi} - m(X_2)_{\theta=\pi}$. This implies that

$$\begin{aligned} \langle c_2(\mathbf{x}_{1a}) \rangle_F^{\theta=0} + \langle c_2(\mathbf{x}_{1a}) \rangle_F^{\theta=\pi} &= 4m(\Gamma_1)_{\theta=0} - 2\nu + 2[X_1], \\ \langle c_2(\mathbf{x}_{1a}) \rangle_F^{\theta=0} - \langle c_2(\mathbf{x}_{1a}) \rangle_F^{\theta=\pi} &= -2[X_1], \end{aligned} \quad (43)$$

where ν denotes the filling, i.e., $m(\Gamma_1)_{\theta=0} + m(\Gamma_2)_{\theta=0} = m(X_1)_{\theta=\pi} + m(X_2)_{\theta=\pi} = \nu$. We recall in this context that that $[X_1] \equiv m(X_1)_{\theta=\pi} - m(\Gamma_1)_{\theta=0}$.

The correspondence between the TCMs for the even and odd unit cell cases, is summarized in Table VIII. Using Eq. (43), when the system has an odd number of

unit cells we can now easily determine quantities such as the bulk polarization, or, since our model has chiral symmetry, the parity of the chiral winding number w . The bulk polarization \mathbf{P} for the SSH chain is determined by the number of Wannier orbitals localized at the $1b$ WP. That is,

$$\mathbf{P} = \frac{e}{2} n_{1b} \mathbf{a}_1. \quad (44)$$

For the even unit cell SSH chain, it is established that the relationship between the chiral winding number, bulk polarization, and the fully traced TCM (even in the absence of translation symmetry) is given as follows [72],

$$2ew = 4|\mathbf{P}| = e \langle c_2(\mathbf{x}_{1b}) \rangle_F^{\theta=0} \pmod{4}. \quad (45)$$

Now for the odd unit cell case, having shown that both periodic and anti-periodic boundary conditions are necessary to distinguish the trivial and obstructed atomic limits, we can now modify the relationship given by Eq. (45) in the following manner,

$$2ew = 4|\mathbf{P}| = e (\langle c_2(\mathbf{x}_{1a}) \rangle_F^{\theta=0} - \langle c_2(\mathbf{x}_{1a}) \rangle_F^{\theta=\pi}) \pmod{4}. \quad (46)$$

Hence, in order to determine the bulk polarization and the parity of the chiral winding number from the symmetry data for an odd number of unit cells, we take a linear combination of the fully traced TCMs for periodic ($\theta = 0$) and anti-periodic ($\theta = \pi$) boundary conditions.

B. Generalizing the procedure to 2D

As demonstrated on a one-dimensional lattice, twisting boundary conditions is a useful way generalizing the mapping between symmetry data in momentum-space and position-space in order to properly distinguish the phases of rotation-symmetric insulators. The procedure discussed for the one-dimensional atomic insulator can be generalized to both C_n -symmetric Chern insulators and atomic insulators in two dimensions by twisting boundary conditions via Eq. (37) and utilizing Eq. (38).

Before discussing the procedure for two-dimensional lattices, we need to understand the geometric features of periodic lattices when they do not satisfy the constraints given by Eq. (3). Figure 6 illustrates the invariant, multiplicity 1 WPs of C_2 and C_3 -symmetric lattices that have dimensions $N_1 \times N_2$ which do not respect the constraints, and therefore do not support the maximal set of high symmetry points. Comparing these lattices to those that were shown in Fig. 1 which do follow the constraints, there is a crucial difference between the set of invariant positions for C_2 , C_3 , and C_4 -symmetric lattices. In Fig. 1, each rotation center leaves invariant the multiplicity 1 WPs of the same type, which is depicted as those corresponding to the same color and shape. That is, if our rotation center is a $1a$ WP then the other invariant points of the periodic lattice are also $1a$ WPs.

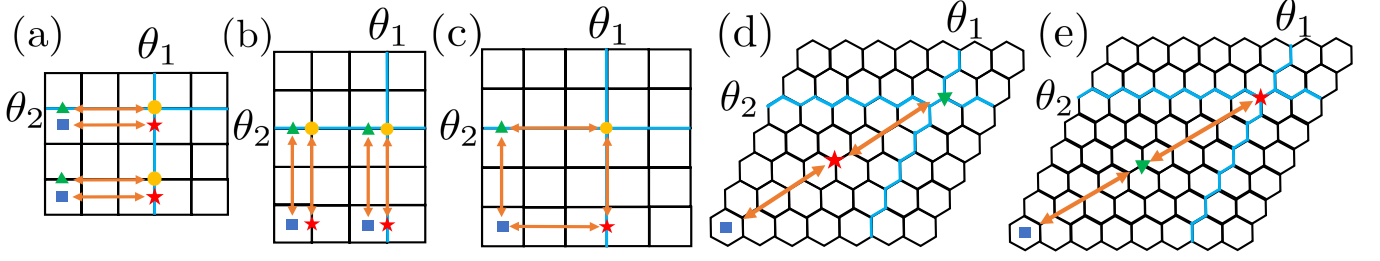


FIG. 6. Set of invariant positions $\mathcal{X}[c_n(\mathbf{r}_o)]$ for finite lattices that do not obey the constraints on the linear dimensions (N_1, N_2) given by Eq. (3). The origin $\mathbf{R} = \mathbf{0}$ is located at the unit cell at the lower left corner of each lattice shown in (a)-(e). Each rotation center is specified by a multiplicity 1 WP for two-dimensional lattices of various dimensions having C_2 symmetry [(a)-(c)] and C_3 symmetry [(d)-(e)]. The dimensions of the lattices are given by (a) $(N_1, N_2) = (1, 0) \bmod 2$, (b) $(N_1, N_2) = (0, 1) \bmod 2$, (c) $(N_1, N_2) = (1, 1) \bmod 2$, (d) $N = 1 \bmod 3$, (e) $N = 2 \bmod 3$. Note that $N_1 = N_2 = N$ for C_3 -symmetric lattices. Each of the lattices in (a)-(e) have periodic boundary conditions, which means that the top and bottom edges are identified with each other, and separately, the left and right edges are identified with each other. The light blue lines indicate the location of the bonds modified by Peierls factors to generate fluxes θ_1 and θ_2 that parameterize the twisted boundary conditions. The location of these fluxes is specifically chosen such that the resulting Hamiltonian with twisted boundary conditions commutes with the rotation operator, i.e., $[H_{\text{TBC}}, c_n(\mathbf{r}_o)] = 0$. The orange double-headed arrows are a visual indicator that two positions in $\mathcal{X}[c_n(\mathbf{r}_o)]$ lie on the same rotation axis when periodic boundary conditions are maintained.

This is no longer true for the lattices shown in Fig. 6; in these cases the rotation center(s) can leave invariant different types of multiplicity 1 WPs. We saw this already for the SSH chain where in the case of an odd number of unit cells a $1a$ and $1b$ WP are left invariant by the same symmetry center instead of two WPs of the same type. This is illustrated in Fig. 6, where the orange arrows serve to indicate which WPs are fixed by the same rotation center. Thus, the dimensions of the lattice, specified by the number of unit cells along each primitive lattice vector, determine the invariant, multiplicity 1 WPs associated with each rotation center. Since there is not a unique choice of label for the WPs associated to each rotation center, then for the lattices shown in Fig. 6 we will label the rotation center by the WP located in the unit cell at the origin of the lattice. The origin is chosen to be the lower left corner of each lattice shown in Figs. 6(a)-(e).

We can now develop a straightforward generalization of the procedure for the odd unit cell SSH chain. That is, for each of the 2D lattices that do not satisfy Eq. (3), we can adjust the boundary conditions by threading fluxes θ_1 and θ_2 along each of the cycles along the primitive lattice vectors \mathbf{a}_1 and \mathbf{a}_2 . This yields a general momentum quantization condition given by Eq. (38). The boundary conditions need to be adjusted only for the dimension(s) of the lattice do not satisfy the constraints in Eq. (3). The necessary boundary conditions that must be considered for each finite-size lattice with C_n symmetry are given in Table IX. Taking into account the complete set of boundary conditions for each C_n -symmetric lattice allows one to distinguish insulating phases. Furthermore, we can reconstruct the full set of momentum-space symmetry data specified by the irrep multiplicities at all the high symmetry points in the BZ, and map the momentum data to the fully traced TCMs, which themselves

are defined for various boundary condition choices. This allows us to classify insulating phases using momentum or position space data on any finite lattice.

To demonstrate this, we can establish a mapping between (i) the fully traced TCMs over each multiplicity 1 WP rotation center for C_n -symmetric lattices having periodic boundary conditions and satisfying the constraints Eq. (3), and (ii) the fully traced TCMs over each multiplicity 1 WP corresponding to a rotation center for different twisted periodic boundary conditions for C_n -symmetric lattices that does not satisfy the constraints in Eq. (3). We recall that we have already accomplished this mapping for a 1D C_2 symmetric lattice as shown in Table VIII.

As an example, let us consider a C_2 -symmetric lattice with dimensions $N_1 \times N_2$. When $(N_1, N_2) = (0, 0) \bmod 2$, only untwisted periodic boundary conditions need to be considered. From Fig. 1 we see there should be four distinct, fully traced TCMs; one for each of the four distinct rotation centers at multiplicity 1 WPs:

$$\{ \langle c_2(\mathbf{x}_{1a}) \rangle_F^{(0,0)}, \langle c_2(\mathbf{x}_{1b}) \rangle_F^{(0,0)}, \langle c_2(\mathbf{x}_{1c}) \rangle_F^{(0,0)}, \langle c_2(\mathbf{x}_{1d}) \rangle_F^{(0,0)} \}. \quad (47)$$

Now, consider the lattice with dimensions such that $(N_1, N_2) = (1, 1) \bmod 2$. From Fig. 6(c) we see that, for this lattice, there is only one type of fully traced TCM given by $\langle c_2(\mathbf{x}_{1a}) \rangle_F^\theta$. According to Table IX, we must take into account three additional twisted boundary conditions in addition to periodic boundary conditions: $\boldsymbol{\theta} = (\theta_1, \theta_2) \in \{(0, 0), (\pi, 0), (0, \pi), (\pi, \pi)\}$. This means the full set of fully traced TCMs for this lattice is

$$\{ \langle c_2(\mathbf{x}_{1a}) \rangle_F^{(0,0)}, \langle c_2(\mathbf{x}_{1a}) \rangle_F^{(\pi,0)}, \langle c_2(\mathbf{x}_{1a}) \rangle_F^{(0,\pi)}, \langle c_2(\mathbf{x}_{1a}) \rangle_F^{(\pi,\pi)} \}. \quad (48)$$

TABLE IX. The required set of boundary conditions $\boldsymbol{\theta} = (\theta_1, \theta_2)$ for each C_n -symmetric lattice with dimensions $N_1 \times N_2$ that do not obey the dimension constraints in Eq. (3). We have specified the dimensions (N_1, N_2) modulo n , where $N_{1,2} > 0$. For C_4 -symmetric systems, also, note that the boundary conditions $\boldsymbol{\theta} = (\pi, 0)$ and $(0, \pi)$ apply only to C_2 TCMs. For C_6 -symmetric systems, the boundary conditions $\boldsymbol{\theta} = (-\frac{2\pi}{3}, \frac{2\pi}{3})$ and $(\frac{2\pi}{3}, -\frac{2\pi}{3})$ apply only to C_3 TCMs, and the boundary conditions $\boldsymbol{\theta} = (\pi, 0)$, $(0, \pi)$, and (π, π) apply only to C_2 TCMs.

C_n	(N_1, N_2)	$\{\boldsymbol{\theta}\}$
C_2	$(1, 0) \bmod 2$	$\{(0, 0), (\pi, 0)\}$
	$(0, 1) \bmod 2$	$\{(0, 0), (0, \pi)\}$
	$(1, 1) \bmod 2$	$\{(0, 0), (\pi, 0), (0, \pi), (\pi, \pi)\}$
C_3	$\pm(1, 1) \bmod 3$	$\{(0, 0), (-\frac{2\pi}{3}, \frac{2\pi}{3}), (\frac{2\pi}{3}, -\frac{2\pi}{3})\}$
C_4	$(1, 1) \bmod 2$	$\{(0, 0), (\pi, 0), (0, \pi), (\pi, \pi)\}$
C_6	$\pm(1, 1) \bmod 6$	$\{(0, 0), (-\frac{2\pi}{3}, \frac{2\pi}{3}), (\frac{2\pi}{3}, -\frac{2\pi}{3}), (\pi, 0), (0, \pi), (\pi, \pi)\}$
	$\pm(2, 2) \bmod 6$	$\{(0, 0), (-\frac{2\pi}{3}, \frac{2\pi}{3}), (\frac{2\pi}{3}, -\frac{2\pi}{3})\}$
	$\pm(3, 3) \bmod 6$	$\{(0, 0), (\pi, 0), (0, \pi), (\pi, \pi)\}$

Now, the key question is how these two sets of TCMs in Eqs. (47) and (48) are related to each other. The mapping of fully traced TCMs corresponding to the lattice with $(N_1, N_2) = (0, 0) \bmod 2$ to the fully traced TCMs corresponding to the lattice with $(N_1, N_2) = (1, 1) \bmod 2$ is given as follows,

$$\begin{aligned}
\langle c_2(\mathbf{x}_{1a}) \rangle_F^{(0,0)} &\leftrightarrow \sum_{\boldsymbol{\theta}} \langle c_2(\mathbf{x}_{1a}) \rangle_F^{\boldsymbol{\theta}}, \\
\langle c_2(\mathbf{x}_{1b}) \rangle_F^{(0,0)} &\leftrightarrow \sum_{\boldsymbol{\theta}} e^{i\theta_1} \langle c_2(\mathbf{x}_{1a}) \rangle_F^{\boldsymbol{\theta}}, \\
\langle c_2(\mathbf{x}_{1c}) \rangle_F^{(0,0)} &\leftrightarrow \sum_{\boldsymbol{\theta}} e^{i\theta_2} \langle c_2(\mathbf{x}_{1a}) \rangle_F^{\boldsymbol{\theta}}, \\
\langle c_2(\mathbf{x}_{1d}) \rangle_F^{(0,0)} &\leftrightarrow \sum_{\boldsymbol{\theta}} e^{i(\theta_1+\theta_2)} \langle c_2(\mathbf{x}_{1a}) \rangle_F^{\boldsymbol{\theta}}, \quad (49)
\end{aligned}$$

where $\sum_{\boldsymbol{\theta}}$ means that we sum over the four combinations of $\boldsymbol{\theta} \in \{(0, 0), (\pi, 0), (0, \pi), (\pi, \pi)\}$ as specified in Table IX. Eq. (49) is a key result that encodes the connection between the four distinct TCMs for $(N_1, N_2) = (0, 0) \bmod 2$ and the same TCM for four distinct boundary conditions when $(N_1, N_2) = (1, 1) \bmod 2$.

To illustrate further, for a C_3 -symmetric system, one can construct a similar mapping between the fully traced TCMs corresponding to the lattice with $N_1 = N_2 = 0 \bmod 3$ and the TCMs corresponding to the lattice with $N_1 = N_2 = 1 \bmod 3$,

$$\begin{aligned}
\langle c_3(\mathbf{x}_{1a}) \rangle_F^{(0,0)} &\leftrightarrow \sum_{\theta \in \{0, \pm 2\pi/3\}} \langle c_3(\mathbf{x}_{1a}) \rangle_F^{(\theta, -\theta)}, \\
\langle c_3(\mathbf{x}_{1b}) \rangle_F^{(0,0)} &\leftrightarrow \sum_{\theta \in \{0, \pm 2\pi/3\}} e^{-i\theta} \langle c_3(\mathbf{x}_{1a}) \rangle_F^{(\theta, -\theta)}, \\
\langle c_3(\mathbf{x}_{1c}) \rangle_F^{(0,0)} &\leftrightarrow \sum_{\theta \in \{0, \pm 2\pi/3\}} e^{i\theta} \langle c_3(\mathbf{x}_{1a}) \rangle_F^{(\theta, -\theta)}. \quad (50)
\end{aligned}$$

The complete details for these maps for every finite-size C_n -symmetric lattice with dimensions (N_1, N_2) are provided in the Supplemental Material [59].

With these results, we are able to reformulate the Chern number, bulk polarization, and sector charge shown in Tables II-VII in terms of fully traced TCMs for any finite-size C_n -symmetric lattice. Since we know how the TCMs for lattices satisfying Eq. (3) can be used to determine the Chern number, etc., we can use the mappings in, e.g., Eqs. (49) and (50), to convert to the data for any finite lattice. For instance, consider a spinless C_2 -symmetric class A insulator in a lattice satisfying Eq. (3), i.e., $(N_1, N_2) = (0, 0) \bmod 2$. In this case, the Chern number mod 2 is indicated by $\frac{1}{2} \langle c_2(\mathbf{x}_W) \rangle_F$ for any maximal WP $W \in \{1a, 1b, 1c, 1d\}$ (see Table II). For other lattice types, say $(N_1, N_2) = (1, 0) \bmod 2$, we replace $\langle c_2(\mathbf{x}_W) \rangle_F$ in the formula with a linear combination of fully traced TCMs with twisted boundary conditions. This linear combination is determined by Eq. (49) and Table IX; if we choose $W = 1b$, two different twisted boundary conditions $\boldsymbol{\theta} = (0, 0)$ and $(\pi, 0)$ are considered to compute $\sum_{\boldsymbol{\theta}} e^{i\theta_1} \langle c_2(\mathbf{x}_{1a}) \rangle_F^{\boldsymbol{\theta}} = \langle c_2(\mathbf{x}_{1a}) \rangle_F^{(0,0)} - \langle c_2(\mathbf{x}_{1a}) \rangle_F^{(\pi,0)}$.

This demonstrates that bulk invariants and physical observables can still be evaluated using symmetry data for any finite lattice, so long as the boundary conditions are taken into consideration.

VI. APPLICATIONS OF TOPOLOGICAL CRYSTALLINE MARKERS

Throughout this article we have focused on the global topological information contained in the fully traced TCMs. We will now show that if the system has ro-

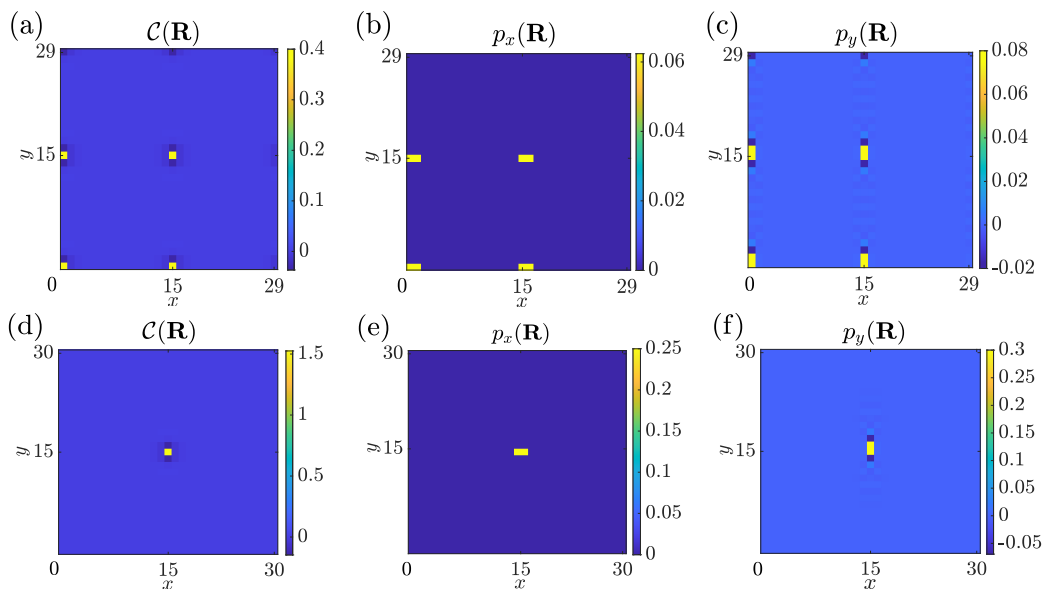


FIG. 7. Density plots of the Chern number [(a) and (d)], the x -component of the bulk polarization [(b) and (e)], and the y -component of the bulk polarization [(c) and (f)] for a $N_x \times N_y = 30 \times 30$ lattice [(a)-(c)] and a $N_x \times N_y = 31 \times 31$ lattice [(d)-(f)] (unit cell coordinates (n_x, n_y) are such that $n_i \in \{0, \dots, N_i - 1\}$ for $i = x, y$). Model parameters (m, m_H, t_x, t_y) of $H_{2D}(\mathbf{k})$ in Eq. (51) used were (a) (3, 0.5, 1, 1.5) (Chern insulator phase), (b) (1, 0, 1, 0.9) (obstructed atomic insulator with bulk polarization $\mathbf{P} = e(1/2, 0)$), and (c) (1, 0.5, 1, 4) (obstructed atomic insulator with bulk polarization $\mathbf{P} = e(0, 1/2)$).

tation symmetry (or more generally, point-group symmetry), even in the absence of translation symmetry, we can use TCMs to characterize crystalline topology. Along these lines, in this section, we discuss some of the unique applications of TCM *densities* for diagnosing bulk crystalline topology in position space. In addition, we build on the TCM mesh method introduced in Ref. 56 to diagnose topological properties in inhomogeneous insulators where translation symmetry, and even point-group symmetry, is broken globally.

To accomplish this we recall from Sec. III that it is possible to expand TCMs in the position-space basis as shown in Eq. (6). This yields a spatially-resolved density function. In Sec. VIA, we will discuss how the *spatially-resolved densities* of bulk invariants such as the bulk Chern number, or the components of the bulk polarization, can be obtained from the TCM densities (c.f., the formulae shown in Tables II-VII). We will demonstrate that this allows one to plot the distribution of topological crystalline invariants over the position-space lattice and identify which points in space directly contribute to the invariants.

Then, in Sec. VIB, we use the TCM localization property encoded in Eq. (8) to develop an application of the TCMs for resolving the bulk crystalline topology when spatial inhomogeneities such as domain walls are present. In such configurations, both translation and rotation symmetry can be broken, but there is a remnant of the crystalline symmetry that survives when we look more than a correlation length away from strong inhomogeneities, e.g., within the bulk of each region separated

by the domain wall. Explicitly, as we detail below, we evaluate a mesh of TCMs at every multiplicity 1 WP on the entire position-space lattice, not just for one global rotation center. This mesh encodes the local robustness of topological crystalline phenomena.

In the following subsections where we discuss these applications, the representative tight-binding model we use to evaluate the TCMs is a simple, two-band model that can describe Chern insulators and 2D weak topological insulators (i.e., polarized obstructed atomic limits). This model can be described as a set of 1D SSH chains extended along the x -direction and stacked along the y -direction. Each unit cell consists of two sublattice sites denoted by A and B . When expressed in terms of Pauli matrices σ_i where $i \in \{x, y, z\}$ acting on the sublattice sites within each unit cell, the tight-binding Hamiltonian for this model is

$$H_{2D}(\mathbf{k}) = m_H \sin k_y \sigma_z + t_x \sin k_x \sigma_y + (1 - m - t_x \cos k_x - t_y \cos k_y) \sigma_x, \quad (51)$$

with intra-cell hopping strength m , inter-cell hopping strengths t_x and t_y along the x and y directions respectively, and a time-reversal breaking, inter-cell hopping strength m_H . This model is C_2 invariant, where σ_x is the C_2 transformation in the sublattice basis. In the following subsections, we use this model to study Chern insulators and obstructed atomic insulators having non-vanishing polarization.

Our approach of using the densities of TCMs as topological indicators, can be compared to the existing mark-

ers for local Chern number from, e.g., Refs. 48 and 49. The local Chern number from these references is defined as a trace per unit cell of the commutator of the position operators projected onto the ground-state. This quantity indicates the Chern number locally at each unit cell position, has non-vanishing support over essentially the entire lattice in a Chern insulator, and its spatial average evaluates to the Chern number (even when there is spatial inhomogeneity). On the other hand, the TCMs we present here exhibit sharp peaks (with widths determined by the correlation length) in the neighborhoods of only a finite number of rotation-invariant positions, and can determine $\mathcal{C} \bmod n$ instead of the full Chern number. Interestingly, while there are no previously proposed markers for polarization or sector charge, our TCM densities also capture them. Hence, there are advantages and disadvantages to the various marker types, and the choice of which marker to use depends on the application.

A. Symmetry-based spatial resolution of bulk topological invariants and physical observables

We will begin by studying the spatial localization of bulk crystalline invariants described by TCM densities. Combining the results shown in Tables II-VII with the TCMs defined in Eq. (6), one can obtain densities of topological invariants such as the Chern number, and the bulk polarization, in terms of the TCMs. Consider a periodic, C_2 -symmetric lattice having an even number of unit cells along each dimension. If we assume the C_2 rotation axis is at the unit cell located at the origin, then the complete set of TCMs⁵ for this lattice is given by

$$\{\langle c_2(\mathbf{x}_{1a}) \rangle_{\mathbf{R}}, \langle c_2(\mathbf{x}_{1b}) \rangle_{\mathbf{R}}, \langle c_2(\mathbf{x}_{1c}) \rangle_{\mathbf{R}}, \langle c_2(\mathbf{x}_{1d}) \rangle_{\mathbf{R}}\}. \quad (52)$$

Since the model we plan to study is in class A, we can refer to Tables II and IV to determine the Chern number *density*, and the densities of the x and y -components of the bulk polarization, as

$$\begin{aligned} \mathcal{C}(\mathbf{R}) &= \frac{1}{2} \langle c_2(\mathbf{x}_W) \rangle_{\mathbf{R}} \pmod{2}, \\ p_x(\mathbf{R}) &= -\frac{e}{2} (\langle c_2(\mathbf{x}_{1b}) \rangle_{\mathbf{R}} + \langle c_2(\mathbf{x}_{1d}) \rangle_{\mathbf{R}}), \\ p_y(\mathbf{R}) &= -\frac{e}{2} (\langle c_2(\mathbf{x}_{1c}) \rangle_{\mathbf{R}} + \langle c_2(\mathbf{x}_{1d}) \rangle_{\mathbf{R}}). \end{aligned} \quad (53)$$

We can now use these formulae to compute the densities of the Chern number and polarization. In Fig. 7(a) we show the density of the bulk Chern number for a Chern insulating phase of our model Eq. (51). In Figs. 7(b) and (c), we show and the x and y -components of the bulk polarization for two different obstructed phases having quantized, non-vanishing polarization in

the x and y direction respectively. The specific model parameters are listed in the caption of Fig. 7.

Let us consider these figures in more detail. The density plot of the Chern number in Fig. 7(a) was obtained from the TCM for rotation axis at the $1a$ Wyckoff position at the unit cell located at $\mathbf{R} = \mathbf{0}$. Since this calculation was done for periodic boundary conditions, this rotation operator fixes the $1a$ WP at the unit cells having coordinates $(0, 0)$, $(N_x/2, 0)$, $(0, N_y/2)$, and $(N_x/2, N_y/2)$ (i.e., the positions contained in $\mathcal{X}[c_2(\mathbf{x}_{1a})]$). For our $N_x \times N_y = 30 \times 30$ lattice, this would be the coordinates $(0, 0)$, $(15, 0)$, $(0, 15)$, and $(15, 15)$. Indeed, we see that in the neighborhood of these unit cells, the density of the Chern number is sharply localized. This is a direct consequence of Eq. (8). Evaluating the fully traced TCM by summing the TCM over all the unit cells of the lattice yields $\mathcal{C} = 1 \bmod 2$, demonstrating that the system has a non-vanishing Chern number.

In the obstructed atomic insulator phases of the model Eq. (51), the system has a quantized bulk polarization and vanishing bulk Chern number $\mathcal{C} = 0$. Figures 7(b)-(c) illustrate density plots of the x and y -components of the bulk polarization respectively for different obstructed atomic limit phases. In both plots, the density of the bulk polarization is peaked at the unit cells contained in $\mathcal{X}[c_2(\mathbf{0})]$. Similar to the Chern number, summing the bulk polarization density over all the unit cells of the lattice yields $p_x = e/2 \bmod e$ and $p_y = e/2 \bmod e$ for Figs. 7(b) and (c) respectively.

The calculations so far have been for lattices obeying the dimension constraints in Eq. (3). Let us now take advantage of our results in Sec. V to construct densities of the Chern number and bulk polarization for finite-size lattices having an arbitrary number of unit cells along each direction, including those that do not support all the high symmetry momenta in the BZ. Specifically, consider a C_2 -symmetric lattice having an odd number of unit cells along both dimensions. The mapping between the fully traced C_2 TCMs for the lattice with an even number of unit cells in each direction, and the fully traced C_2 TCMs for the lattice with an odd number of unit cells in each direction, is given by Eq. (49). This same map directly applies to the TCM densities $\mathcal{C}(\mathbf{R})$, $p_x(\mathbf{R})$, and $p_y(\mathbf{R})$ resulting in

$$\begin{aligned} \mathcal{C}(\mathbf{R}) &= \frac{1}{2} \sum_{\theta_1=0,\pi} \sum_{\theta_2=0,\pi} \langle c_2(\mathbf{x}_{1a}) \rangle_{\mathbf{R}}^{\theta} \pmod{2}, \\ p_x(\mathbf{R}) &= -\frac{e}{2} \left(\langle c_2(\mathbf{x}_{1a}) \rangle_{\mathbf{R}}^{(0,0)} - \langle c_2(\mathbf{x}_{1a}) \rangle_{\mathbf{R}}^{(\pi,0)} \right), \\ p_y(\mathbf{R}) &= -\frac{e}{2} \left(\langle c_2(\mathbf{x}_{1a}) \rangle_{\mathbf{R}}^{(0,0)} - \langle c_2(\mathbf{x}_{1a}) \rangle_{\mathbf{R}}^{(0,\pi)} \right). \end{aligned} \quad (54)$$

To confirm this result, in Figs. 7(d)-(f) we show density plots of the Chern number and the x - and y -components of the bulk polarization for the same model parameters as Figs. 7(a)-(c), but for a C_2 -symmetric lattice having an odd number of unit cells along both dimensions. To generate the plots shown in Figs. 7(d)-(f),

⁵ Note that these are not fully traced as we have been previously considering.

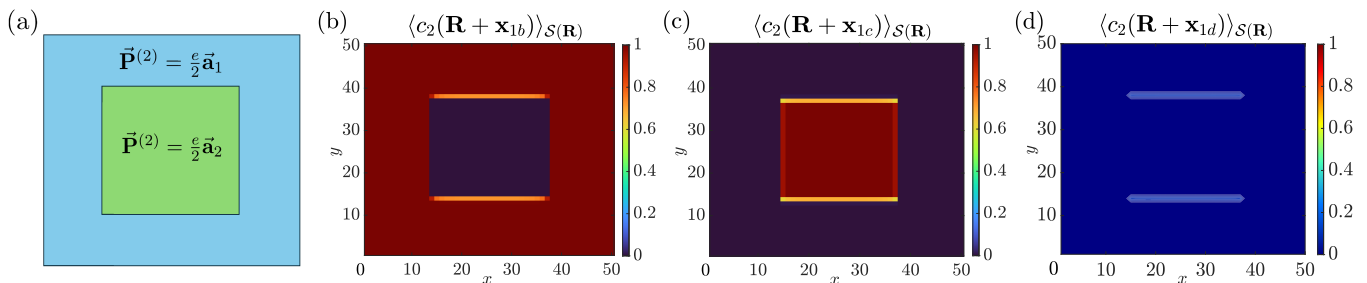


FIG. 8. (a) Illustration of a domain wall configuration separating two obstructed atomic insulator regions having different bulk polarizations. The Hamiltonian is given by Eq. (51) with periodic boundary conditions. Plot of the mesh of traced TCMs for (b) $\{\langle c_n(\mathbf{R} + \mathbf{x}_{1b}) \rangle_{\mathcal{S}(\mathbf{R})}\}$, (c) $\{\langle c_n(\mathbf{R} + \mathbf{x}_{1c}) \rangle_{\mathcal{S}(\mathbf{R})}\}$, and (d) $\{\langle c_n(\mathbf{R} + \mathbf{x}_{1d}) \rangle_{\mathcal{S}(\mathbf{R})}\}$. The outer region is in an obstructed atomic insulator phase with bulk polarization $\mathbf{P} = \frac{e}{2}\mathbf{a}_1$ for model parameters $(m_1, m_{H,1}, t_{x,1}, t_{y,1}) = (0.9, 0, 1, 0)$, whereas the inner region is in an obstructed atomic insulator phase with bulk polarization $\mathbf{P} = \frac{e}{2}\mathbf{a}_2$ for model parameters $(m_2, m_{H,2}, t_{x,2}, t_{y,2}) = (0.8, 1, 0, 1)$. $\mathcal{S}(\mathbf{R})$ was chosen to be a 6×6 window centered around a peak for each traced TCM in the mesh.

we implement a (gauge) choice of anti-periodic boundary conditions that commutes with the rotation operator with its origin at the unit cell with coordinates $((N_x - 1)/2, (N_y - 1)/2)$. For the $N_x \times N_y = 31 \times 31$ lattice we used, this would correspond to the point (15, 15) on the lattice. For this lattice geometry, the rotation center fixes a $1a$, $1b$, $1c$, and $1d$ WP at four different unit cells. In fact, Figs. 7(d)-(f) illustrate that the densities of each respective bulk quantity are peaked at unit cells having coordinates $((N_x - 1)/2, (N_y - 1)/2)$, $((N_x - 1)/2, N_y)$, $(N_x, (N_y - 1)/2)$, and $(N_x - 1, N_y - 1)$ (i.e., (15, 15), (15, 29), (29, 15), and (29, 29)).

The distributions of the Chern number density, and the densities of the components of the bulk polarization, reveal that the largest weight of the distribution is sharply peaked at the unit cell with coordinates $((N_x - 1)/2, (N_y - 1)/2)$, while the other three unit cells that comprise the invariant positions have small weight. In particular, as shown in Fig. 7(e), the density $p_x(\mathbf{R})$ is sharply localized at the $1b$ WP, which corresponds to the location of the electronic Wannier orbitals in the obstructed atomic limit phase with bulk polarization $\mathbf{P} = (e/2)\mathbf{a}_1$. Similar reasoning holds for Fig. 7(f), in which the density $p_y(\mathbf{R})$ is sharply localized at the $1c$ WP. We find that integrating each of the densities shown in Figs. 7(d)-(f) yields $\mathcal{C} = 1$, $p_x = e/2 \pmod{e}$, and $p_y = e/2 \pmod{e}$ respectively.

For the plots shown in Fig. 7(a) and (d), it is worth noting that although the ground state of the Chern insulator presents an obstruction to a Wannier representation, the Chern density itself is exponentially localized at the invariant positions on the lattice. For example, in Fig. 7(a), the peaks occur at the invariant positions contained in $\mathcal{X}[c_2(\mathbf{0})]$. Therefore, when expressed in terms of the traced TCMs, the densities of \mathcal{C} , p_x , and p_y all contain *exponentially* localized peaks in their distributions despite the contrasting Wannierizable nature of their ground state wavefunctions. This is because the traced TCMs rely solely on the ground state projector, which always exhibits short-ranged, exponentially decay-

ing behavior when a single-particle gap is present, i.e., when there is a finite correlation length. Hence, using the TCM densities, the bulk properties of strong topological insulators (e.g., Chern insulators) and atomic insulators can be resolved in position-space despite the differences in the Wannierizability of the ground states of these systems. In the next subsection, we will leverage the sharp localization of the densities to spatially resolve topological properties in inhomogeneous systems.

B. Diagnosing crystalline topology in insulators with spatial inhomogeneities

In this subsection, we will discuss the construction of a mesh of local topological crystalline invariants derived from the partially traced TCMs, and apply the mesh to determining the properties of inhomogeneous insulators in domain wall configurations. This mesh construction was introduced in Ref. 56 where it was used to justify the stability of crystalline topology to symmetry breaking disorder. For a periodic lattice, any WP W located at $\mathbf{R} + \mathbf{x}_W$ can serve as the rotation center for a TCM, with $\mathcal{X}[c_n(\mathbf{R} + \mathbf{x}_W)]$ [c.f., Eq. (1)] denoting the set of positions invariant under the rotation (recall the rotation operator with origin at $\mathbf{R} + \mathbf{x}_W$ is denoted as $c_n(\mathbf{R} + \mathbf{x}_W)$).

The key step is that for *every unit cell* on the periodic lattice, one can enumerate the set of TCMs: $\{\langle c_n(\mathbf{R} + \mathbf{x}_W) \rangle_{\mathbf{R}'}\}$. We know from Eq. (8), and as illustrated in the previous subsection, that the quantities $\langle c_n(\mathbf{R} + \mathbf{x}_W) \rangle_{\mathbf{R}'}$ are sharply peaked when \mathbf{R}' is in the neighborhood of the invariant positions $\mathcal{X}[c_n(\mathbf{R} + \mathbf{x}_W)]$. One of these invariant positions is the rotation center within the unit cell \mathbf{R} itself. For the neighborhood $\mathcal{S}(\mathbf{R})$ of this center we can consider a traced TCM with the support $\mathcal{S}(\mathbf{R})$. Furthermore, as we scan \mathbf{R} across the lattice we can define a *mesh* of traced TCMs, one for each \mathbf{R} . Explicitly, as defined in Eq. (9), we compute the

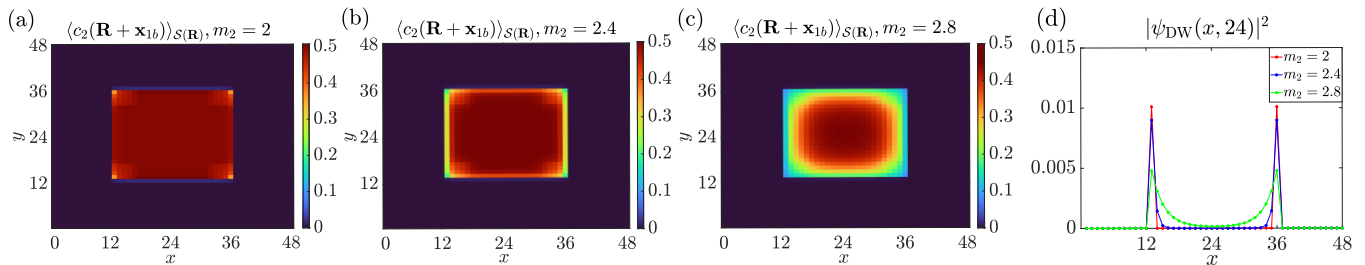


FIG. 9. Mesh plot data and probability distribution plots of a domain wall boundary mode for a domain wall configuration identical to Fig. 8(a), with the inner green region being a Chern insulator with $\mathcal{C} = 1$ and the outer blue region being a trivial atomic insulator. (a)-(c) Plot of the mesh of traced TCMs $\{\langle c_n(\mathbf{R} + \mathbf{x}_{1b}) \rangle_{\mathcal{S}(\mathbf{R})}\}$. The model parameters used for the trivial atomic insulator are $(m_1, m_{H,1}, t_{x,1}, t_{y,1}) = (4, 0, 0.1, 0.1)$ and the Chern insulator are $(m_2, m_{H,2}, t_{x,2}, t_{y,2}) = (m_2, 1, 1, 1)$ where $m_2 = 2, 2.4, 2.8$. For this choice of $m_{H,2}$, $t_{x,2}$, and $t_{y,2}$, $m_2 = 3$ is gapless. As m_2 is increased towards this value, the region where the mesh is quantized to 0.5 reduces in size because of the increase in correlation length, as indicated by each of the plots of the probability distribution of a wavefunction $|\psi_{\text{DW}}(x, 24)|^2$ corresponding to a domain wall boundary mode in (d). $\mathcal{S}(\mathbf{R})$ was chosen to be a 4×4 window centered around a peak for each traced TCM in the mesh.

partially traced TCM,

$$\langle c_n(\mathbf{R} + \mathbf{x}_W) \rangle_{\mathcal{S}(\mathbf{R})} = \sum_{\mathbf{R}' \in \mathcal{S}(\mathbf{R})} \langle c_n(\mathbf{R} + \mathbf{x}_W) \rangle_{\mathbf{R}'}. \quad (55)$$

For simplicity, we choose a square neighborhood, and when the linear size of $\mathcal{S}(\mathbf{R})$ is ξ_S , the sum/partial trace receives contributions only from \mathbf{R}' such that $|\mathbf{R}' - \mathbf{R}| < \xi_S$. Thus, to give meaningful results for insulators, we expect ξ_S must be chosen to be comparable to, or larger than, their correlation length ζ .

This construction generates a mesh of traced TCMs $\{\langle c_n(\mathbf{R} + \mathbf{x}_W) \rangle_{\mathcal{S}(\mathbf{R})}\}$, at the W WP within every unit cell on the position-space lattice. The TCM mesh provides a set of spatially-resolved crystalline topological data. That is, each partially traced TCM specified by Eq. (55) yields a local topological invariant at that position. For a translationally invariant lattice having periodic boundaries, such a mesh of invariants is uniform and quantized. However, if translation-symmetry breaking defects such as open boundaries, or domain walls are present, we expect that some of the traced TCMs contained in the mesh will no longer be quantized because the rotational symmetry is not exactly preserved at every rotation center. Despite this, the exponentially localized nature of the single-particle projector implies that the deviation of each traced TCM from its quantized value in the translationally-invariant limit depends on the relative size of $\mathcal{S}(\mathbf{R})$ with respect to the correlation length ζ . Indeed, the mesh gives quantitative support to the intuition that locally the system can still appear to have crystal symmetry even if it is broken globally.

To demonstrate the utility of the traced TCM mesh, we consider the model given by Eq. (51) and set up a configuration having distinct phases separated by a domain wall. In Fig. 8 we show the results for a domain wall separating two obstructed atomic insulators having different bulk polarizations, while in Fig. 9 we show a domain wall separating a Chern insulator and a trivial atomic insulator. We find that within each region separated by the

domain wall, the local values of the mesh of traced TCMs for a specific multiplicity 1 WP is approximately equal to a quantized value. In contrast, the traced TCMs along the domain wall are not quantized, possibly because of low-energy modes on the domain wall (see Fig. 9(d) for an illustration of this). In each of the cases it is clear that the mesh is able to distinguish the spatial structure of the phases with a resolution controlled by the correlation length.

To understand why the partially traced TCMs $\langle c_n(\mathbf{R} + \mathbf{x}_W) \rangle_{\mathcal{S}(\mathbf{R})}$ evaluate to symmetry-protected topological invariants having certain quantized values, let us first understand the quantitative relationship between the fully traced and *partially traced* TCMs in a periodic and homogeneous system. To this end, we focus on the rotation operator $c_2(\mathbf{x}_W)$ located within the unit cell $\mathbf{R} = \mathbf{0}$. As shown in Fig. 7, the TCM densities for periodic boundaries are exponentially localized around four rotation centers defined by $\mathcal{X}[c_2(\mathbf{x}_W)]$, according to Eq. (8). For a homogeneous system with linear dimensions obeying Eq. (3), the four rotation-invariant positions correspond to the same type of WP W , and the partially traced TCMs around these centers are all identical. For instance, consider the intensity of the center peak around \mathbf{x}_W as shown in Fig. 7(b). The intensity can be computed by the partially traced TCM $\langle c_2(\mathbf{x}_W) \rangle_{\mathcal{S}(\mathbf{0})}$, where the window $\mathcal{S}(\mathbf{0})$ is a neighborhood of the center peak. Since the other three peaks in Fig. 7(b) have the same intensity, we can conclude that

$$\langle c_2(\mathbf{x}_W) \rangle_{\mathcal{S}(\mathbf{0})} = \frac{1}{4} \langle c_2(\mathbf{x}_W) \rangle_F, \quad (56)$$

up to an exponentially small correction $O(e^{-\xi_S/\zeta})$ determined by the correlation length ζ and the linear window size ξ_S . This relation is implied by Eq. (12).

Since one can compute topological invariants like the Chern number, polarization, etc. from the fully traced TCMs, the partially traced TCMs, which we have just argued are proportional to the fully traced ones, also

indicate the topological invariants. Moreover, we find $\langle c_2(\mathbf{x}_W) \rangle_{S(0)}$ is approximately quantized as $\mathbb{Z}/4$. This is because $\langle c_2(\mathbf{x}_W) \rangle_F$ is the group theory character for spinless C_2 rotation of a given ground state, and takes an integer value, i.e., $\langle c_2(\mathbf{x}_W) \rangle_F \in \mathbb{Z}$.

So far, we have focused on the TCMS for $c_2(\mathbf{x}_W)$ in a homogeneous and periodic system where $c_2(\mathbf{x}_W)$ is indeed a symmetry of the system. However, the connection between the partially traced TCMS and topological invariants holds even when open boundaries are used, or if the rotation symmetry is globally broken, but approximately preserved locally. To illustrate, we can consider the domain wall configurations we introduced in Figs. 8 and 9. Although the system is homogeneous away from the domain wall, $c_2(\mathbf{R} + \mathbf{x}_W)$ is not preserved for a general unit cell \mathbf{R} within a homogeneous region. However, because of the exponential localization of the TCMS [Eq. (8)], the value of the partially traced TCMS $\langle c_2(\mathbf{R} + \mathbf{x}_W) \rangle_{S(\mathbf{R})}$ is insensitive to the change of boundary condition (if the correlation length is sufficiently shorter than the linear window size). Thus, $\langle c_2(\mathbf{R} + \mathbf{x}_W) \rangle_{S(\mathbf{R})}$ diagnoses topological invariants in a broader class of systems than the fully traced ones.

With the above conclusion, we now understand clearly how the distribution of our partially traced TCMS distinguishes the phases shown in Fig. 8. In Fig. 8(b), the mesh of $\langle c_2(\mathbf{R} + \mathbf{x}_{1b}) \rangle_{S(\mathbf{R})}$ is shown. For the obstructed atomic insulator outside the domain wall, the partially traced TCMS evaluate to $\langle c_2(\mathbf{R} + \mathbf{x}_{1b}) \rangle_{S(\mathbf{R})} \simeq 1$, when \mathbf{R} is within the homogeneous region, and the size ξ_S of the window S is larger than the correlation length ζ . These values of partially traced TCMS imply that $\langle c_2(\mathbf{x}_{1b}) \rangle_F = 4$ for the outer obstructed atomic insulator if it were homogeneous and periodic. By doing a similar analysis for $\langle c_2(\mathbf{R} + \mathbf{x}_{1c,1d}) \rangle$, as shown in Figs. 8(c)-(d), we infer that the fully traced TCMS of this insulator would be $\langle c_2(\mathbf{x}_{1c,1d}) \rangle_F = 0$ for a periodic and homogeneous case. By recalling that $(\mathbf{P})_x = -\frac{e}{8}(\langle c_2(\mathbf{x}_{1b}) \rangle_F + \langle c_2(\mathbf{x}_{1d}) \rangle_F) \bmod e$, and $(\mathbf{P})_y = -\frac{e}{8}(\langle c_2(\mathbf{x}_{1c}) \rangle_F + \langle c_2(\mathbf{x}_{1d}) \rangle_F) \bmod e$ [Table IV], we conclude that the bulk polarization of this insulator is $\mathbf{P} = (e/2)\mathbf{a}_1$. In comparison, the partially traced TCMS for the obstructed insulator inside the domain wall, are $\langle c_2(\mathbf{R} + \mathbf{x}_{1c}) \rangle_F \simeq 1$ and $\langle c_2(\mathbf{R} + \mathbf{x}_{1b,1d}) \rangle_F \simeq 0$ for \mathbf{R} in the homogeneous region. These values imply the bulk polarization $\mathbf{P} = (e/2)\mathbf{a}_2$. In this way, the TCM mesh for the $1b, 1c, 1d$ positions distinguishes atomic insulators with different polarizations.

Finally, we obtain a similar conclusion for a Chern insulating phase. For a Chern phase with C_2 symmetry, the Chern number \mathcal{C} modulo 2 can be indicated by the traced TCMS $\langle c_2(\mathbf{R} + \mathbf{x}_W) \rangle_{S(\mathbf{R})}$. As discussed in Sec. IV A, and shown in Table II, $\mathcal{C} \bmod 2$ is determined by the fully traced TCM: $\mathcal{C} = \frac{1}{2} \langle c_2(\mathbf{x}_W) \rangle_F \bmod 2$ for any $W \in \{1a, 1b, 1c, 1d\}$. For the domain wall between a trivial insulator and a Chern insulator with $\mathcal{C} = 1$, we computed the distribution of partially traced TCMS for $\langle c_2(\mathbf{x}_{1a}) \rangle$, as shown in Fig. 9(a). Note that

we find this distribution is similar to the ones for the C_2 rotations centered at other WPs, $c_2(\mathbf{x}_{1b,1c,1d})$. The relationship between fully and partially traced TCMS [Eq. (56)] implies that $\mathcal{C} \simeq 2 \langle c_2(\mathbf{R} + \mathbf{x}_W) \rangle_{S(\mathbf{R})} \bmod 2$ for a unit cell \mathbf{R} within the homogeneous region. Thus, the nontrivial Chern number of the insulator inside the domain wall is indicated by $\langle c_2(\mathbf{R} + \mathbf{x}_W) \rangle_{S(\mathbf{R})} \simeq \frac{1}{2}$ for $W \in \{1a, 1b, 1c, 1d\}$, i.e., $\mathcal{C} = 1 \bmod 2$.

Our analysis using the quantitative relationship between the fully and partially traced TCMS can be extended to other rotation symmetric insulators by figuring out how many times the WPs W are included in $\mathcal{X}[c_n(\mathbf{R} + \mathbf{x}_W)]$. For example, for a C_3 -symmetric insulator obeying Eq. (3), three invariant positions with the same type of WP form $\mathcal{X}[c_3(\mathbf{R} + \mathbf{x}_W)]$. In this case, the relationship between the fully and partially traced TCMS changes to $\langle c_3(\mathbf{x}_W) \rangle_{S(0)} = \frac{1}{3} \langle c_3(\mathbf{x}_W) \rangle_F$. The quantization of $\langle c_3(\mathbf{x}_W) \rangle_{S(0)}$ also follows from the fact that $\langle c_3(\mathbf{x}_W) \rangle_F$ is the group theory character for C_3 rotation of the ground state. This means that, for the spinless (spinful) case, $\langle c_3(\mathbf{x}_W) \rangle_F$ is always expressed as $\sum_{\ell=0}^2 n_\ell e^{\frac{2\pi\ell i}{3}}$ ($\sum_{\ell=0}^2 n_\ell e^{\frac{2\pi\ell i + \pi i}{3}}$) for integers n_ℓ . Thus, the real and imaginary parts of partially traced TCMS around the center peak are quantized accordingly. For the lattice types that do not satisfy Eq. (3), a similar analysis can be achieved by applying necessary twisted boundary conditions according to the procedure developed in Sec. V.

In summary, as shown in Figs. 8 and 9, the mesh of traced TCMS clearly distinguishes the different phases of our model within each region separated by the domain wall, thereby demonstrating how TCMS can be utilized to evaluate bulk topological crystalline invariants over a position-space lattice that does not globally preserve translational and crystalline symmetries. The spatial resolution of this method is limited by the size of the correlation length ζ , but this is expected since a bulk insulating region is only stably established in spatial regions of size larger than ζ .

VII. CONCLUSION

In this work, we explored the properties of topological crystalline markers (TCMS) that are locally calculable in position space. We demonstrated how the TCMS can detect crystalline topology in gapped systems protected by C_n -symmetry. This reformulation of bulk topological invariants and responses using the TCMS encompasses a wide range of insulators, classified under the AZ symmetry classes A, AI, AII, and D. The basis-independent formulation of topological crystalline invariants presented here, as well as in Ref. 56, shows that bulk invariants can be extracted directly from the ground-state wavefunction using projected symmetry operators, without the need to assume translational invariance. This approach allows us to characterize the bulk crystalline topology of finite-size lattices with arbitrary numbers of unit cells, even when

such lattices do not generate all high-symmetry points in the Brillouin zone. More crucially, we show that TCMs can spatially resolve bulk crystalline topology, making them a powerful tool for calculating topological crystalline invariants at any point on the crystalline lattice, even in the presence of translation-symmetry breaking.

Our work on the TCMs is closely connected to other works, and can be extended to other systems beyond non-interacting insulators. For instance, the mapping between the fully traced TCMs and the Wannier orbital configuration discussed in Sec. IV B implies that the fully traced TCMs are directly related to the recently discovered real-space invariants (RSIs) [73–75]. In the Supplemental Material [59], we explicitly derive this mapping between the fully traced TCMs and the RSIs for all C_n symmetries in classes A, AI, and AII. Additionally, the results presented in this work are similar in spirit to recent approaches of extracting topological invariants directly from the ground state wavefunction [76] using expectation values of partial rotation operators [77–80]. This implies at least one route for extending TCMs to interacting systems.

Since the TCMs are expressed solely in terms of the symmetry operators and the ground state projector in any basis, our results can be used to study a wide

breadth of systems with broken translation symmetry, including disordered topological phases [81–84], amorphous systems which weakly preserve the point-group symmetry [85–94], and quasicrystalline lattices [90, 95, 96].

ACKNOWLEDGMENTS

We thank Barry Bradlyn and Penghao Zhu for several useful discussions and guidance during the development of this work. S.V. thanks Kunal Marwaha, Yuxuan Zhang, Naren Manjunath, Jonah Herzog-Arbeitman, Alexander Cerjan, Pratik Sathe, and Ammar Jahin for insightful discussions on related works and feedback on the results presented in this work. Y.H. and T.L.H. are supported by the US Office of Naval Research (ONR) Multidisciplinary University Research Initiative (MURI) grant N00014-20-1-2325. Y.H. is also supported by Air Force Office of Scientific Research under award number FA9550-21-1-0131. S.V. was partly supported by the NSF Graduate Research Fellowship Program under Grant No. DGE-1746047 when this work was initiated and later supported by the University of Illinois.

-
- [1] Barry Bradlyn, L. Elcoro, Jennifer Cano, M. G. Vergniory, Zhijun Wang, C. Felser, M. I. Aroyo, and B. Andrei Bernevig, “Topological quantum chemistry,” *Nature* **547**, 298–305 (2017).
 - [2] Hoi Chun Po, Ashvin Vishwanath, and Haruki Watanabe, “Symmetry-based indicators of band topology in the 230 space groups,” *Nature Communications* **8**, 50 (2017).
 - [3] Jorrit Kruthoff, Jan de Boer, Jasper van Wezel, Charles L. Kane, and Robert-Jan Slager, “Topological Classification of Crystalline Insulators through Band Structure Combinatorics,” *Phys. Rev. X* **7**, 041069 (2017).
 - [4] Barry Bradlyn, L. Elcoro, M. G. Vergniory, Jennifer Cano, Zhijun Wang, C. Felser, M. I. Aroyo, and B. Andrei Bernevig, “Band connectivity for topological quantum chemistry: Band structures as a graph theory problem,” *Phys. Rev. B* **97**, 035138 (2018).
 - [5] Jennifer Cano, Barry Bradlyn, Zhijun Wang, L. Elcoro, M. G. Vergniory, C. Felser, M. I. Aroyo, and B. Andrei Bernevig, “Building blocks of topological quantum chemistry: Elementary band representations,” *Phys. Rev. B* **97**, 035139 (2018).
 - [6] Zhida Song, Tiantian Zhang, Zhong Fang, and Chen Fang, “Quantitative mappings between symmetry and topology in solids,” *Nature Communications* **9**, 3530 (2018).
 - [7] Eslam Khalaf, Hoi Chun Po, Ashvin Vishwanath, and Haruki Watanabe, “Symmetry Indicators and Anomalous Surface States of Topological Crystalline Insulators,” *Phys. Rev. X* **8**, 031070 (2018).
 - [8] Seishiro Ono and Haruki Watanabe, “Unified understanding of symmetry indicators for all internal symmetry classes,” *Phys. Rev. B* **98**, 115150 (2018).
 - [9] Hoi Chun Po, “Symmetry indicators of band topology,” *Journal of Physics: Condensed Matter* **32**, 263001 (2020).
 - [10] Jennifer Cano and Barry Bradlyn, “Band Representations and Topological Quantum Chemistry,” *Annual Review of Condensed Matter Physics* **12**, 225–246 (2021).
 - [11] Luis Elcoro, Benjamin J. Wieder, Zhida Song, Yuanfeng Xu, Barry Bradlyn, and B. Andrei Bernevig, “Magnetic topological quantum chemistry,” *Nature Communications* **12**, 5965 (2021).
 - [12] Seishiro Ono, Hoi Chun Po, and Ken Shiozaki, “ \mathbb{Z}_2 -enriched symmetry indicators for topological superconductors in the 1651 magnetic space groups,” *Phys. Rev. Res.* **3**, 023086 (2021).
 - [13] Tiantian Zhang and Shuichi Murakami, “Predicting topological materials: symmetry-based indicator theories and beyond,” *Journal of Physics D: Applied Physics* **54**, 414002 (2021).
 - [14] Ken Shiozaki, Masatoshi Sato, and Kiyonori Gomi, “Atiyah-Hirzebruch spectral sequence in band topology: General formalism and topological invariants for 230 space groups,” *Phys. Rev. B* **106**, 165103 (2022).
 - [15] Benjamin J. Wieder, Barry Bradlyn, Jennifer Cano, Zhijun Wang, Maia G. Vergniory, Luis Elcoro, Alexey A. Soluyanov, Claudia Felser, Titus Neupert, Nicolas Regnault, and B. Andrei Bernevig, “Topological materials discovery from crystal symmetry,” *Nature Reviews Materials* **7**, 196–216 (2022).
 - [16] Liang Fu and C. L. Kane, “Topological insulators with inversion symmetry,” *Phys. Rev. B* **76**, 045302 (2007).
 - [17] Ari M. Turner, Yi Zhang, and Ashvin Vishwanath, “Entanglement and inversion symmetry in topological insu-

- lators,” *Phys. Rev. B* **82**, 241102 (2010).
- [18] Taylor L. Hughes, Emil Prodan, and B. Andrei Bernevig, “Inversion-symmetric topological insulators,” *Phys. Rev. B* **83**, 245132 (2011).
- [19] Liang Fu, “Topological Crystalline Insulators,” *Phys. Rev. Lett.* **106**, 106802 (2011).
- [20] Chen Fang, Matthew J. Gilbert, and B. Andrei Bernevig, “Bulk topological invariants in noninteracting point group symmetric insulators,” *Phys. Rev. B* **86**, 115112 (2012).
- [21] Timothy H. Hsieh, Hsin Lin, Junwei Liu, Wenhui Duan, Arun Bansil, and Liang Fu, “Topological crystalline insulators in the SnTe material class,” *Nature Communications* **3**, 982 (2012).
- [22] Ching-Kai Chiu, Hong Yao, and Shinsei Ryu, “Classification of topological insulators and superconductors in the presence of reflection symmetry,” *Phys. Rev. B* **88**, 075142 (2013).
- [23] Priyamvada Jadaun, Di Xiao, Qian Niu, and Sanjay K. Banerjee, “Topological classification of crystalline insulators with space group symmetry,” *Phys. Rev. B* **88**, 085110 (2013).
- [24] Robert-Jan Slager, Andrej Mesaros, Vladimir Juričić, and Jan Zaanen, “The space group classification of topological band-insulators,” *Nature Physics* **9**, 98–102 (2013).
- [25] Wladimir A. Benalcazar, Jeffrey C. Y. Teo, and Taylor L. Hughes, “Classification of two-dimensional topological crystalline superconductors and Majorana bound states at disclinations,” *Phys. Rev. B* **89**, 224503 (2014).
- [26] Chen Fang, Matthew J. Gilbert, and B. Andrei Bernevig, “New Class of Topological Superconductors Protected by Magnetic Group Symmetries,” *Phys. Rev. Lett.* **112**, 106401 (2014).
- [27] Ken Shiozaki and Masatoshi Sato, “Topology of crystalline insulators and superconductors,” *Phys. Rev. B* **90**, 165114 (2014).
- [28] Chen Fang and Liang Fu, “New classes of three-dimensional topological crystalline insulators: Nonsymmorphic and magnetic,” *Phys. Rev. B* **91**, 161105 (2015).
- [29] A. Alexandradinata, Zhijun Wang, and B. Andrei Bernevig, “Topological Insulators from Group Cohomology,” *Phys. Rev. X* **6**, 021008 (2016).
- [30] Ching-Kai Chiu, Jeffrey C. Y. Teo, Andreas P. Schnyder, and Shinsei Ryu, “Classification of topological quantum matter with symmetries,” *Rev. Mod. Phys.* **88**, 035005 (2016).
- [31] Wladimir A. Benalcazar, B. Andrei Bernevig, and Taylor L. Hughes, “Quantized electric multipole insulators,” *Science* **357**, 61–66 (2017).
- [32] Wladimir A. Benalcazar, B. Andrei Bernevig, and Taylor L. Hughes, “Electric multipole moments, topological multipole moment pumping, and chiral hinge states in crystalline insulators,” *Phys. Rev. B* **96**, 245115 (2017).
- [33] Zhida Song, Zhong Fang, and Chen Fang, “ $(d - 2)$ -Dimensional Edge States of Rotation Symmetry Protected Topological States,” *Phys. Rev. Lett.* **119**, 246402 (2017).
- [34] Guido van Miert and Carmine Ortix, “Higher-order topological insulators protected by inversion and rotoinversion symmetries,” *Phys. Rev. B* **98**, 081110 (2018).
- [35] Wladimir A. Benalcazar, Tianhe Li, and Taylor L. Hughes, “Quantization of fractional corner charge in C_n -symmetric higher-order topological crystalline insulators,” *Phys. Rev. B* **99**, 245151 (2019).
- [36] Frank Schindler, Marta Brzezińska, Wladimir A. Benalcazar, Mikel Iraola, Adrien Bouhon, Stepan S. Tsirkin, Maia G. Vergniory, and Titus Neupert, “Fractional corner charges in spin-orbit coupled crystals,” *Phys. Rev. Res.* **1**, 033074 (2019).
- [37] Yoonseok Hwang, Junyeong Ahn, and Bohm-Jung Yang, “Fragile topology protected by inversion symmetry: Diagnosis, bulk-boundary correspondence, and Wilson loop,” *Phys. Rev. B* **100**, 205126 (2019).
- [38] Motoaki Hirayama, Ryo Takahashi, Satoru Matsuishi, Hideo Hosono, and Shuichi Murakami, “Higher-order topological crystalline insulating phase and quantized hinge charge in topological electride apatite,” *Phys. Rev. Res.* **2**, 043131 (2020).
- [39] Yutaro Tanaka, Ryo Takahashi, Tiantian Zhang, and Shuichi Murakami, “Theory of inversion- F_4 protected topological chiral hinge states and its applications to layered antiferromagnets,” *Phys. Rev. Res.* **2**, 043274 (2020).
- [40] Yuan Fang and Jennifer Cano, “Filling anomaly for general two- and three-dimensional C_4 symmetric lattices,” *Phys. Rev. B* **103**, 165109 (2021).
- [41] Ryo Takahashi, Tiantian Zhang, and Shuichi Murakami, “General corner charge formula in two-dimensional C_n -symmetric higher-order topological insulators,” *Phys. Rev. B* **103**, 205123 (2021).
- [42] Frank Schindler, Stepan S. Tsirkin, Titus Neupert, B. Andrei Bernevig, and Benjamin J. Wieder, “Topological zero-dimensional defect and flux states in three-dimensional insulators,” *Nature Communications* **13**, 5791 (2022).
- [43] Yutaro Tanaka, Tiantian Zhang, Makio Uwaha, and Shuichi Murakami, “Anomalous Crystal Shapes of Topological Crystalline Insulators,” *Phys. Rev. Lett.* **129**, 046802 (2022).
- [44] Katsuaki Naito, Ryo Takahashi, Haruki Watanabe, and Shuichi Murakami, “Fractional hinge and corner charges in various crystal shapes with cubic symmetry,” *Phys. Rev. B* **105**, 045126 (2022).
- [45] Yutaro Tanaka and Shuichi Murakami, “Effects of first- and second-order topological phases on equilibrium crystal shapes,” *Phys. Rev. B* **107**, 245148 (2023).
- [46] Sachin Vaidya, Ali Ghorashi, Thomas Christensen, Mikael C. Rechtsman, and Wladimir A. Benalcazar, “Topological phases of photonic crystals under crystalline symmetries,” *Phys. Rev. B* **108**, 085116 (2023).
- [47] Hidetoshi Wada, Katsuaki Naito, Seishiro Ono, Ken Shiozaki, and Shuichi Murakami, “General corner charge formulas in various tetrahedral and cubic space groups,” *Phys. Rev. B* **109**, 085114 (2024).
- [48] Alexei Kitaev, “Anyons in an exactly solved model and beyond,” *Annals of Physics* **321**, 2–111 (2006), January Special Issue.
- [49] Raffaello Bianco and Raffaele Resta, “Mapping topological order in coordinate space,” *Phys. Rev. B* **84**, 241106 (2011).
- [50] Nicolas Baù and Antimo Marrazzo, “Local Chern marker for periodic systems,” *Phys. Rev. B* **109**, 014206 (2024).
- [51] Terry A Loring, “A guide to the bott index and localizer index,” *arXiv preprint arXiv:1907.11791* (2019).
- [52] Edgar Lozano Viesca, Jonas Schober, and Hermann Schulz-Baldes, “Chern numbers as half-signature of the spectral localizer,” *Journal of Mathematical Physics* **60**,

- 072101 (2019).
- [53] Alexander Cerjan and Terry A. Loring, “An operator-based approach to topological photonics,” *Nanophotonics* **11**, 4765–4780 (2022).
- [54] Alexander Cerjan, Lars Koekenbier, and Hermann Schulz-Baldes, “Spectral localizer for line-gapped non-Hermitian systems,” *Journal of Mathematical Physics* **64**, 082102 (2023).
- [55] Alexander Cerjan, Terry A. Loring, and Hermann Schulz-Baldes, “Local Markers for Crystalline Topology,” *Phys. Rev. Lett.* **132**, 073803 (2024).
- [56] Ian Mondragon-Shem and Taylor L. Hughes, “Robust topological invariants of topological crystalline phases in the presence of impurities,” *Phys. Rev. B* **110**, 035146 (2024).
- [57] Alexander Altland and Martin R. Zirnbauer, “Non-standard symmetry classes in mesoscopic normal-superconducting hybrid structures,” *Phys. Rev. B* **55**, 1142–1161 (1997).
- [58] Alexei Kitaev, “Periodic table for topological insulators and superconductors,” *AIP Conference Proceedings* **1134**, 22–30 (2009).
- [59] See the Supplemental Material for more details.
- [60] Seishiro Ono, Youichi Yanase, and Haruki Watanabe, “Symmetry indicators for topological superconductors,” *Physical Review Research* **1**, 013012 (2019).
- [61] Max Geier, Piet W. Brouwer, and Luka Trifunovic, “Symmetry-based indicators for topological Bogoliubov-de Gennes Hamiltonians,” *Phys. Rev. B* **101**, 245128 (2020).
- [62] Seishiro Ono, Hoi Chun Po, and Haruki Watanabe, “Refined symmetry indicators for topological superconductors in all space groups,” *Science Advances* **6**, eaaz8367 (2020).
- [63] R. D. King-Smith and David Vanderbilt, “Theory of polarization of crystalline solids,” *Phys. Rev. B* **47**, 1651–1654 (1993).
- [64] Christopher W. Peterson, Tianhe Li, Wladimir A. Benalcazar, Taylor L. Hughes, and Gaurav Bahl, “A fractional corner anomaly reveals higher-order topology,” *Science* **368**, 1114–1118 (2020).
- [65] W. P. Su, J. R. Schrieffer, and A. J. Heeger, “Solitons in Polyacetylene,” *Phys. Rev. Lett.* **42**, 1698–1701 (1979).
- [66] Haruki Watanabe and Seishiro Ono, “Corner charge and bulk multipole moment in periodic systems,” *Phys. Rev. B* **102**, 165120 (2020).
- [67] Sander Kooi, Guido van Miert, and Carmine Ortix, “The bulk-corner correspondence of time-reversal symmetric insulators,” *npj Quantum Materials* **6**, 1 (2021).
- [68] Jeffrey C. Y. Teo, Liang Fu, and C. L. Kane, “Surface states and topological invariants in three-dimensional topological insulators: Application to $\text{Bi}_{1-x}\text{Sb}_x$,” *Phys. Rev. B* **78**, 045426 (2008).
- [69] Yutaro Tanaka, Ryo Takahashi, and Shuichi Murakami, “Appearance of hinge states in second-order topological insulators via the cutting procedure,” *Phys. Rev. B* **101**, 115120 (2020).
- [70] Ryo Takahashi, Yutaro Tanaka, and Shuichi Murakami, “Bulk-edge and bulk-hinge correspondence in inversion-symmetric insulators,” *Phys. Rev. Res.* **2**, 013300 (2020).
- [71] Ari M. Turner, Yi Zhang, Roger S. K. Mong, and Ashvin Vishwanath, “Quantized response and topology of magnetic insulators with inversion symmetry,” *Phys. Rev. B* **85**, 165120 (2012).
- [72] Saavanth Velury, Barry Bradlyn, and Taylor L. Hughes, “Topological crystalline phases in a disordered inversion-symmetric chain,” *Phys. Rev. B* **103**, 024205 (2021).
- [73] Zhi-Da Song, Luis Elcoro, and B. Andrei Bernevig, “Twisted bulk-boundary correspondence of fragile topology,” *Science* **367**, 794–797 (2020).
- [74] Jonah Herzog-Arbeitman, Zhi-Da Song, Luis Elcoro, and B. Andrei Bernevig, “Hofstadter Topology with Real Space Invariants and Reentrant Projective Symmetries,” *Phys. Rev. Lett.* **130**, 236601 (2023).
- [75] Jonah Herzog-Arbeitman, B. Andrei Bernevig, and Zhi-Da Song, “Interacting topological quantum chemistry in 2D with many-body real space invariants,” *Nature Communications* **15**, 1171 (2024).
- [76] Ruihua Fan, Pengfei Zhang, and Yingfei Gu, “Generalized real-space Chern number formula and entanglement hamiltonian,” *SciPost Phys.* **15**, 249 (2023).
- [77] Yuxuan Zhang, Naren Manjunath, Ryohei Kobayashi, and Maissam Barkeshli, “Complete Crystalline Topological Invariants from Partial Rotations in $(2+1)\text{D}$ Invertible Fermionic States and Hofstadter’s Butterfly,” *Phys. Rev. Lett.* **131**, 176501 (2023).
- [78] Yuxuan Zhang, Naren Manjunath, Gautam Nambiar, and Maissam Barkeshli, “Quantized Charge Polarization as a Many-Body Invariant in $(2+1)\text{D}$ Crystalline Topological States and Hofstadter Butterflies,” *Phys. Rev. X* **13**, 031005 (2023).
- [79] Naren Manjunath, Vladimir Calvera, and Maissam Barkeshli, “Characterization and classification of interacting $(2+1)$ -dimensional topological crystalline insulators with orientation-preserving wallpaper groups,” *Phys. Rev. B* **109**, 035168 (2024).
- [80] Ryohei Kobayashi, Taige Wang, Tomohiro Soejima, Roger S. K. Mong, and Shinsei Ryu, “Extracting Higher Central Charge from a Single Wave Function,” *Phys. Rev. Lett.* **132**, 016602 (2024).
- [81] Liang Fu and C. L. Kane, “Topology, Delocalization via Average Symmetry and the Symplectic Anderson Transition,” *Phys. Rev. Lett.* **109**, 246605 (2012).
- [82] I. C. Fulga, B. van Heck, J. M. Edge, and A. R. Akhmerov, “Statistical topological insulators,” *Phys. Rev. B* **89**, 155424 (2014).
- [83] M. Diez, D. I. Pikulin, I. C. Fulga, and J. Tworzydło, “Extended topological group structure due to average reflection symmetry,” *New Journal of Physics* **17**, 043014 (2015).
- [84] Juntao Song and Emil Prodan, “Quantization of topological invariants under symmetry-breaking disorder,” *Phys. Rev. B* **92**, 195119 (2015).
- [85] Adhip Agarwala and Vijay B. Shenoy, “Topological Insulators in Amorphous Systems,” *Phys. Rev. Lett.* **118**, 236402 (2017).
- [86] Noah P. Mitchell, Lisa M. Nash, Daniel Hexner, Ari M. Turner, and William T. M. Irvine, “Amorphous topological insulators constructed from random point sets,” *Nature Physics* **14**, 380–385 (2018).
- [87] Adhip Agarwala, Vladimir Juričić, and Bitan Roy, “Higher-order topological insulators in amorphous solids,” *Phys. Rev. Res.* **2**, 012067 (2020).
- [88] Helene Spring, Anton R. Akhmerov, and Daniel Varjas, “Amorphous topological phases protected by continuous rotation symmetry,” *SciPost Phys.* **11**, 022 (2021).
- [89] Julia D. Hannukainen, Miguel F. Martínez, Jens H. Bardarson, and Thomas Klein Kvorning, “Local Topological

- Markers in Odd Spatial Dimensions and Their Application to Amorphous Topological Matter,” *Phys. Rev. Lett.* **129**, 277601 (2022).
- [90] Dexin Li, Citian Wang, and Huaqing Huang, “Real-space formalism for the euler class and fragile topology in quasicrystals and amorphous lattices,” *arXiv preprint arXiv:2311.01557* (2023).
- [91] Xiaoyu Cheng, Tiantao Qu, Liantuan Xiao, Suotang Jia, Jun Chen, and Lei Zhang, “Topological Anderson amorphous insulator,” *Phys. Rev. B* **108**, L081110 (2023).
- [92] Yu-Liang Tao, Jiong-Hao Wang, and Yong Xu, “Average symmetry protected higher-order topological amorphous insulators,” *SciPost Phys.* **15**, 193 (2023).
- [93] Adolfo G Grushin, “Topological phases of amorphous matter,” in *Low-Temperature Thermal and Vibrational Properties of Disordered Solids: A Half-Century of Universal “Anomalies” of Glasses* (World Scientific, 2023) pp. 435–486.
- [94] Paul Corbae, Julia D. Hannukainen, Quentin Marsal, Daniel Muñoz-Segovia, and Adolfo G. Grushin, “Amorphous topological matter: Theory and experiment,” *Europhysics Letters* **142**, 16001 (2023).
- [95] Ai-Lei He, Lu-Rong Ding, Yuan Zhou, Yi-Fei Wang, and Chang-De Gong, “Quasicrystalline Chern insulators,” *Phys. Rev. B* **100**, 214109 (2019).
- [96] Joseph Sykes and Ryan Barnett, “1D quasicrystals and topological markers,” *Materials for Quantum Technology* **2**, 025005 (2022).

Supplemental Material for “Global and Local Topological Crystalline Markers for Rotation-Symmetric Insulators”

Saavanth Velury,^{*} Yoonseok Hwang, and Taylor L. Hughes
*Department of Physics and Anthony J. Leggett Institute for Condensed Matter Theory,
 University of Illinois at Urbana-Champaign, Urbana, Illinois 61801-3080, USA*

CONTENTS

I. Review of tight-binding Hamiltonian and symmetry transformations	1
II. Derivation of topological crystalline marker decomposition in momentum space	4
III. Construction of mappings between topological crystalline markers, momentum-space irrep multiplicities, rotation invariants, and wannier orbital irrep multiplicities/real-space invariants (RSI)	5
IV. Elementary band representations for C_n -symmetric atomic insulators	6
V. Comments on class D superconductors and pairing symmetry	6
VI. Matrices for mappings for each symmetry class and C_n symmetry	9
VII. Derivation of momentum quantization condition under twisted boundary conditions	27
VIII. Fully traced TCMs for arbitrary finite-size C_n -symmetric lattice utilizing twisted boundary conditions	28
References	31

I. REVIEW OF TIGHT-BINDING HAMILTONIAN AND SYMMETRY TRANSFORMATIONS

In this section, we briefly review the properties of the tight-binding Hamiltonian and the action of symmetry operators on the associated single-particle basis.

1. Tight-binding Hamiltonian

Consider a periodic lattice in d -dimensions with N unit cells, and a tight-binding basis (e.g., a set of basis atomic orbitals) which can be denoted by the single-particle kets $|\mathbf{R}, \alpha\rangle$ where \mathbf{R} denotes a (Bravais) lattice vector corresponding to the position of a unit cell, and $\alpha = 1, \dots, N_{\text{int}}$ is an index for the internal degree of freedom within the unit cell, denoting an orbital index, sublattice site, etc. Usually, we express $\mathbf{R} = \sum_{i=1}^d n_i \mathbf{a}_i$, where $n_i \in \mathbb{Z}$ for $i \in \{1, \dots, d\}$ and $\{\mathbf{a}_i\}_{i=1}^d$ denotes the set of independent (primitive) lattice vectors spanning the lattice. The tight-binding basis state $|\mathbf{R}, \alpha\rangle$ represents an electron localized at the position $\mathbf{R} + \mathbf{x}_\alpha$, where \mathbf{x}_α denotes the sublattice site of the α^{th} orbital with respect to the unit cell origin. Note that $\{|\mathbf{R}, \alpha\rangle\}$ forms an orthonormal basis, i.e. $\langle \mathbf{R}, \alpha | \mathbf{R}', \beta \rangle = \delta_{\mathbf{R}, \mathbf{R}'} \delta_{\alpha, \beta}$. The single-particle Hamiltonian can be expanded in the tight-binding basis, known as the tight-binding Hamiltonian, as follows,

$$H = \sum_{\mathbf{R}, \mathbf{R}'} \sum_{\alpha, \beta} t_{(\mathbf{R}, \alpha), (\mathbf{R}', \beta)} |\mathbf{R}, \alpha\rangle \langle \mathbf{R}', \beta|, \quad (1)$$

^{*} svelury2@illinois.edu

where $t_{(\mathbf{R},\alpha),(\mathbf{R}',\beta)}$ denotes the hopping amplitude between the α^{th} and β^{th} orbitals located at $\mathbf{R} + \mathbf{x}_\alpha$ and $\mathbf{R}' + \mathbf{x}_\beta$ respectively.

For a tight-binding Hamiltonian on a periodic lattice with translational symmetry, it is useful to consider the Fourier transform. Typically, there are two different conventions one can use when considering the Fourier transform of $|\mathbf{R}, \alpha\rangle$,

$$\begin{aligned} |\mathbf{k}, \alpha\rangle &\equiv \frac{1}{\sqrt{N}} \sum_{\mathbf{R}} e^{i\mathbf{k}\cdot\mathbf{R}} |\mathbf{R}, \alpha\rangle \\ |\{\mathbf{k}, \alpha\}\rangle &\equiv \frac{1}{\sqrt{N}} \sum_{\mathbf{R}} e^{i\mathbf{k}\cdot(\mathbf{R}+\mathbf{x}_\alpha)} |\mathbf{R}, \alpha\rangle. \end{aligned} \quad (2)$$

The states $\{|\mathbf{k}, \alpha\rangle\}$ span a periodic basis, because $|\mathbf{k} + \mathbf{G}, \alpha\rangle = |\mathbf{k}, \alpha\rangle$ where \mathbf{G} denotes a reciprocal lattice vector. On the other hand, the states $\{|\{\mathbf{k}, \alpha\}\rangle\}$ span a non-periodic basis, because $|\mathbf{k} + \mathbf{G}, \alpha\rangle \neq |\mathbf{k}, \alpha\rangle$ because $\mathbf{G} \cdot \mathbf{x}_\alpha \neq 0 \pmod{2\pi}$. However, a basis transformation can be applied to the non-periodic basis states to obtain the periodic basis states,

$$|\mathbf{k}, \alpha\rangle = \sum_{\beta} [V(\mathbf{k})]_{\beta\alpha} |\{\mathbf{k}, \beta\}\rangle, \quad (3)$$

where $[V(\mathbf{k})]_{\beta\alpha} = e^{-i\mathbf{k}\cdot\mathbf{x}_\beta} \delta_{\beta\alpha}$ is the sublattice embedding matrix for this unitary transformation. Note that with the sublattice embedding matrix, one can now implement periodicity on the non-periodic basis states as $|\{\mathbf{k} + \mathbf{G}, \alpha\}\rangle = \sum_{\beta} V(\mathbf{G})_{\beta\alpha}^{-1} |\{\mathbf{k}, \beta\}\rangle$, which is called the periodic gauge. Both the periodic basis states and the non-periodic basis states satisfy orthonormality (i.e., $\langle \mathbf{k}, \alpha | \mathbf{k}', \beta \rangle = \langle \{\mathbf{k}, \alpha\} | \{\mathbf{k}', \beta\} \rangle = \delta_{\mathbf{k}, \mathbf{k}'} \delta_{\alpha, \beta}$). Using Eqs. (2) and (3), the tight-binding Hamiltonian can be expanded in either the periodic or non-periodic basis states,

$$H = \sum_{\mathbf{k}} \sum_{\alpha, \beta} |\mathbf{k}, \alpha\rangle H(\mathbf{k})_{\alpha\beta} \langle \mathbf{k}, \beta| = \sum_{\mathbf{k}} \sum_{\alpha, \beta} |\{\mathbf{k}, \alpha\}\rangle \tilde{H}(\mathbf{k})_{\alpha\beta} \langle \{\mathbf{k}, \beta\}|, \quad (4)$$

where $H(\mathbf{k})_{\alpha\beta} \equiv \langle \mathbf{k}, \alpha | H(\mathbf{k}) | \mathbf{k}, \beta \rangle$ and $\tilde{H}(\mathbf{k})_{\alpha\beta} \equiv \langle \{\mathbf{k}, \alpha\} | \tilde{H}(\mathbf{k}) | \{\mathbf{k}, \beta\} \rangle$. From Eq. (4), one has

$$\begin{aligned} \tilde{H}(\mathbf{k}) &= V(\mathbf{k}) H(\mathbf{k}) V(\mathbf{k})^{-1}, \\ H(\mathbf{k} + \mathbf{G}) &= H(\mathbf{k}), \\ \tilde{H}(\mathbf{k} + \mathbf{G}) &= V(\mathbf{G}) \tilde{H}(\mathbf{k}) V(\mathbf{G})^{-1}, \end{aligned} \quad (5)$$

The matrix elements of the tight-binding Hamiltonian can be explicitly evaluated in either the periodic or non-periodic bases when implementing the Fourier transform given by Eq. (2) on the tight-binding Hamiltonian given by Eq. (1),

$$\begin{aligned} H(\mathbf{k})_{\alpha\beta} &= \sum_{\mathbf{R}} t_{(\mathbf{R},\alpha),(\mathbf{R}',\beta)} e^{-i\mathbf{k}\cdot\mathbf{R}}, \\ \tilde{H}(\mathbf{k})_{\alpha\beta} &= \sum_{\mathbf{R}} t_{(\mathbf{R},\alpha),(\mathbf{R}',\beta)} e^{-i\mathbf{k}\cdot(\mathbf{R}+\mathbf{x}_\alpha-\mathbf{x}_\beta)}, \end{aligned} \quad (6)$$

Note that the matrix elements in the non-periodic basis are equivalent to the matrix elements in the periodic basis if *all* the orbitals are located at the unit cell origin (e.g., $\mathbf{x}_\alpha = \mathbf{0}$ for all α). $H(\mathbf{k})$ and $\tilde{H}(\mathbf{k})$ are the Bloch Hamiltonians for the periodic or non-periodic bases respectively. Diagonalization of the Bloch Hamiltonian yields the following in each basis,

$$\begin{aligned} \sum_{\beta} H(\mathbf{k})_{\alpha\beta} |u_n(\mathbf{k})\rangle_{\beta} &= E_n(\mathbf{k}) |u_n(\mathbf{k})\rangle_{\alpha} \\ \sum_{\beta} \tilde{H}(\mathbf{k})_{\alpha\beta} |\{u_n(\mathbf{k})\}\rangle_{\beta} &= E_n(\mathbf{k}) |\{u_n(\mathbf{k})\}\rangle_{\alpha} \end{aligned} \quad (7)$$

The states $|\{u_n(\mathbf{k})\}\rangle$ in the non-periodic basis can be related to the states $|u_n(\mathbf{k})\rangle$ via the sublattice embedding matrix, i.e. $|\{u_n(\mathbf{k})\}\rangle = V(\mathbf{k}) |u_n(\mathbf{k})\rangle$. The $|u_n(\mathbf{k})\rangle$ states in the periodic basis automatically satisfy the periodic gauge since $|u_n(\mathbf{k} + \mathbf{G})\rangle = |u_n(\mathbf{k})\rangle$, whereas the $|\{u_n(\mathbf{k})\}\rangle$ states in the non-periodic basis require the sublattice embedding matrix to satisfy the periodic gauge, i.e., $|\{u_n(\mathbf{k} + \mathbf{G})\}\rangle = V(\mathbf{G}) |\{u_n(\mathbf{k})\}\rangle$. (Thus, in both bases, the Bloch wavefunction $|\psi_n(\mathbf{k})\rangle = \sum_{\alpha} |u_n(\mathbf{k})\rangle_{\alpha} |\mathbf{k}, \alpha\rangle = \sum_{\alpha} |\{u_n(\mathbf{k})\}\rangle_{\alpha} |\{\mathbf{k}, \alpha\}\rangle$ is periodic such that $|\psi_n(\mathbf{k})\rangle = |\psi_n(\mathbf{k} + \mathbf{G})\rangle$. Here, $|u_n(\mathbf{k})\rangle_{\alpha}$ ($|\{u_n(\mathbf{k})\}\rangle_{\alpha}$) denotes the α^{th} component of $|u_n(\mathbf{k})\rangle$ ($|\{u_n(\mathbf{k})\}\rangle$).

Throughout this Supplemental Material, specifically for Secs. II, and Sec. VII, we will work in the periodic basis and the Bloch Hamiltonian $H(\mathbf{k})$ to present the derivations in the most algebraically simple way possible. It is straightforward to re-derive the results in the non-periodic basis and the corresponding Bloch Hamiltonian $\tilde{H}(\mathbf{k})$ using the basis transformations shown in Eqs. (3) and (5).

2. Symmetry transformations

Consider an element χ of the space group G where $\chi = \{R_\chi | \boldsymbol{\delta}_\chi\}$ which acts on a point in space as follows,

$$\chi : \mathbf{r} \rightarrow R_\chi \mathbf{r} + \boldsymbol{\delta}_\chi \quad (8)$$

where R_χ is an orthogonal matrix. On the tight-binding basis states, χ is a unitary operator that acts as follows,

$$\chi |\mathbf{R}, \alpha\rangle = \sum_{\beta} [U(\chi)]_{\beta\alpha} |\mathbf{R}_\chi(\alpha), \beta\rangle, \quad (9)$$

where $\mathbf{R}_\chi(\alpha) = R_\chi(\mathbf{R} + \mathbf{x}_\alpha) + \boldsymbol{\delta}_\chi - \mathbf{x}_\beta$ and $U(\chi)$ is a unitary matrix representing χ in the orbital basis. On the periodic basis states, the action of χ can be determined by combining Eqs. (2) and (9),

$$\begin{aligned} \chi |\mathbf{k}, \alpha\rangle &= \frac{1}{\sqrt{N}} \sum_{\mathbf{R}} e^{i\mathbf{k}\cdot\mathbf{R}} \chi |\mathbf{R}, \alpha\rangle = \frac{1}{\sqrt{N}} \sum_{\mathbf{R}} \sum_{\beta} e^{i\mathbf{k}\cdot\mathbf{R}} [U(\chi)]_{\beta\alpha} |\mathbf{R}_\chi(\alpha), \beta\rangle \\ &\equiv \frac{1}{\sqrt{N}} \sum_{\mathbf{R}} \sum_{\beta} e^{i\mathbf{k}\cdot(R_\chi^{-1}(\mathbf{R} + \mathbf{x}_\beta - \boldsymbol{\delta}_\chi) - \mathbf{x}_\alpha)} [U(\chi)]_{\beta\alpha} |\mathbf{R}, \beta\rangle \\ &= \sum_{\beta} e^{i(R_\chi \mathbf{k}) \cdot (\mathbf{x}_\beta - R_\chi \mathbf{x}_\alpha - \boldsymbol{\delta}_\chi)} [U(\chi)]_{\beta\alpha} \left(\frac{1}{\sqrt{N}} \sum_{\mathbf{R}} e^{i(R_\chi \mathbf{k}) \cdot \mathbf{R}} |\mathbf{R}, \beta\rangle \right) \\ &= \sum_{\beta} e^{i(R_\chi \mathbf{k}) \cdot (\mathbf{x}_\beta - R_\chi \mathbf{x}_\alpha - \boldsymbol{\delta}_\chi)} [U(\chi)]_{\beta\alpha} |R_\chi \mathbf{k}, \beta\rangle, \\ &\equiv \sum_{\beta} [U_\chi(\mathbf{k})]_{\beta\alpha} |R_\chi \mathbf{k}, \beta\rangle. \end{aligned} \quad (10)$$

In the above, we have introduced the unitary matrix $U_\chi(\mathbf{k})$ which is the momentum-space representation of U_χ and is defined as follows,

$$[U_\chi(\mathbf{k})]_{\beta\alpha} = e^{i(R_\chi \mathbf{k}) \cdot (\mathbf{x}_\beta - R_\chi \mathbf{x}_\alpha - \boldsymbol{\delta}_\chi)} U(\chi) \equiv \left[V(R_\chi \mathbf{k})^\dagger \left(e^{-i(R_\chi \mathbf{k}) \cdot \boldsymbol{\delta}_\chi} U(\chi) \right) V(\mathbf{k}) \right]_{\beta\alpha}. \quad (11)$$

where $V(\mathbf{k})$ is the sublattice embedding matrix (note that it is unitary) defined in Sec. I 1. If the tight-binding Hamiltonian is symmetric under χ , it is invariant under conjugation by χ , e.g., $H = \chi H \chi^{-1}$. This implies the Bloch Hamiltonian transforms as follows,

$$H(R_\chi \mathbf{k}) = U_\chi(\mathbf{k}) H(\mathbf{k}) U_\chi(\mathbf{k})^\dagger \quad (12)$$

Consider the group element corresponding to a C_n rotation at the unit cell origin, i.e., $c_n(\mathbf{0}) = \{C_n | \mathbf{0}\}$, where $c_n(\mathbf{0})$ is the rotation operator for a rotation axis located at the unit cell origin (we also assume this to be the $1a$ Wyckoff position (WP), $\mathbf{x}_{1a} = \mathbf{0}$). The rotation operator $c_n(\mathbf{0})$ maps a position \mathbf{r} to $c_n(\mathbf{0})\mathbf{r}$. From Eq. (11), we have

$$c_n(\mathbf{0}, \mathbf{k}) = V(C_n \mathbf{k})^\dagger c_n(\mathbf{0}) V(\mathbf{k}), \quad (13)$$

Additionally, consider a WP at \mathbf{r}_o . The group element

$$c_n(\mathbf{r}_o) = \{C_n | \mathbf{r}_o - c_n(\mathbf{0})\mathbf{r}_o\} = \{E | \mathbf{r}_o\} \{C_n | \mathbf{0}\} \{E | -\mathbf{r}_o\} \equiv t(\mathbf{r}_o) c_n(\mathbf{0}) t(\mathbf{r}_o)^{-1} \quad (14)$$

is the rotation operator for a rotation axis at \mathbf{r}_o and maps a position \mathbf{r} to $c_n(\mathbf{r}_o)\mathbf{r} = c_n(\mathbf{0})\mathbf{r} + \mathbf{r}_o - c_n(\mathbf{0})\mathbf{r}_o$. Note that $\{E | \mathbf{x}\} \equiv t(\mathbf{x})$ is the group element corresponding to translation by \mathbf{x} . From Eq. (11), identifying $\boldsymbol{\delta}_{c_n(\mathbf{0})} = \mathbf{r}_o - c_n(\mathbf{0})\mathbf{r}_o$, it follows that

$$c_n(\mathbf{r}_o, \mathbf{k}) = e^{-i\mathbf{k}\cdot((c_n(\mathbf{0}))^{-1}\mathbf{r}_o - \mathbf{r}_o)} V(C_n \mathbf{k})^\dagger c_n(\mathbf{0}, \mathbf{k}) V(\mathbf{k}) = e^{-i(C_n \mathbf{k} - \mathbf{k}) \cdot \mathbf{r}_o} V(C_n \mathbf{k})^\dagger c_n(\mathbf{0}, \mathbf{k}) V(\mathbf{k}) \quad (15)$$

This is a generalized version of the result presented in Eq. (15) of the main text, which can be easily obtained assuming that all orbitals within the unit cell lie at the origin (e.g., $\mathbf{x}_\alpha = \mathbf{0}$ for all α). Then $V(\mathbf{k})$ becomes the identity matrix and Eq. (15) is equivalent to Eq. (15) of the main text.

II. DERIVATION OF TOPOLOGICAL CRYSTALLINE MARKER DECOMPOSITION IN MOMENTUM SPACE

Here, we will go over the decomposition of the fully traced topological crystalline marker (TCM) for C_n point groups in the momentum-space basis, which is given by Eq. (17) in the main text. This is used to establish the mapping between the fully traced TCMs and the momentum-space irrep multiplicities which is covered in Secs. III and VI of this Supplemental Material. Working in the periodic basis, diagonalizing the Bloch Hamiltonian yields Eq. (7). The ground state projector P_{GS} can be expanded in terms of the Bloch states,

$$P_{GS} = \sum_{j=1}^{\nu} \sum_{\mathbf{k}} |\psi_j(\mathbf{k})\rangle \langle \psi_j(\mathbf{k})|, \quad (16)$$

where ν is the number of filled bands. The Bloch states are expressed in the periodic basis as $|\psi_n(\mathbf{k})\rangle = \sum_{\alpha} |u_n(\mathbf{k})\rangle_{\alpha} |\mathbf{k}, \alpha\rangle$, and satisfy the orthogonality relation $\langle \psi_m(\mathbf{k}) | \psi_n(\mathbf{k}') \rangle = \delta_{mn} \delta_{\mathbf{k}, \mathbf{k}'}$ (note that $\langle u_m(\mathbf{k}) | u_n(\mathbf{k}') \rangle \neq \delta_{mn} \delta_{\mathbf{k}, \mathbf{k}'}$ in general, but $\langle u_m(\mathbf{k}) | u_n(\mathbf{k}) \rangle = \delta_{mn}$). The fully traced TCM can be expanded in momentum-space as follows,

$$\langle c_n(\mathbf{r}_o) \rangle_F = \text{Tr}[c_n(\mathbf{r}_o) P_{GS}] = \sum_{\mathbf{k}} \sum_{m=1}^{N_{\text{int}}} \langle \psi_m(\mathbf{k}) | c_n(\mathbf{r}_o, \mathbf{k}) P_{GS} | \psi_m(\mathbf{k}) \rangle. \quad (17)$$

Substituting Eq. (16) into Eq. (17) yields the following,

$$\langle c_n(\mathbf{r}_o) \rangle_F = \sum_{\mathbf{k}, \mathbf{k}'} \sum_{m=1}^{N_{\text{int}}} \sum_{j=1}^{\nu} \langle \psi_m(\mathbf{k}) | c_n(\mathbf{r}_o, \mathbf{k}) | \psi_j(\mathbf{k}') \rangle \langle \psi_j(\mathbf{k}') | \psi_m(\mathbf{k}) \rangle. \quad (18)$$

Given $c_n(\mathbf{r}_o, \mathbf{k})$ maps $\mathbf{k} \rightarrow C_n \mathbf{k}$, the non-zero contributions in the fully traced TCMs only occur at the high-symmetry momenta $\bar{\mathbf{k}}$ where $C_n \bar{\mathbf{k}} = \bar{\mathbf{k}}$ modulo \mathbf{b} , where \mathbf{b} is a reciprocal lattice vector. This means the sum in Eq. (18) is non-zero only for $\mathbf{k} = \mathbf{k}' = \bar{\mathbf{k}}$. Therefore, Eq. (18) reduces to the following using the orthogonality relation of the Bloch states $\langle \psi_m(\mathbf{k}) | \psi_n(\mathbf{k}') \rangle = \delta_{mn} \delta_{\mathbf{k}, \mathbf{k}'}$,

$$\langle c_n(\mathbf{r}_o) \rangle_F = \sum_{\bar{\mathbf{k}} \in \text{HSM}_n} \sum_{j=1}^{\nu} \langle \psi_j(\bar{\mathbf{k}}) | c_n(\mathbf{r}_o, \bar{\mathbf{k}}) | \psi_j(\bar{\mathbf{k}}) \rangle, \quad (19)$$

where HSM_n is the set of C_n -invariant high-symmetry momenta. For every $\bar{\mathbf{k}} \in \text{HSM}_n$, because $[c_n(\mathbf{r}_o, \bar{\mathbf{k}}), H(\bar{\mathbf{k}})] = 0$, this means $|\psi_j(\bar{\mathbf{k}})\rangle$ is a simultaneous eigenstate of both $H(\bar{\mathbf{k}})$ and $c_n(\mathbf{r}_o, \bar{\mathbf{k}})$. Eq. (19) is the trace (over the filled bands) of the *sewing matrix* $B_{mn}(\mathbf{k}) = \langle \psi_m(\mathbf{k}) | c_n(\mathbf{r}_o, \mathbf{k}) | \psi_n(\mathbf{k}) \rangle$ evaluated at the high-symmetry momenta $\bar{\mathbf{k}} \in \text{HSM}_n$. This matrix can be diagonalized to yield the rotation eigenvalues $\{e^{i\phi_{n,p}(\mathbf{r}_o, \bar{\mathbf{k}})}\}_{p=1}^n$ and their irrep multiplicities $m(\bar{\mathbf{k}}_p)$ at each $\bar{\mathbf{k}} \in \text{HSM}_n$. Thus,

$$\langle c_n(\mathbf{r}_o) \rangle_F = \sum_{\bar{\mathbf{k}} \in \text{HSM}_n} \sum_{p=1}^n e^{i\phi_{n,p}(\mathbf{r}_o, \bar{\mathbf{k}})} m(\bar{\mathbf{k}}_p), \quad (20)$$

where $\phi_{n,p}(\mathbf{r}_o, \bar{\mathbf{k}}) = \frac{2\pi}{n} \ell - \bar{\mathbf{k}} \cdot ((c_n(\mathbf{0}))^{-1} \mathbf{r}_o - \mathbf{r}_o) = \frac{2\pi}{n} \ell - (C_n \bar{\mathbf{k}} - \bar{\mathbf{k}}) \cdot \mathbf{r}_o$ with the orbital angular momentum $\ell = p - 1$ for spinless electrons and $\ell = p - 1/2$ for spin-1/2 electrons ($p = 1, \dots, n$) as defined in the main text. The irrep multiplicity $m(\bar{\mathbf{k}}_p)$ is the number of occupied states at $\bar{\mathbf{k}}$ for the irrep $\bar{\mathbf{k}}_p$, and

$$\sum_{p=1}^n m(\bar{\mathbf{k}}_p) = \nu. \quad (21)$$

Eq. (21) directly applies to C_2 and C_3 point groups. For C_n point groups that contain a $C_{m \leq n}$ -invariant subgroup, there exist high-symmetry momenta $\bar{\mathbf{k}} \neq \Gamma$ which are only invariant under the $C_{m \leq n}$ subgroup, which is true for C_4 and C_6 point groups. Therefore, a generalized version of Eq. (21) is,

$$\sum_{p=1}^m m(\bar{\mathbf{k}}_p) = \sum_{p=1}^n m(\Gamma_p) = \nu \rightarrow \sum_{p=1}^m [\bar{\mathbf{k}}_p] = 0 \quad (22)$$

where we have used the rotation invariants $[\bar{\mathbf{k}}_p]$ to simplify the expression for this constraint.

III. CONSTRUCTION OF MAPPINGS BETWEEN TOPOLOGICAL CRYSTALLINE MARKERS, MOMENTUM-SPACE IRREP MULTIPLICITIES, ROTATION INVARIANTS, AND WANNIER ORBITAL IRREP MULTIPLICITIES/REAL-SPACE INVARIANTS (RSI)

Eq. (20) explicitly demonstrates that the fully traced TCMs can be expressed in terms of the momentum-space irrep multiplicities, thereby demonstrating the existence of a mapping between the fully traced TCMs and the momentum-space irrep multiplicities. Furthermore, for atomic insulators, the ground state can be expressed in terms of symmetric, exponentially-localized Wannier orbitals, which implies the existence of a mapping between momentum-space irrep multiplicities and Wannier orbital irrep multiplicities. These mappings can be used to express strong topological invariants, such as the Chern number, and the quantized responses of atomic insulators such as the bulk polarization and sector charge, in terms of one unified set of quantities, which is the set of fully traced TCMs for a given space group. In this section, we will provide an overview of how these mappings are constructed.

The TCM and the fully traced TCM can be constructed for any group element $\chi = \{R_\chi | \delta_\chi\} \in G$,

$$\langle \chi \rangle = \sum_{\alpha} \langle \mathbf{R}, \alpha | \chi P_{GS} | \mathbf{R}, \alpha \rangle \rightarrow \langle \chi \rangle_F = \text{Tr}[\chi P_{GS}]. \quad (23)$$

The minimal complete set of fully traced TCMs for a given space group G can be constructed from the generators of the little group $G_{\mathbf{r}_o}$ for each *maximal* WP \mathbf{r}_o . This includes a fully traced TCM for the identity element (e.g., $\{E | \mathbf{0}\}$) and a fully traced TCM for the inverse element (e.g., $\chi^{-1} = \{(R_\chi)^{-1} | - (R_\chi)^{-1} \delta_\chi\}$). Focusing on C_n point groups, we introduce a column vector $\mathbf{v}_{\text{TCM}}^{(n)}$, which contains the minimal, complete set of independent fully traced TCMs. As an example, for a C_2 point group, the unit cell contains four WPs (1a, 1b, 1c, and 1d), so $\mathbf{v}_{\text{TCM}}^{(2)}$ is given as follows,

$$\mathbf{v}_{\text{TCM}}^{(2)} = (\nu, \langle c_2(\mathbf{x}_{1a}) \rangle_F, \langle c_2(\mathbf{x}_{1b}) \rangle_F, \langle c_2(\mathbf{x}_{1c}) \rangle_F, \langle c_2(\mathbf{x}_{1d}) \rangle_F)^T. \quad (24)$$

where $\nu = \text{Tr}[P_{GS}]$ is the filling and is equivalent to the TCM for the identity element. The remaining $\mathbf{v}_{\text{TCM}}^{(3)}$, $\mathbf{v}_{\text{TCM}}^{(4)}$, and $\mathbf{v}_{\text{TCM}}^{(6)}$ for the C_3 , C_4 , and C_6 point groups can be determined in a similar manner,

$$\begin{aligned} \mathbf{v}_{\text{TCM}}^{(3)} &= (\nu, \langle c_3(\mathbf{x}_{1a}) \rangle_F, \langle c_3(\mathbf{x}_{1b}) \rangle_F, \langle c_3(\mathbf{x}_{1c}) \rangle_F, \langle (c_3(\mathbf{x}_{1a}))^{-1} \rangle_F, \langle (c_3(\mathbf{x}_{1b}))^{-1} \rangle_F, \langle (c_3(\mathbf{x}_{1c}))^{-1} \rangle_F)^T, \\ \mathbf{v}_{\text{TCM}}^{(4)} &= (\nu, \langle c_4(\mathbf{x}_{1a}) \rangle_F, \langle c_4(\mathbf{x}_{1b}) \rangle_F, \langle (c_4(\mathbf{x}_{1a}))^{-1} \rangle_F, \langle (c_4(\mathbf{x}_{1b}))^{-1} \rangle_F, \langle c_2(\mathbf{x}_{1a}) \rangle_F, \langle c_2(\mathbf{x}_{1b}) \rangle_F, \langle c_2(\mathbf{x}_{2c}) \rangle_F)^T, \\ \mathbf{v}_{\text{TCM}}^{(6)} &= (\nu, \langle c_6(\mathbf{x}_{1a}) \rangle_F, \langle (c_6(\mathbf{x}_{1a}))^{-1} \rangle_F, \langle c_3(\mathbf{x}_{1a}) \rangle_F, \langle c_3(\mathbf{x}_{2b}) \rangle_F, \langle (c_3(\mathbf{x}_{1a}))^{-1} \rangle_F, \\ &\quad \langle (c_3(\mathbf{x}_{2b}))^{-1} \rangle_F, \langle c_2(\mathbf{x}_{1a}) \rangle_F, \langle c_2(\mathbf{x}_{3c}) \rangle_F)^T. \end{aligned} \quad (25)$$

We now consider the complete set of momentum-space irrep multiplicities for each C_n point group. In order to do so, we utilize the momentum-space rotation invariants for each C_n point group as defined in Eq. (21) of the main text. Constraints arising from filling (as shown in Eq. (22)) and internal symmetries such as time-reversal and/or particle-hole can easily be expressed in terms of the rotation invariants. Therefore, we introduce a column vector $\mathbf{v}_{\text{MS}}^{(n)}$ which contains the minimal complete set of rotation invariants for each C_n point group,

$$\begin{aligned} \mathbf{v}_{\text{MS}}^{(2)} &= (\nu, m(\Gamma_1), [X_1], [Y_1], [M_1])^T, \\ \mathbf{v}_{\text{MS}}^{(3)} &= (\nu, m(\Gamma_1), m(\Gamma_2), [K_1], [K_2], [K'_1], [K'_2])^T, \\ \mathbf{v}_{\text{MS}}^{(4)} &= (\nu, m(\Gamma_1), m(\Gamma_2), m(\Gamma_3), [X_1], [M_1], [M_2], [M_3])^T, \\ \mathbf{v}_{\text{MS}}^{(6)} &= (\nu, m(\Gamma_1), m(\Gamma_2), m(\Gamma_3), m(\Gamma_4), m(\Gamma_5), [K_1], [K_2], [M_1])^T. \end{aligned} \quad (26)$$

Finally, pertaining to atomic insulators, we consider the complete set of Wannier orbital irrep multiplicities over the maximal WPs for each C_n point group. Similar to rotation invariants, we utilize real-space invariants (RSIs) [1], which can be expressed in terms of the Wannier orbital irrep multiplicities for each C_n point group for spinless electrons,

$$\begin{aligned} C_2 : \delta_W &= n_W^{(1)} - n_W^{(0)} \text{ for } W \in \{1a, 1b, 1c, 1d\}, \\ C_3 : \delta_W^{(\ell)} &= n_W^{(\ell)} - n_W^{(0)} \text{ for } W \in \{1a, 1b, 1c\} \text{ and } \ell \in \{1, 2\}, \\ C_4 : \delta_W^{(\ell)} &= n_W^{(\ell)} - n_W^{(0)} \text{ for } W \in \{1a, 1b\} \text{ and } \ell \in \{1, 2, 3\}, \\ \delta_{2c} &= n_{2c}^{(1)} - n_{2c}^{(0)}, \\ C_6 : \delta_{1a}^{(\ell)} &= n_{1a}^{(\ell)} - n_{1a}^{(0)} \text{ for } \ell \in \{1, 2, 3, 4, 5\}, \end{aligned}$$

$$\begin{aligned}\delta_{2b}^{(\ell)} &= n_{2b}^{(\ell)} - n_{2b}^{(0)} \text{ for } \ell \in \{1, 2\}, \\ \delta_{3c} &= n_{3c}^{(1)} - n_{3c}^{(0)}.\end{aligned}\tag{27}$$

and for spin-1/2 electrons,

$$\begin{aligned}C_2 : \delta_W &= n_W^{(3/2)} - n_W^{(1/2)} \text{ for } W \in \{1a, 1b, 1c, 1d\}, \\ C_3 : \delta_W^{(\ell-1/2)} &= n_W^{(\ell)} - n_W^{(1/2)} \text{ for } W \in \{1a, 1b, 1c\} \text{ and } \ell \in \{3/2, 5/2\}, \\ C_4 : \delta_W^{(\ell-1/2)} &= n_W^{(\ell)} - n_W^{(1/2)} \text{ for } W \in \{1a, 1b\} \text{ and } \ell \in \{3/2, 5/2, 7/2\}, \\ &\delta_{2c} = n_{2c}^{(3/2)} - n_{2c}^{(1/2)}, \\ C_6 : \delta_{1a}^{(\ell-1/2)} &= n_{1a}^{(\ell)} - n_{1a}^{(1/2)} \text{ for } \ell \in \{3/2, 5/2, 7/2, 9/2, 11/2\}, \\ &\delta_{2b}^{(\ell-1/2)} = n_{2b}^{(\ell)} - n_{2b}^{(1/2)} \text{ for } \ell \in \{3/2, 5/2\}, \\ &\delta_{3c} = n_{3c}^{(3/2)} - n_{3c}^{(1/2)}.\end{aligned}\tag{28}$$

Additionally, the filling ν can be expressed in terms of the Wannier orbital irrep multiplicities,

$$\nu = \sum_{W, \ell} M_W n_W^{(\ell)}\tag{29}$$

where M_W is the multiplicity of the maximal WP W . We introduce the column vector $\mathbf{v}_{\text{RSI}}^{(n)}$ which contains the minimal complete set of RSIs for each C_n point group,

$$\begin{aligned}\mathbf{v}_{\text{RSI}}^{(2)} &= (\nu, \delta_{1a}, \delta_{1b}, \delta_{1c}, \delta_{1d})^T, \\ \mathbf{v}_{\text{RSI}}^{(3)} &= (\nu, \delta_{1a}^{(1)}, \delta_{1a}^{(2)}, \delta_{1b}^{(1)}, \delta_{1b}^{(2)}, \delta_{1c}^{(1)}, \delta_{1c}^{(2)})^T, \\ \mathbf{v}_{\text{RSI}}^{(4)} &= (\nu, \delta_{1a}^{(1)}, \delta_{1a}^{(2)}, \delta_{1a}^{(3)}, \delta_{1b}^{(1)}, \delta_{1b}^{(2)}, \delta_{1b}^{(3)}, \delta_{2c})^T, \\ \mathbf{v}_{\text{RSI}}^{(6)} &= (\nu, \delta_{1a}^{(1)}, \delta_{1a}^{(2)}, \delta_{1a}^{(3)}, \delta_{1a}^{(4)}, \delta_{1a}^{(5)}, \delta_{2b}^{(1)}, \delta_{2b}^{(2)}, \delta_{3c})^T.\end{aligned}\tag{30}$$

Crucially, $\mathbf{v}_{\text{TCM}}^{(n)}$, $\mathbf{v}_{\text{MS}}^{(n)}$, and $\mathbf{v}_{\text{RSI}}^{(n)}$ all have the same rank, which means that *bijective* mappings exist between each of these quantities,

$$\mathbf{v}_{\text{TCM}}^{(n)} = M_{\text{TCM} \leftarrow \text{MS}}^{(n)} \mathbf{v}_{\text{MS}}^{(n)} \text{ and } \mathbf{v}_{\text{MS}}^{(n)} = M_{\text{MS} \leftarrow \text{RSI}}^{(n)} \mathbf{v}_{\text{RSI}}^{(n)} \rightarrow \mathbf{v}_{\text{TCM}}^{(n)} = M_{\text{TCM} \leftarrow \text{RSI}}^{(n)} \mathbf{v}_{\text{RSI}}^{(n)},\tag{31}$$

with $M_{\text{TCM} \leftarrow \text{RSI}}^{(n)} = M_{\text{TCM} \leftarrow \text{MS}}^{(n)} M_{\text{MS} \leftarrow \text{RSI}}^{(n)}$. $M_{\text{TCM} \leftarrow \text{MS}}^{(n)}$ is a matrix for the mapping from the momentum-space rotation invariants to the fully traced TCMs, and similarly, $M_{\text{MS} \leftarrow \text{RSI}}^{(n)}$ is the matrix for the mapping from the real-space invariants to the momentum-space rotation invariants. Note that $M_{\text{MS} \leftarrow \text{TCM}}^{(n)} = \left(M_{\text{TCM} \leftarrow \text{MS}}^{(n)}\right)^{-1}$ and $M_{\text{RSI} \leftarrow \text{MS}}^{(n)} = \left(M_{\text{MS} \leftarrow \text{RSI}}^{(n)}\right)^{-1}$. The entries of $M_{\text{TCM} \leftarrow \text{MS}}$ are calculated using Eq. (20), and the entries of $M_{\text{MS} \leftarrow \text{RSI}}$ are determined from elementary band representation tables.

IV. ELEMENTARY BAND REPRESENTATIONS FOR C_n -SYMMETRIC ATOMIC INSULATORS

In this section, we provide tables of the elementary band representations for spinless and spin-1/2 systems for each C_n symmetry for symmetry class A systems. Although we do not provide a review of band representation theory in this Supplemental Material, Ref. [2] provides an excellent review on the subject, and the elementary band representations for C_n point groups specifically are also derived in Refs. [3, 4].

V. COMMENTS ON CLASS D SUPERCONDUCTORS AND PAIRING SYMMETRY

The mappings between the fully traced TCMs and the rotation invariants provided in Sec. VI are for symmetry classes A, AI, AII, and D of the Altland-Zirnbauer (AZ) classification. However, class D topological crystalline

TABLE I. Representation of bands induced from Wannier orbitals for a C_2 -symmetric lattice. Each Wannier orbital type can take one of maximal WPs, $W = 1a, 1b, 1c, 1d$ with an angular momentum $\ell = 0$ or 1 (spinless) or angular momentum $\ell = 1/2$ or $3/2$ (spin-1/2). The 2nd-5th columns denote C_2 eigenvalue of bands at high-symmetry points in momentum space. The 6th-8th columns represent the rotation invariants.

(ℓ, W)	HSP ₂				Rotation Invariants		
	Γ	X	Y	M	$[X_1]$	$[Y_1]$	$[M_1]$
(0, 1a)	1	1	1	1	0	0	0
(1, 1a)	-1	-1	-1	-1	0	0	0
(0, 1b)	1	-1	1	-1	-1	0	-1
(1, 1b)	-1	1	-1	1	1	0	1
(0, 1c)	1	1	-1	-1	0	-1	-1
(1, 1c)	-1	-1	1	1	0	1	1
(0, 1d)	1	-1	-1	1	-1	-1	0
(1, 1d)	-1	1	1	-1	1	1	0

(ℓ, W)	HSP ₂				Rotation Invariants		
	Γ	X	Y	M	$[X_1]$	$[Y_1]$	$[M_1]$
(1/2, 1a)	i	i	i	1	0	0	0
(3/2, 1a)	$-i$	$-i$	$-i$	-1	0	0	0
(1/2, 1b)	i	$-i$	i	-1	-1	0	-1
(3/2, 1b)	$-i$	i	$-i$	1	1	0	1
(1/2, 1c)	i	i	$-i$	-1	0	-1	-1
(3/2, 1c)	$-i$	$-i$	i	1	0	1	1
(1/2, 1d)	i	$-i$	$-i$	1	-1	-1	0
(3/2, 1d)	$-i$	i	i	-1	1	1	0

TABLE II. Representation of bands induced from Wannier orbitals for a C_3 -symmetric lattice. Each Wannier orbital type can take one of maximal WPs, $W = 1a, 1b, 1c$ with an angular momentum $\ell = 0, 1, 2$ (spinless) or angular momentum $\ell = 1/2, 3/2, 5/2$ (spin-1/2). The 2nd-4th columns denote C_3 eigenvalue $\omega = e^{2\pi i/3}$ and $\zeta = e^{\pi i/3}$ (and their complex conjugates, $\bar{\omega}$ and $\bar{\zeta}$ respectively) of bands at high-symmetry points in momentum space. The 5th-8th columns represent the rotation invariants.

(ℓ, W)	HSP ₃			Rotation Invariants			
	Γ	K	K'	$[K_1]$	$[K_2]$	$[K'_1]$	$[K'_2]$
(0, 1a)	1	1	1	0	0	0	0
(1, 1a)	ω	ω	ω	0	0	0	0
(2, 1a)	$\bar{\omega}$	$\bar{\omega}$	$\bar{\omega}$	0	0	0	0
(0, 1b)	1	ω	$\bar{\omega}$	-1	1	-1	0
(1, 1b)	ω	$\bar{\omega}$	1	0	-1	1	-1
(2, 1b)	$\bar{\omega}$	1	ω	1	0	0	1
(0, 1c)	1	$\bar{\omega}$	ω	-1	0	-1	1
(1, 1c)	ω	1	$\bar{\omega}$	1	-1	0	-1
(2, 1c)	$\bar{\omega}$	ω	1	0	1	1	0

(ℓ, W)	HSP ₃			Rotation Invariants			
	Γ	K	K'	$[K_1]$	$[K_2]$	$[K'_1]$	$[K'_2]$
(1/2, 1a)	ζ	ζ	ζ	0	0	0	0
(3/2, 1a)	-1	-1	-1	0	0	0	0
(5/2, 1a)	$\bar{\zeta}$	$\bar{\zeta}$	$\bar{\zeta}$	0	0	0	0
(1/2, 1b)	ζ	-1	$\bar{\zeta}$	-1	1	-1	0
(3/2, 1b)	-1	$\bar{\zeta}$	ζ	0	-1	1	-1
(5/2, 1b)	$\bar{\zeta}$	ζ	-1	1	0	0	1
(1/2, 1c)	ζ	$\bar{\zeta}$	-1	-1	0	-1	1
(3/2, 1c)	-1	ζ	$\bar{\zeta}$	1	-1	0	-1
(5/2, 1c)	$\bar{\zeta}$	-1	ζ	0	1	1	0

TABLE III. Representation of bands induced from Wannier orbitals for a C_4 -symmetric lattice. Each Wannier orbital type can take one of maximal WPs, $W = 1a, 1b$ with an angular momentum $\ell = 0, 1, 2, 3$ (spinless) or angular momentum $\ell = 1/2, 3/2, 5/2, 7/2$ (spin-1/2) or take the $W = 2c$ WP with angular momentum $\ell = 0$ or $\ell = 1$ (spinless) or angular momentum $\ell = 1/2$ or $\ell = 3/2$ (spin-1/2). The 2nd-4th columns denote C_4 eigenvalues ($\eta = e^{i\pi/4}$ and its complex conjugate $\bar{\eta}$) or C_2 eigenvalues of bands at high-symmetry points in momentum space. Note that X (and X') are C_2 -invariant HSPs contained in HSP₂, whereas Γ and M are C_4 -invariant HSPs contained in HSP₄. The 5th-8th columns represent the rotation invariants.

(ℓ, W)	HSP ₄ /HSP ₂			Rotation Invariants			
	Γ	X	M	$[X_1]$	$[M_1]$	$[M_2]$	$[M_3]$
(0, 1a)	1	1	1	0	0	0	0
(1, 1a)	i	-1	i	0	0	0	0
(2, 1a)	-1	1	-1	0	0	0	0
(3, 1a)	$-i$	-1	$-i$	0	0	0	0
(0, 1b)	1	-1	-1	-1	-1	0	1
(1, 1b)	i	1	$-i$	1	0	-1	0
(2, 1b)	-1	-1	1	-1	1	0	-1
(3, 1b)	$-i$	1	i	1	0	1	0
(0, 2c)	{1, -1}	{1, -1}	{ $i, -i$ }	-1	-1	1	-1
(1, 2c)	{ $i, -i$ }	{1, -1}	{1, -1}	1	1	-1	1

(ℓ, W)	HSP ₄ /HSP ₂			Rotation Invariants			
	Γ	X	M	$[X_1]$	$[M_1]$	$[M_2]$	$[M_3]$
(1/2, 1a)	η	i	η	0	0	0	0
(3/2, 1a)	$-\bar{\eta}$	$-i$	$-\bar{\eta}$	0	0	0	0
(5/2, 1a)	$-\eta$	i	$-\eta$	0	0	0	0
(7/2, 1a)	$\bar{\eta}$	$-i$	$\bar{\eta}$	0	0	0	0
(1/2, 1b)	η	$-i$	$-\eta$	-1	-1	0	1
(3/2, 1b)	$-\bar{\eta}$	i	$\bar{\eta}$	1	0	-1	0
(5/2, 1b)	$-\eta$	$-i$	η	-1	1	0	-1
(7/2, 1b)	$\bar{\eta}$	i	$-\bar{\eta}$	1	0	1	0
(1/2, 2c)	{ $\eta, -\eta$ }	{ $i, -i$ }	{ $-\bar{\eta}, \bar{\eta}$ }	-1	-1	1	-1
(3/2, 2c)	{ $-\bar{\eta}, \bar{\eta}$ }	{ $i, -i$ }	{ $\eta, -\eta$ }	1	1	-1	1

TABLE IV. Representation of bands induced from Wannier orbitals on a C_6 -symmetric lattice. Each Wannier orbital type can take one of maximal WPs, $W = 1a$ with angular momentum $\ell = 0, 1, 2, 3, 4, 5$ (spinless) or angular momentum $\ell = 1/2, 3/2, 5/2, 7/2, 11/2$ (spin-1/2), or take the $W = 2b$ WP with angular momentum $\ell = 0, 1, 2$ (spinless) or angular momentum $\ell = 1/2, 3/2, 5/2$, or take the $W = 3c$ WP with angular momentum $\ell = 0, 1$ (spinless) or angular momentum $\ell = 1/2, 3/2$ (spin-1/2). The 2nd-4th columns denote C_6 eigenvalues or C_3 eigenvalues ($\gamma = e^{\pi i/6}$, $\zeta = e^{\pi i/3}$, $\omega = e^{2\pi i/3}$ and their complex conjugates $\bar{\gamma}$, $\bar{\zeta}$, and $\bar{\omega}$ respectively) or C_2 eigenvalues of bands at high-symmetry points in momentum space. Note that K (and K') are C_3 invariant HSPs contained in HSP_3 and M (and M', M'') are C_2 invariants HSPs contained in HSP_2 , whereas Γ is a C_6 invariant HSP contained in HSP_6 . The 5th-7th columns represent the rotation invariants.

(ℓ, W)	HSP ₆ /HSP ₃ /HSP ₂			Rotation Invariants		
	Γ	K	M	$[K_1]$	$[K_2]$	$[M_1]$
(0, 1a)	1	1	1	0	0	0
(1, 1a)	ζ	ω	-1	0	0	0
(2, 1a)	ω	$\bar{\omega}$	1	0	0	0
(3, 1a)	-1	1	-1	0	0	0
(4, 1a)	$\bar{\omega}$	ω	1	0	0	0
(5, 1a)	$\bar{\zeta}$	$\bar{\omega}$	-1	0	0	0
(0, 2b)	{1, -1}	{ $\omega, \bar{\omega}$ }	{1, -1}	-2	1	0
(1, 2b)	{ $\zeta, \bar{\omega}$ }	{ $\bar{\omega}, 1$ }	{1, -1}	1	-2	0
(2, 2b)	{ $\omega, \bar{\zeta}$ }	{1, ω }	{1, -1}	1	1	0
(0, 3c)	{1, $\omega, \bar{\omega}$ }	{1, $\omega, \bar{\omega}$ }	{1, -1, -1}	0	0	-2
(1, 3c)	{ $\zeta, -1, \bar{\zeta}$ }	{ $\zeta, -1, \bar{\zeta}$ }	{1, 1, -1}	0	0	2

(ℓ, W)	HSP ₆ /HSP ₃ /HSP ₂			Rotation Invariants		
	Γ	K	M	$[K_1]$	$[K_2]$	$[M_1]$
(1/2, 1a)	γ	ζ	i	0	0	0
(3/2, 1a)	i	-1	$-i$	0	0	0
(5/2, 1a)	$-\bar{\gamma}$	$\bar{\zeta}$	i	0	0	0
(7/2, 1a)	$-\gamma$	ζ	$-i$	0	0	0
(9/2, 1a)	$-i$	-1	i	0	0	0
(11/2, 1a)	$\bar{\gamma}$	$\bar{\zeta}$	$-i$	0	0	0
(1/2, 2b)	{ $\gamma, -\gamma$ }	{-1, $\bar{\zeta}$ }	{ $i, -i$ }	-2	1	0
(3/2, 2b)	{ $i, -i$ }	{ $\bar{\zeta}, \zeta$ }	{ $i, -i$ }	1	-2	0
(5/2, 2b)	{ $-\bar{\gamma}, \bar{\gamma}$ }	{ $\zeta, -1$ }	{ $i, -i$ }	1	1	0
(1/2, 3c)	{ $\gamma, -\bar{\gamma}, -i$ }	{ $\zeta, -1, \bar{\zeta}$ }	{ $i, -i, -i$ }	0	0	-2
(3/2, 3c)	{ $i, -\gamma, \bar{\gamma}$ }	{ $\zeta, -1, \bar{\zeta}$ }	{ $i, i, -i$ }	0	0	2

superconductors (TCS), unlike class A, AI, and AII insulators, are expressed in terms of Bogoliubov de-Gennes (BdG) Hamiltonians. The BdG Hamiltonian is typically given as follows,

$$H_{\text{BdG}}(\mathbf{k}) = \begin{pmatrix} H(\mathbf{k}) & \Delta(\mathbf{k}) \\ \Delta^\dagger(\mathbf{k}) & -H^*(-\mathbf{k}) \end{pmatrix}, \quad (32)$$

where $H(\mathbf{k})$ is the Hamiltonian encoding the band structure in the normal phase, and the BdG Hamiltonian $H_{\text{BdG}}(\mathbf{k})$ encodes the band structure for the superconducting phase, and $\Delta(\mathbf{k})$ denotes the gap function. Since class D TCSs must obey particle-hole symmetry, the BdG Hamiltonian in Eq. (32) satisfies $\Xi H_{\text{BdG}}(\mathbf{k}) \Xi^{-1} = -H_{\text{BdG}}(-\mathbf{k})$ with $\Delta^\dagger(-\mathbf{k}) = -\Delta^*(\mathbf{k})$, where $\Xi = \tau_1 K$ is the particle-hole operator, τ_1 is the Pauli matrix in the Nambu basis, and K is the complex conjugation operator. Consider a spatial symmetry $\chi = \{R_\chi | \delta_\chi\} \in G$, the momentum-space representation of which is given by $U_\chi(\mathbf{k})$. In order for the BdG Hamiltonian to be symmetric under χ , the following relations must be satisfied,

$$\begin{aligned} U_\chi(\mathbf{k}) H(\mathbf{k}) U_\chi^\dagger(\mathbf{k}) &= H(R_\chi \mathbf{k}), \\ U_\chi(\mathbf{k}) \Delta(\mathbf{k}) U_\chi^T(-\mathbf{k}) &= \Theta(\chi) \Delta(R_\chi \mathbf{k}), \end{aligned} \quad (33)$$

where a $U(1)$ phase factor $\Theta(\chi)$ takes one-dimensional representation of wallpaper or space group. This allows for $U_{\text{BdG}, \chi}(\mathbf{k}) H_{\text{BdG}}(\mathbf{k}) U_{\text{BdG}, \chi}^\dagger(\mathbf{k}) = H_{\text{BdG}}(R_\chi \mathbf{k})$ where $U_{\text{BdG}, \chi}(\mathbf{k})$ is the momentum-space representation of χ in the

Nambu basis. Here, $U_{\text{BdG},\chi}(\mathbf{k})$ is defined as follows,

$$U_{\text{BdG},\chi}(\mathbf{k}) = \begin{pmatrix} U_\chi(\mathbf{k}) & 0 \\ 0 & \Theta(\chi)U_\chi^*(-\mathbf{k}) \end{pmatrix} \quad (34)$$

which implies the following,

$$\Xi\chi\Xi^{-1} = \Theta^*(\chi)\chi \leftrightarrow \Xi U_{\text{BdG},\chi}^*(\mathbf{k})\Xi^\dagger = \Theta^*(\chi)U_{\text{BdG},\chi}(-\mathbf{k}) \quad (35)$$

According to Eqs. (33)-(35), $\Theta(\chi)$ determines the *pairing symmetry*, which is the symmetry associated with the gap function $\Delta(\mathbf{k})$. Both χ and $\Theta(\chi)$ determine the symmetries of the BdG Hamiltonian. For this work, we focus only on the trivial pairing symmetry for C_n rotations, where $\Theta(c_n(\mathbf{r}_o)) = 1$ and $[\Xi, c_n(\mathbf{r}_o)] = 0$. Thus, in Sec. VI, all class D results obtained are for TCSs with pairing symmetries that allow for commuting particle-hole and rotation operators.

Different values of $\Theta(\chi)$ can change the pairing symmetry of the BdG Hamiltonian, but it is not always possible to apply symmetry indicators to properly diagnose the bulk topological properties of the TCS for certain values of $\Theta(\chi)$ [5, 6]. However, if the bulk topology is symmetry-indicated for a particular non-trivial $\Theta(\chi)$, then it is possible to also express the bulk topology in terms of the fully traced TCMs. This can lead to an issue where the spatial symmetry χ and the particle-hole operator Ξ no longer commute as per Eq. (35) (although this can be partially resolved through a redefinition of the unitary operator for χ , e.g., see Ref. 7.) This implies that a broader characterization of the bulk topology in terms of the fully traced TCMs exists for class D TCSs for different pairing symmetries. For each pairing symmetry that exhibits symmetry-indicated bulk topology, the mapping between the fully traced TCMs and the momentum-space data (e.g., rotation invariants for C_n rotations) can be modified by properly incorporating the $U(1)$ phase factor $\Theta(\chi)$, which remains to be studied.

VI. MATRICES FOR MAPPINGS FOR EACH SYMMETRY CLASS AND C_n SYMMETRY

In this section, we derive the matrices $M_{\text{TCM} \leftarrow \text{MS}}^{(n)}$, $M_{\text{MS} \leftarrow \text{RSI}}^{(n)}$, and consequently, $M_{\text{TCM} \leftarrow \text{RSI}}^{(n)}$ for every C_n symmetry and symmetry class (classes A, AI, AII, and D). Then, using these matrices, we explain how to determine the bulk Chern number, bulk polarization, and sector charge in terms of the fully traced TCMs. The definitions of $\mathbf{v}_{\text{TCM}}^{(n)}$, $\mathbf{v}_{\text{MS}}^{(n)}$, and $\mathbf{v}_{\text{RSI}}^{(n)}$ are given by Eqs. (24)-(26), and (30). The results derived in this section only hold for lattices that satisfy the constraint given as,

$$\begin{aligned} C_2 : (N_1, N_2) &= (0, 0) \pmod{2} \\ C_4 : N &= 0 \pmod{2} \\ C_{n=3,6} : N &= 0 \pmod{n}. \end{aligned} \quad (36)$$

Note that the matrices $M_{\text{MS} \leftarrow \text{RSI}}^{(n)}$ only apply to symmetry classes A, AI, and AII, since atomic insulators fall under these symmetry classes. In this section, note that the expressions for the bulk polarization are stated as “ $\mathbf{P} = p_1 \mathbf{a}_1 + p_2 \mathbf{a}_2 \pmod{e}$ ”, which means $p_1 \pmod{e}$ and $p_2 \pmod{e}$.

1. C_2 symmetry

For a C_2 -symmetric system, the filling ν constrains the rotation invariants, the $m(\Gamma_p)$ irrep multiplicities, and the Wannier orbital irrep multiplicities to satisfy the following equation,

$$\nu = \sum_{p=1}^2 m(\Gamma_p) = \sum_W \sum_\ell n_W^{(\ell)} \rightarrow \sum_{p=1}^2 [X_p] = \sum_{p=1}^2 [Y_p] = \sum_{p=1}^2 [M_p] = 0 \quad (37)$$

Using Eq. (20) and Table I, we can determine the $M_{\text{TCM} \leftarrow \text{MS}}^{(2)}$ and $M_{\text{MS} \leftarrow \text{RSI}}^{(2)}$ matrices for symmetry classes A and AI pertaining to spinless electrons,

$$\begin{aligned} \mathbf{v}_{\text{TCM}}^{(2)} = M_{\text{TCM} \leftarrow \text{MS}}^{(2)} \mathbf{v}_{\text{MS}}^{(2)} &\rightarrow \begin{pmatrix} \nu \\ \langle c_2(\mathbf{x}_{1a}) \rangle_F \\ \langle c_2(\mathbf{x}_{1b}) \rangle_F \\ \langle c_2(\mathbf{x}_{1c}) \rangle_F \\ \langle c_2(\mathbf{x}_{1d}) \rangle_F \end{pmatrix} = \begin{pmatrix} 1 & 0 & 0 & 0 & 0 \\ -4 & 8 & 2 & 2 & 2 \\ 0 & 0 & -2 & 2 & -2 \\ 0 & 0 & 2 & -2 & -2 \\ 0 & 0 & -2 & -2 & 2 \end{pmatrix} \begin{pmatrix} \nu \\ m(\Gamma_1) \\ [X_1] \\ [Y_1] \\ [M_1] \end{pmatrix}, \\ \mathbf{v}_{\text{MS}}^{(2)} = M_{\text{MS} \leftarrow \text{RSI}}^{(2)} \mathbf{v}_{\text{RSI}}^{(2)} &\rightarrow \begin{pmatrix} \nu \\ m(\Gamma_1) \\ [X_1] \\ [Y_1] \\ [M_1] \end{pmatrix} = \begin{pmatrix} 1 & 0 & 0 & 0 & 0 \\ 1/2 & -1/2 & -1/2 & -1/2 & -1/2 \\ 0 & 0 & 1 & 0 & 1 \\ 0 & 0 & 0 & 1 & 1 \\ 0 & 0 & 1 & 1 & 0 \end{pmatrix} \begin{pmatrix} \nu \\ \delta_{1a} \\ \delta_{1b} \\ \delta_{1c} \\ \delta_{1d} \end{pmatrix}. \end{aligned} \quad (38)$$

From Eq. (38), the matrix $M_{\text{MS} \leftarrow \text{TCM}}^{(2)} = (M_{\text{TCM} \leftarrow \text{MS}}^{(2)})^{-1}$ can be computed and the following relations can be determined,

$$\begin{aligned} 2\nu + \frac{1}{2} \langle c_2(\mathbf{x}_{1a}) \rangle_F &= 4m(\Gamma_1) + [X_1] + [Y_1] + [M_1], \\ \frac{1}{2} \langle c_2(\mathbf{x}_{1b}) \rangle_F &= -[X_1] + [Y_1] - [M_1], \\ \frac{1}{2} \langle c_2(\mathbf{x}_{1c}) \rangle_F &= [X_1] - [Y_1] - [M_1], \\ \frac{1}{2} \langle c_2(\mathbf{x}_{1d}) \rangle_F &= -[X_1] - [Y_1] + [M_1], \end{aligned} \quad (39)$$

which leads to the relation

$$\mathcal{C} = [X_1] + [Y_1] + [M_1] = \frac{1}{2} \langle c_2(\mathbf{x}_W) \rangle_F \pmod{2} \text{ for } W \in \{1a, 1b, 1c, 1d\} \quad (40)$$

for the Chern number for symmetry classes A and D pertaining to spinless electrons. The matrix $M_{\text{RSI} \leftarrow \text{TCM}}^{(2)} = (M_{\text{TCM} \leftarrow \text{RSI}}^{(2)})^{-1}$ can also be computed and the following relations can be determined,

$$\delta_W = -\frac{1}{4} \langle c_2(\mathbf{x}_W) \rangle_F \text{ for } W \in \{1a, 1b, 1c, 1d\}. \quad (41)$$

Note that for atomic insulators, the Chern number must be zero, which enforces a constraint between the rotation invariants as $[X_1] = -([Y_1] + [M_1]) \pmod{2}$. In terms of RSIs and TCMs, the bulk polarization and the sector charge can be expressed as follows (for symmetry classes A and AI pertaining to spinless electrons),

$$\begin{aligned} \mathbf{P} &= \frac{e}{2} [(\delta_{1b} + \delta_{1d}) \mathbf{a}_1 + (\delta_{1c} + \delta_{1d}) \mathbf{a}_2] \pmod{e} \\ &= -\frac{e}{8} [(\langle c_2(\mathbf{x}_{1b}) \rangle_F + \langle c_2(\mathbf{x}_{1d}) \rangle_F) \mathbf{a}_1 + (\langle c_2(\mathbf{x}_{1c}) \rangle_F + \langle c_2(\mathbf{x}_{1d}) \rangle_F) \mathbf{a}_2] \pmod{e}, \\ Q_{\text{sector}} &= -\frac{e}{2} \delta_{1d} = -\frac{e}{8} \langle c_2(\mathbf{x}_{1d}) \rangle_F \pmod{e}. \end{aligned} \quad (42)$$

For symmetry class A pertaining to spin-1/2 electrons, the matrix $M_{\text{MS} \leftarrow \text{RSI}}^{(2)}$ is the same as determined by Table I, but the matrix $M_{\text{TCM} \leftarrow \text{MS}}^{(2)}$ is

$$\mathbf{v}_{\text{TCM}}^{(2)} = M_{\text{TCM} \leftarrow \text{MS}}^{(2)} \mathbf{v}_{\text{MS}}^{(2)} \rightarrow \begin{pmatrix} \nu \\ \langle c_2(\mathbf{x}_{1a}) \rangle_F \\ \langle c_2(\mathbf{x}_{1b}) \rangle_F \\ \langle c_2(\mathbf{x}_{1c}) \rangle_F \\ \langle c_2(\mathbf{x}_{1d}) \rangle_F \end{pmatrix} = \begin{pmatrix} 1 & 0 & 0 & 0 & 0 \\ -4i & 8i & 2i & 2i & 2i \\ 0 & 0 & -2i & 2i & -2i \\ 0 & 0 & 2i & -2i & -2i \\ 0 & 0 & -2i & -2i & 2i \end{pmatrix} \begin{pmatrix} \nu \\ \delta_{1a} \\ \delta_{1b} \\ \delta_{1c} \\ \delta_{1d} \end{pmatrix}, \quad (43)$$

which implies the following relations

$$\begin{aligned} 2i\nu - \frac{i}{2} \langle c_2(\mathbf{x}_{1a}) \rangle_F &= 4m(\Gamma_1) + [X_1] + [Y_1] + [M_1], \\ -\frac{i}{2} \langle c_2(\mathbf{x}_{1b}) \rangle_F &= -[X_1] + [Y_1] - [M_1], \\ -\frac{i}{2} \langle c_2(\mathbf{x}_{1c}) \rangle_F &= [X_1] - [Y_1] - [M_1], \\ -\frac{i}{2} \langle c_2(\mathbf{x}_{1d}) \rangle_F &= -[X_1] - [Y_1] + [M_1]. \end{aligned} \quad (44)$$

This means the Chern number for symmetry classes A and D pertaining to spin-1/2 electrons is

$$\mathcal{C} = -\frac{i}{2} \langle c_2(\mathbf{x}_W) \rangle_F \pmod{2}. \quad (45)$$

Computing $M_{\text{RSI} \leftarrow \text{TCM}}^{(2)} = (M_{\text{TCM} \leftarrow \text{RSI}}^{(2)})^{-1}$ from Eq. (43) yields the following relation,

$$\delta_W = \frac{i}{4} \langle c_2(\mathbf{x}_W) \rangle_F \text{ for } W \in \{1a, 1b, 1c, 1d\} \quad (46)$$

Thus, the bulk polarization and the sector charge can be expressed as follows for symmetry class A pertaining to spin-1/2 electrons,

$$\begin{aligned} \mathbf{P} &= \frac{ie}{8} [(\langle c_2(\mathbf{x}_{1b}) \rangle_F + \langle c_2(\mathbf{x}_{1d}) \rangle_F) \mathbf{a}_1 + (\langle c_2(\mathbf{x}_{1c}) \rangle_F + \langle c_2(\mathbf{x}_{1d}) \rangle_F) \mathbf{a}_2] \pmod{e}, \\ Q_{\text{sector}} &= \frac{ie}{8} \langle c_2(\mathbf{x}_{1d}) \rangle_F \pmod{e}. \end{aligned} \quad (47)$$

For symmetry class AII, time-reversal symmetry imposes the constraint that $[X_p] = [Y_p] = [M_p] = 0$ for $p \in \{1, 2\}$. This also implies that

$$\delta_W = 0 \quad \text{and} \quad \langle c_2(\mathbf{x}_W) \rangle_F = 0 \quad \text{for } W \in \{1a, 1b, 1c, 1d\}, \quad (48)$$

as a consequence of Kramers' theorem, which means $\mathbf{P} = \mathbf{0} \pmod{e}$ and $Q_{\text{sector}} = 0 \pmod{e}$ for symmetry class AII.

2. C_3 symmetry

For a C_3 -symmetric system, the filling ν constrains the rotation invariants, the $m(\Gamma_p)$ irrep multiplicities, and the Wannier orbital irrep multiplicities to satisfy the following equation,

$$\nu = \sum_{p=1}^3 m(\Gamma_p) = \sum_W \sum_{\ell} n_W^{(\ell)} \rightarrow \sum_{p=1}^3 [K_p] = \sum_{p=1}^3 [K'_p] = 0 \quad (49)$$

Using Eq. (20) and Table II, we can determine the $M_{\text{TCM} \leftarrow \text{MS}}^{(3)}$ and $M_{\text{MS} \leftarrow \text{RSI}}^{(3)}$ matrices for symmetry class A pertaining to spinless electrons,

$$\begin{pmatrix} \nu \\ \langle c_3(\mathbf{x}_{1a}) \rangle_F \\ \langle c_3(\mathbf{x}_{1b}) \rangle_F \\ \langle c_3(\mathbf{x}_{1c}) \rangle_F \\ \langle (c_3(\mathbf{x}_{1a}))^{-1} \rangle_F \\ \langle (c_3(\mathbf{x}_{1b}))^{-1} \rangle_F \\ \langle (c_3(\mathbf{x}_{1c}))^{-1} \rangle_F \end{pmatrix} = \begin{pmatrix} 1 & 0 & 0 & 0 & 0 & 0 & 0 \\ 3\bar{\omega} & 3(1-\bar{\omega}) & 3(\omega-\bar{\omega}) & 1-\bar{\omega} & \omega-\bar{\omega} & 1-\bar{\omega} & \omega-\bar{\omega} \\ 0 & 0 & 0 & -(\omega-\bar{\omega}) & -(\omega-1) & \omega-1 & -(1-\bar{\omega}) \\ 0 & 0 & 0 & \omega-1 & -(1-\bar{\omega}) & -(\omega-\bar{\omega}) & -(\omega-1) \\ 3\omega & -3(\omega-1) & -3(\omega-\bar{\omega}) & -(\omega-1) & -(\omega-\bar{\omega}) & -(\omega-1) & -(\omega-\bar{\omega}) \\ 0 & 0 & 0 & \omega-\bar{\omega} & 1-\bar{\omega} & -(1-\bar{\omega}) & \omega-1 \\ 0 & 0 & 0 & -(1-\bar{\omega}) & \omega-1 & \omega-\bar{\omega} & 1-\bar{\omega} \end{pmatrix} \begin{pmatrix} \nu \\ m(\Gamma_1) \\ m(\Gamma_2) \\ [K_1] \\ [K_2] \\ [K'_1] \\ [K'_2] \end{pmatrix},$$

$$\begin{pmatrix} \nu \\ m(\Gamma_1) \\ m(\Gamma_2) \\ [K_1] \\ [K_2] \\ [K'_1] \\ [K'_2] \end{pmatrix} = \begin{pmatrix} 1 & 0 & 0 & 0 & 0 & 0 & 0 \\ 1/3 & -1/3 & -1/3 & -1/3 & -1/3 & -1/3 & -1/3 \\ 1/3 & 2/3 & -1/3 & 2/3 & -1/3 & 2/3 & -1/3 \\ 0 & 0 & 0 & 0 & 1 & 1 & 0 \\ 0 & 0 & 0 & -1 & 0 & -1 & 1 \\ 0 & 0 & 0 & 1 & 0 & 0 & 1 \\ 0 & 0 & 0 & -1 & 1 & -1 & 0 \end{pmatrix} \begin{pmatrix} \nu \\ \delta_{1a}^{(1)} \\ \delta_{1a}^{(2)} \\ \delta_{1b}^{(1)} \\ \delta_{1b}^{(2)} \\ \delta_{1c}^{(1)} \\ \delta_{1c}^{(2)} \end{pmatrix}, \quad (50)$$

where $\omega = e^{2\pi i/3}$ and $\bar{\omega} = e^{-2\pi i/3}$. Note that the entries of the rows of $M_{\text{TCM} \leftarrow \text{MS}}^{(3)}$ corresponding to $\langle (c_3(\mathbf{x}_W))^{-1} \rangle_F$ are complex conjugates of the entries of the rows corresponding to $\langle c_3(\mathbf{x}_W) \rangle_F$, for $W \in \{1a, 1b, 1c\}$ (e.g., $\langle (c_3(\mathbf{x}_W)) \rangle_F^* = \langle (c_3(\mathbf{x}_W))^{-1} \rangle_F$). From Eq. (50) and computing $M_{\text{MS} \leftarrow \text{TCM}}^{(3)} = (M_{\text{TCM} \leftarrow \text{MS}}^{(3)})^{-1}$, the following relations can be determined,

$$\begin{aligned} (\omega-\bar{\omega})^{-1}(\langle c_3(\mathbf{x}_{1a}) \rangle_F - \langle (c_3(\mathbf{x}_{1a}))^{-1} \rangle_F) &= -3\nu + 3m(\Gamma_1) + 6m(\Gamma_2) + [K_1] + 2[K_2] + [K'_1] + 2[K'_2], \\ (\omega-\bar{\omega})^{-1}(\langle c_3(\mathbf{x}_{1b}) \rangle_F - \langle (c_3(\mathbf{x}_{1b}))^{-1} \rangle_F) &= -2[K_1] - [K_2] + [K'_1] - [K'_2], \\ (\omega-\bar{\omega})^{-1}(\langle c_3(\mathbf{x}_{1c}) \rangle_F - \langle (c_3(\mathbf{x}_{1c}))^{-1} \rangle_F) &= [K_1] - [K_2] - 2[K'_1] - [K'_2], \end{aligned} \quad (51)$$

which leads to the relation

$$\mathcal{C} = [K_1] + 2[K_2] + [K'_1] + 2[K'_2] = \frac{2}{\sqrt{3}} \text{Im}[\langle c_3(\mathbf{x}_W) \rangle_F] \pmod{3} \text{ for } W \in \{1a, 1b, 1c\} \quad (52)$$

for the Chern number for spinless electron systems in symmetry class A. The matrix $M_{\text{RSI} \leftarrow \text{TCM}}^{(3)} = (M_{\text{TCM} \leftarrow \text{RSI}}^{(3)})^{-1}$ can also be computed and the following relations can be determined,

$$\begin{aligned} \delta_W^{(1)} &= \frac{i}{3\sqrt{3}} \omega \langle c_3(\mathbf{x}_W) \rangle_F + \frac{1}{9} (\omega-1) \langle (c_3(\mathbf{x}_W)) \rangle_F^*, \\ \delta_W^{(2)} &= \frac{1}{9} (\omega-1) \langle c_3(\mathbf{x}_W) \rangle_F + \frac{i}{3\sqrt{3}} \omega \langle (c_3(\mathbf{x}_W)) \rangle_F^*, \end{aligned} \quad (53)$$

for $W \in \{1a, 1b, 1c\}$. Note that for atomic insulators, the Chern number must be zero, which enforces a constraint between the rotation invariants as $[K_1] + [K'_1] = [K_2] + [K'_2] \pmod{3}$. In terms of RSIs and TCMs, the bulk polarization and the sector charge can be expressed as follows (for symmetry class A pertaining to spinless electrons),

$$\mathbf{P} = \frac{e}{3} (\delta_{1b}^{(1)} + \delta_{1b}^{(2)} - \delta_{1c}^{(1)} - \delta_{1c}^{(2)}) (\mathbf{a}_1 + \mathbf{a}_2) = -\frac{2e}{3} (\delta_{1b}^{(1)} + \delta_{1b}^{(2)} - \delta_{1c}^{(1)} - \delta_{1c}^{(2)}) (\mathbf{a}_1 + \mathbf{a}_2)$$

$$\begin{aligned}
&= \frac{4e}{9} \text{Re}[\langle c_3(\mathbf{x}_{1b}) \rangle_F - \langle c_3(\mathbf{x}_{1c}) \rangle_F](\mathbf{a}_1 + \mathbf{a}_2) \pmod{e}, \\
Q_{\text{sector}} &= \frac{e}{3}(\delta_{1a}^{(1)} + \delta_{1a}^{(2)}) = -\frac{2e}{3}(\delta_{1a}^{(1)} + \delta_{1a}^{(2)}) = \frac{4e}{9} \text{Re}[\langle c_3(\mathbf{x}_{1a}) \rangle_F] \pmod{e}.
\end{aligned} \tag{54}$$

For symmetry class AI systems, time-reversal symmetry introduces the following constraints on the rotation invariants, $[K_2] = -([K'_1] + [K'_2])$ and $[K'_2] = -([K_1] + [K_2])$, which implies $[K_1] = [K'_1]$. Furthermore, time-reversal symmetry also imposes a constraint that $m(\Gamma_2) = m(\Gamma_3)$, which implies $\nu = m(\Gamma_1) + 2m(\Gamma_2)$, as well as $\delta_W^{(1)} = \delta_W^{(2)} \equiv \delta_W$ which also implies $\langle c_3(\mathbf{x}_W) \rangle_F = \langle (c_3(\mathbf{x}_W))^{-1} \rangle_F = \langle \langle c_3(\mathbf{x}_W) \rangle_F \rangle^*$ for all $W \in \{1a, 1b, 1c\}$. Therefore, to evaluate the matrices for symmetry class AI, we must incorporate the additional constraints imposed by the symmetries and modify $\mathbf{v}_{\text{TCM}}^{(3)}$, $\mathbf{v}_{\text{MS}}^{(3)}$, and $\mathbf{v}_{\text{RSI}}^{(3)}$ to include only the independent set of quantities for each,

$$\begin{aligned}
\mathbf{v}_{\text{TCM}}^{(3)} &= (\nu, \langle c_3(\mathbf{x}_{1a}) \rangle_F, \langle c_3(\mathbf{x}_{1b}) \rangle_F, \langle c_3(\mathbf{x}_{1c}) \rangle_F)^T, \\
\mathbf{v}_{\text{MS}}^{(3)} &= (\nu, m(\Gamma_1), [K_1], [K_2])^T, \\
\mathbf{v}_{\text{RSI}}^{(3)} &= (\nu, \delta_{1a}, \delta_{1b}, \delta_{1c})^T.
\end{aligned} \tag{55}$$

Thus, $M_{\text{TCM} \leftarrow \text{MS}}^{(3)}$ and $M_{\text{MS} \leftarrow \text{RSI}}^{(3)}$ for symmetry class AI are given as follows,

$$\begin{aligned}
\begin{pmatrix} \nu \\ \langle c_3(\mathbf{x}_{1a}) \rangle_F \\ \langle c_3(\mathbf{x}_{1b}) \rangle_F \\ \langle c_3(\mathbf{x}_{1c}) \rangle_F \end{pmatrix} &= \begin{pmatrix} 1 & 0 & 0 & 0 \\ -3/2 & 9/2 & 3 & 0 \\ 0 & 0 & 0 & 3 \\ 0 & 0 & -3 & -3 \end{pmatrix} \begin{pmatrix} \nu \\ m(\Gamma_1) \\ [K_1] \\ [K_2] \end{pmatrix}, \\
\begin{pmatrix} \nu \\ m(\Gamma_1) \\ [K_1] \\ [K_2] \end{pmatrix} &= \begin{pmatrix} 1 & 0 & 0 & 0 \\ 1/3 & -2/3 & -2/3 & -2/3 \\ 0 & 0 & 1 & 1 \\ 0 & 0 & -1 & 0 \end{pmatrix} \begin{pmatrix} \nu \\ \delta_{1a} \\ \delta_{1b} \\ \delta_{1c} \end{pmatrix}.
\end{aligned} \tag{56}$$

Computing $M_{\text{RSI} \leftarrow \text{TCM}}^{(3)} = (M_{\text{TCM} \leftarrow \text{RSI}}^{(3)})^{-1}$ yields the following relation,

$$\delta_W = -\frac{1}{3} \langle c_3(\mathbf{x}_W) \rangle_F \text{ for } W \in \{1a, 1b, 1c\} \tag{57}$$

which means the bulk polarization and the sector charge for symmetry class AI are,

$$\begin{aligned}
\mathbf{P} &= \frac{2e}{3}(\delta_{1b} - \delta_{1c})(\mathbf{a}_1 + \mathbf{a}_2) = -\frac{e}{3}(\delta_{1b} - \delta_{1c})(\mathbf{a}_1 + \mathbf{a}_2) = \frac{e}{9}(\langle c_3(\mathbf{x}_{1b}) \rangle_F - \langle c_3(\mathbf{x}_{1c}) \rangle_F)(\mathbf{a}_1 + \mathbf{a}_2) \pmod{e}, \\
Q_{\text{sector}} &= \frac{2e}{3}\delta_{1a} = -\frac{e}{3}\delta_{1a} = \frac{e}{9}\langle c_3(\mathbf{x}_{1a}) \rangle_F \pmod{e}.
\end{aligned} \tag{58}$$

Taking the original definitions of $\mathbf{v}_{\text{TCM}}^{(3)}$, $\mathbf{v}_{\text{MS}}^{(3)}$, and $\mathbf{v}_{\text{RSI}}^{(3)}$ given by Eqs. (25), (26), and (30), one can construct the matrix $M_{\text{TCM} \leftarrow \text{MS}}^{(3)}$ once again using Eq. (20) and Table II for symmetry class A systems pertaining to spin-1/2 electrons,

$$\begin{pmatrix} \nu \\ \langle c_3(\mathbf{x}_{1a}) \rangle_F \\ \langle c_3(\mathbf{x}_{1b}) \rangle_F \\ \langle c_3(\mathbf{x}_{1c}) \rangle_F \\ \langle (c_3(\mathbf{x}_{1a}))^{-1} \rangle_F \\ \langle (c_3(\mathbf{x}_{1b}))^{-1} \rangle_F \\ \langle (c_3(\mathbf{x}_{1c}))^{-1} \rangle_F \end{pmatrix} = \begin{pmatrix} 1 & 0 & 0 & 0 & 0 & 0 & 0 \\ 3\bar{\zeta} & 3(\zeta - \bar{\zeta}) & -3(1 + \bar{\zeta}) & \zeta - \bar{\zeta} & -(1 + \bar{\zeta}) & \zeta - \bar{\zeta} & -(1 + \bar{\zeta}) \\ 0 & 0 & 0 & 1 + \bar{\zeta} & 1 + \zeta & -(1 + \zeta) & -(\zeta - \bar{\zeta}) \\ 0 & 0 & 0 & -(1 + \zeta) & -(\zeta - \bar{\zeta}) & 1 + \bar{\zeta} & 1 + \zeta \\ 3\zeta & -3(\zeta - \bar{\zeta}) & -3(1 + \zeta) & -(\zeta - \bar{\zeta}) & -(1 + \zeta) & -(\zeta - \bar{\zeta}) & -(1 + \zeta) \\ 0 & 0 & 0 & 1 + \zeta & 1 + \bar{\zeta} & -(1 + \bar{\zeta}) & \zeta - \bar{\zeta} \\ 0 & 0 & 0 & -(1 + \bar{\zeta}) & \zeta - \bar{\zeta} & 1 + \zeta & 1 + \bar{\zeta} \end{pmatrix} \begin{pmatrix} \nu \\ m(\Gamma_1) \\ m(\Gamma_2) \\ [K_1] \\ [K_2] \\ [K'_1] \\ [K'_2] \end{pmatrix}, \quad (59)$$

where $\zeta = e^{\pi i/3}$ and $\bar{\zeta} = e^{-\pi i/3}$, and $M_{\text{MS} \leftarrow \text{RSI}}^{(3)}$ is identical to Eq. (50). From Eq. (59), the following relations can be determined,

$$\begin{aligned} (\bar{\zeta} - \zeta)^{-1} (\langle c_3(\mathbf{x}_{1a}) \rangle_F - \langle (c_3(\mathbf{x}_{1a}))^{-1} \rangle_F) &= 3\nu - 6m(\Gamma_1) - 3m(\Gamma_2) - 2[K_1] - [K_2] - 2[K'_1] - [K'_2], \\ (\bar{\zeta} - \zeta)^{-1} (\langle c_3(\mathbf{x}_{1b}) \rangle_F - \langle (c_3(\mathbf{x}_{1b}))^{-1} \rangle_F) &= [K_1] - [K_2] + [K'_1] + 2[K'_2], \\ (\bar{\zeta} - \zeta)^{-1} (\langle c_3(\mathbf{x}_{1c}) \rangle_F - \langle (c_3(\mathbf{x}_{1c}))^{-1} \rangle_F) &= [K_1] + 2[K_2] + [K'_1] - [K'_2], \end{aligned} \quad (60)$$

which leads to the relation

$$\mathcal{C} = [K_1] + 2[K_2] + [K'_1] + 2[K'_2] = -\frac{2}{\sqrt{3}} \text{Im}[\langle c_3(\mathbf{x}_W) \rangle_F] \pmod{3} \text{ for } W \in \{1a, 1b, 1c\} \quad (61)$$

for the Chern number for spin-1/2 electron systems in symmetry class A. The matrix $M_{\text{RSI} \leftarrow \text{TCM}}^{(3)} = (M_{\text{TCM} \leftarrow \text{RSI}}^{(3)})^{-1}$ can also be computed and the following relations can be determined,

$$\begin{aligned} \delta_W^{(1)} &= \frac{1}{9}(\omega - 1)\langle c_3(\mathbf{x}_W) \rangle_F + \frac{1}{9}(\bar{\omega} - 1)\langle (c_3(\mathbf{x}_W))^{-1} \rangle_F^*, \\ \delta_W^{(2)} &= \frac{i}{3\sqrt{3}}(\langle c_3(\mathbf{x}_W) \rangle_F - \langle (c_3(\mathbf{x}_W))^{-1} \rangle_F^*), \end{aligned} \quad (62)$$

for $W \in \{1a, 1b, 1c\}$. In terms of the TCMs, the bulk polarization and the sector charge can be expressed as follows (for symmetry class A pertaining to spin-1/2 electrons),

$$\begin{aligned} \mathbf{P} &= \frac{e}{3}(\delta_{1b}^{(1)} + \delta_{1b}^{(2)} - \delta_{1c}^{(1)} - \delta_{1c}^{(2)})(\mathbf{a}_1 + \mathbf{a}_2) = \frac{e}{3}(-2\delta_{1b}^{(1)} + \delta_{1b}^{(1)} + 2\delta_{1c}^{(1)} - \delta_{1c}^{(2)})(\mathbf{a}_1 + \mathbf{a}_2) \\ &= \frac{2e}{9} \text{Re}[\langle c_3(\mathbf{x}_{1b}) \rangle_F - \langle c_3(\mathbf{x}_{1c}) \rangle_F](\mathbf{a}_1 + \mathbf{a}_2) \pmod{e}, \\ Q_{\text{sector}} &= \frac{e}{3}(\delta_{1a}^{(1)} + \delta_{1a}^{(2)}) = \frac{e}{3}(-2\delta_{1a}^{(1)} + \delta_{1a}^{(2)}) = \frac{2e}{9} \text{Re}[\langle c_3(\mathbf{x}_{1a}) \rangle_F] \pmod{e}. \end{aligned} \quad (63)$$

For symmetry class AII systems, time-reversal symmetry introduces the following constraints on the rotation invariants, $[K_1] = -([K'_1] + [K'_2])$ and $[K'_1] = -([K_1] + [K_2])$, which implies $[K_2] = [K'_2]$. Furthermore, time-reversal symmetry also imposes a constraint $m(\Gamma_1) = m(\Gamma_3)$, which implies $\nu = 2m(\Gamma_1) + m(\Gamma_2)$, as well as $\delta_W^{(2)} = 0$ which therefore implies $\delta_W^{(1)} \equiv \delta_W$. As expected, $\langle c_3(\mathbf{x}_W) \rangle_F = \langle (c_3(\mathbf{x}_W))^{-1} \rangle_F = (\langle c_3(\mathbf{x}_W) \rangle_F)^*$ for all $W \in \{1a, 1b, 1c\}$. To evaluate the matrices for symmetry class AII, we will use the modified definition of $\mathbf{v}_{\text{TCM}}^{(3)}$, $\mathbf{v}_{\text{MS}}^{(3)}$ and $\mathbf{v}_{\text{RSI}}^{(3)}$ given by Eq. (55). Thus, $M_{\text{TCM} \leftarrow \text{MS}}^{(3)}$ and $M_{\text{MS} \leftarrow \text{RSI}}^{(3)}$ for symmetry class AII are given as follows,

$$\begin{pmatrix} \nu \\ \langle c_3(\mathbf{x}_{1a}) \rangle_F \\ \langle c_3(\mathbf{x}_{1b}) \rangle_F \\ \langle c_3(\mathbf{x}_{1c}) \rangle_F \end{pmatrix} = \begin{pmatrix} 1 & 0 & 0 & 0 \\ -3 & 9 & 0 & -3 \\ 0 & 0 & 3 & 3 \\ 0 & 0 & -3 & 0 \end{pmatrix} \begin{pmatrix} \nu \\ m(\Gamma_1) \\ [K_1] \\ [K_2] \end{pmatrix},$$

$$\begin{pmatrix} \nu \\ m(\Gamma_1) \\ [K_1] \\ [K_2] \end{pmatrix} = \begin{pmatrix} 1 & 0 & 0 & 0 \\ 1/3 & -1/3 & -1/3 & -1/3 \\ 0 & 0 & 0 & 1 \\ 0 & 0 & -1 & -1 \end{pmatrix} \begin{pmatrix} \nu \\ \delta_{1a} \\ \delta_{1b} \\ \delta_{1c} \end{pmatrix}. \quad (64)$$

Computing $M_{\text{RSI} \leftarrow \text{TCM}}^{(3)} = (M_{\text{TCM} \leftarrow \text{RSI}}^{(3)})^{-1}$ yields the same relations between the RSIs and TCMS given by Eq. (57). Because $\delta_W^{(2)} = 0$ and $\delta_W \equiv \delta_W^{(1)}$, this implies that the bulk polarization and the sector charge for symmetry class AII are,

$$\begin{aligned} \mathbf{P} &= \frac{e}{3}(\delta_{1b} - \delta_{1c})(\mathbf{a}_1 + \mathbf{a}_2) = -\frac{2e}{3}(\delta_{1b} - \delta_{1c})(\mathbf{a}_1 + \mathbf{a}_2) = \frac{2e}{9}(\langle c_3(\mathbf{x}_{1b}) \rangle_F - \langle c_3(\mathbf{x}_{1c}) \rangle_F)(\mathbf{a}_1 + \mathbf{a}_2) \pmod{e}, \\ Q_{\text{sector}} &= \frac{e}{3}(\delta_{1a}^{(1)} + \delta_{1a}^{(2)}) = -\frac{2e}{3}(\delta_{1a}^{(1)} + \delta_{1a}^{(2)}) = \frac{2e}{9}\langle c_3(\mathbf{x}_{1a}) \rangle_F \pmod{e}. \end{aligned} \quad (65)$$

Finally, for symmetry class D systems, we consider both spinless and spin-1/2 electron systems. For both systems, particle-hole symmetry will introduce constraints on the rotation invariants. Therefore, similar to the approach taken for symmetry classes AI and AII, to evaluate the matrices for symmetry class D, we once again incorporate the additional constraints imposed by the symmetries and modify $\mathbf{v}_{\text{TCM}}^{(3)}$ and $\mathbf{v}_{\text{MS}}^{(3)}$ (we do not consider $\mathbf{v}_{\text{RSI}}^{(3)}$ because symmetry class D does not support atomic insulators) to include only the independent set of quantities for each,

$$\begin{aligned} \mathbf{v}_{\text{TCM}}^{(3)} &= (\nu, \langle c_3(\mathbf{x}_{1a}) \rangle_F, \langle c_3(\mathbf{x}_{1b}) \rangle_F, \langle c_3(\mathbf{x}_{1c}) \rangle_F, \langle (c_3(\mathbf{x}_{1a}))^{-1} \rangle_F)^T, \\ \mathbf{v}_{\text{MS}}^{(3)} &= (\nu, m(\Gamma_1), m(\Gamma_2), [K_1], [K_2])^T. \end{aligned} \quad (66)$$

For spinless systems, particle-hole symmetry introduces the following constraints on the rotation invariants, $[K_2] = [K'_1] + [K'_2]$ and $[K'_2] = [K_1] + [K_2]$ which implies $[K_1] = -[K'_1]$. Furthermore, using Eq. (20), it follows that $\langle c_3(\mathbf{x}_W) \rangle_F = -\langle (c_3(\mathbf{x}_W))^{-1} \rangle_F = -\langle (c_3(\mathbf{x}_W)) \rangle_F^*$ only for $W \in \{1b, 1c\}$. Thus, $M_{\text{TCM} \leftarrow \text{MS}}^{(3)}$ for symmetry class D for spinless electrons is given as follows,

$$\begin{pmatrix} \nu \\ \langle c_3(\mathbf{x}_{1a}) \rangle_F \\ \langle c_3(\mathbf{x}_{1b}) \rangle_F \\ \langle c_3(\mathbf{x}_{1c}) \rangle_F \\ \langle (c_3(\mathbf{x}_{1a}))^{-1} \rangle_F \end{pmatrix} = \begin{pmatrix} 1 & 0 & 0 & 0 & 0 \\ 3\bar{\omega} & 3(1 - \bar{\omega}) & 3(\omega - \bar{\omega}) & \omega - \bar{\omega} & 2(\omega - \bar{\omega}) \\ 0 & 0 & 0 & -2(\omega - \bar{\omega}) & -(\omega - \bar{\omega}) \\ 0 & 0 & 0 & \omega - \bar{\omega} & -(\omega - \bar{\omega}) \\ 3\omega & -3(\omega - 1) & -3(\omega - \bar{\omega}) & -(\omega - \bar{\omega}) & -2(\omega - \bar{\omega}) \end{pmatrix} \begin{pmatrix} \nu \\ m(\Gamma_1) \\ m(\Gamma_2) \\ [K_1] \\ [K_2] \end{pmatrix} \quad (67)$$

From Eq. (67), the same relations as Eq. (51) can be obtained, with the additional relations $[K'_2] = [K_1] + [K_2]$, $[K'_1] = -[K_1]$, and $\langle c_3(\mathbf{x}_W) \rangle_F = -\langle (c_3(\mathbf{x}_W))^{-1} \rangle_F = -\langle (c_3(\mathbf{x}_W)) \rangle_F^*$ for $W \in \{1b, 1c\}$. Thus, the Chern number for symmetry class D pertaining to spinless electrons is equivalent to the Chern number for symmetry class for spinless electrons given by Eq. (52) (note that because $\text{Re}[\langle c_3(\mathbf{x}_W) \rangle_F] = 0$ for $W \in \{1b, 1c\}$, the expression for the Chern number can be further simplified). Similarly, for spin-1/2 systems, particle-hole symmetry introduces the following constraints on the rotation invariants, $[K_1] = [K'_1] + [K'_2]$ and $[K'_1] = [K_1] + [K_2]$ which implies $[K_2] = -[K'_2]$. The same constraint of $\langle c_3(\mathbf{x}_W) \rangle_F = -\langle (c_3(\mathbf{x}_W))^{-1} \rangle_F = -\langle (c_3(\mathbf{x}_W)) \rangle_F^*$ also applies for $W \in \{1b, 1c\}$. Thus, $M_{\text{TCM} \leftarrow \text{MS}}^{(3)}$ for symmetry class D is given as follows,

$$\begin{pmatrix} \nu \\ \langle c_3(\mathbf{x}_{1a}) \rangle_F \\ \langle c_3(\mathbf{x}_{1b}) \rangle_F \\ \langle c_3(\mathbf{x}_{1c}) \rangle_F \\ \langle (c_3(\mathbf{x}_{1a}))^{-1} \rangle_F \end{pmatrix} = \begin{pmatrix} 1 & 0 & 0 & 0 & 0 \\ 3\bar{\zeta} & 3(\zeta - \bar{\zeta}) & -3(1 + \bar{\zeta}) & 2(\zeta - \bar{\zeta}) & \zeta - \bar{\zeta} \\ 0 & 0 & 0 & -(\zeta - \bar{\zeta}) & \zeta - \bar{\zeta} \\ 0 & 0 & 0 & -(\zeta - \bar{\zeta}) & -2(\zeta - \bar{\zeta}) \\ 3\zeta & -3(\zeta - \bar{\zeta}) & -3(1 + \zeta) & -2(\zeta - \bar{\zeta}) & -(\zeta - \bar{\zeta}) \end{pmatrix} \begin{pmatrix} \nu \\ m(\Gamma_1) \\ m(\Gamma_2) \\ [K_1] \\ [K_2] \end{pmatrix} \quad (68)$$

From Eq. (68), the same relations as Eq. (60) can be obtained, with the additional relations $[K'_1] = [K_1] + [K_2]$, $[K'_2] = -[K_2]$, and $\langle c_3(\mathbf{x}_W) \rangle_F = -\langle (c_3(\mathbf{x}_W))^{-1} \rangle_F = -\langle (c_3(\mathbf{x}_W)) \rangle_F^*$ for $W \in \{1b, 1c\}$. Thus, the Chern number for symmetry class D for spin-1/2 electrons is equivalent to the Chern number for symmetry class A for spin-1/2 electrons given by Eq. (61) (note that because $\text{Re}[\langle c_3(\mathbf{x}_W) \rangle_F] = 0$ for $W \in \{1b, 1c\}$, the expression for the Chern number can be further simplified).

3. C_4 symmetry

For a C_4 -symmetric system, the filling ν constrains the rotation invariants, the $m(\Gamma_p)$ irrep multiplicities, and the Wannier orbital irrep multiplicities to satisfy the following equation,

$$\nu = \sum_{p=1}^4 m(\Gamma_p) = \sum_W \sum_{\ell} M_W n_W^{(\ell)} \rightarrow \sum_{p=1}^2 [X_p] = \sum_{p=1}^4 [M_p] = 0 \quad (69)$$

where $M_{1a} = M_{1b} = 1$ and $M_{2c} = 2$ are the corresponding Wannier orbital multiplicities at WPs 1a, 1b, and 2c respectively. Using Eq. (20) and Table III, we can determine the $M_{\text{TCM} \leftarrow \text{MS}}^{(4)}$ and $M_{\text{MS} \leftarrow \text{RSI}}^{(4)}$ matrices for symmetry class A pertaining to spinless electrons,

$$\begin{pmatrix} \nu \\ \langle c_4(\mathbf{x}_{1a}) \rangle_F \\ \langle c_4(\mathbf{x}_{1b}) \rangle_F \\ \langle (c_4(\mathbf{x}_{1a}))^{-1} \rangle_F \\ \langle (c_4(\mathbf{x}_{1b}))^{-1} \rangle_F \\ \langle c_2(\mathbf{x}_{1a}) \rangle_F \\ \langle c_2(\mathbf{x}_{1b}) \rangle_F \\ \langle c_2(\mathbf{x}_{2c}) \rangle_F \end{pmatrix} = \begin{pmatrix} 1 & 0 & 0 & 0 & 0 & 0 & 0 & 0 \\ -2i & 2(1+i) & 4i & -2(1-i) & 0 & 1+i & 2i & -(1-i) \\ 0 & 0 & 0 & 0 & 0 & -(1+i) & -2i & 1-i \\ 2i & 2(1-i) & -4i & -2(1+i) & 0 & 1-i & -2i & -(1+i) \\ 0 & 0 & 0 & 0 & 0 & -(1-i) & 2i & 1+i \\ -4 & 8 & 0 & 8 & 4 & 2 & 0 & 2 \\ 0 & 0 & 0 & 0 & -4 & 2 & 0 & 2 \\ 0 & 0 & 0 & 0 & 0 & -2 & 0 & -2 \end{pmatrix} \begin{pmatrix} \nu \\ m(\Gamma_1) \\ m(\Gamma_2) \\ m(\Gamma_3) \\ [X_1] \\ [M_1] \\ [M_2] \\ [M_3] \end{pmatrix}, \quad (70)$$

$$\begin{pmatrix} \nu \\ m(\Gamma_1) \\ m(\Gamma_2) \\ m(\Gamma_3) \\ [X_1] \\ [M_1] \\ [M_2] \\ [M_3] \end{pmatrix} = \begin{pmatrix} 1 & 0 & 0 & 0 & 0 & 0 & 0 & 0 \\ 1/4 & -1/4 & -1/4 & -1/4 & -1/4 & -1/4 & -1/4 & -1/2 \\ 1/4 & 3/4 & -1/4 & -1/4 & 3/4 & -1/4 & -1/4 & 1/2 \\ 1/4 & -1/4 & 3/4 & -1/4 & -1/4 & 3/4 & -1/4 & -1/2 \\ 0 & 0 & 0 & 0 & 1 & -1 & 1 & 1 \\ 0 & 0 & 0 & 0 & 0 & 1 & 0 & 1 \\ 0 & 0 & 0 & 0 & -1 & 0 & 1 & -1 \\ 0 & 0 & 0 & 0 & 0 & -1 & 0 & 1 \end{pmatrix} \begin{pmatrix} \nu \\ \delta_{1a}^{(1)} \\ \delta_{1a}^{(2)} \\ \delta_{1a}^{(3)} \\ \delta_{1b}^{(1)} \\ \delta_{1b}^{(2)} \\ \delta_{1b}^{(3)} \\ \delta_{2c} \end{pmatrix}.$$

Note that the entries of the rows of $M_{\text{TCM} \leftarrow \text{MS}}^{(4)}$ corresponding to $\langle (c_4(\mathbf{x}_W))^{-1} \rangle_F$ are complex conjugates of the entries of the rows corresponding to $\langle c_4(\mathbf{x}_W) \rangle_F$, for $W \in \{1a, 1b\}$ (e.g., $\langle (c_4(\mathbf{x}_W)) \rangle_F^* = \langle (c_4(\mathbf{x}_W))^{-1} \rangle_F$). From Eq. (70) and computing $M_{\text{MS} \leftarrow \text{TCM}}^{(4)} = (M_{\text{TCM} \leftarrow \text{MS}}^{(4)})^{-1}$, the following relations can be determined,

$$2m(\Gamma_1) - 2m(\Gamma_3) + [M_1] - [M_3] = \text{Re}[\langle c_4(\mathbf{x}_{1a}) \rangle_F],$$

$$\begin{aligned}
& -2\nu + 2m(\Gamma_1) + 4m(\Gamma_2) + 2m(\Gamma_3) + [M_1] + 2[M_2] + [M_3] = \text{Im}[\langle c_4(\mathbf{x}_{1a}) \rangle_F], \\
& -2\nu + 4m(\Gamma_1) + 4m(\Gamma_3) + 2[X_1] + [M_1] + [M_3] = \frac{1}{2} \langle c_2(\mathbf{x}_{1a}) \rangle_F, \\
& -[M_1] + [M_3] = \text{Re}[\langle c_4(\mathbf{x}_{1b}) \rangle_F], \\
& -[M_1] - 2[M_2] - [M_3] = \text{Im}[\langle c_4(\mathbf{x}_{1b}) \rangle_F],
\end{aligned} \tag{71}$$

which implies the following *multiple* possible relations for the Chern number for symmetry class A pertaining to spinless electrons,

$$\mathcal{C} = [M_1] + 2[M_2] + 3[M_3] + 2[X_1] = \pm \sqrt{2} \text{Re}[e^{i\pi/4} \langle c_4(\mathbf{x}_W) \rangle_F] + \frac{1}{2} \langle c_2(\mathbf{x}_W) \rangle_F \pmod{4} \text{ for } W \in \{1a, 1b\}, \tag{72}$$

$$\mathcal{C} = [M_1] + 2[M_2] + 3[M_3] + 2[X_1] = \pm \sqrt{2} \text{Re}[e^{-i\pi/4} \langle c_4(\mathbf{x}_W) \rangle_F] - \frac{1}{2} \langle c_2(\mathbf{x}_W) \rangle_F \pmod{4} \text{ for } W \in \{1a, 1b\}. \tag{73}$$

The matrix $M_{\text{TCM} \leftarrow \text{RSI}}^{(4)}$ can also be computed and the following relations can be determined,

$$\begin{aligned}
i\delta_W^{(1)} - \delta_W^{(2)} - i\delta_W^{(3)} &= \frac{1}{2} \langle c_4(\mathbf{x}_W) \rangle_F \text{ for } W \in \{1a, 1b\}, \\
\delta_W^{(1)} - \delta_W^{(2)} + \delta_W^{(3)} &= -\frac{1}{4} \langle c_2(\mathbf{x}_W) \rangle_F \text{ for } W \in \{1a, 1b\}, \\
\delta_{2c} &= -\frac{1}{4} \langle c_2(\mathbf{x}_{2c}) \rangle_F.
\end{aligned} \tag{74}$$

Note that for atomic insulators, the Chern number must be zero, which enforces an additional constraint between the rotation invariants, $[M_3] = [M_1] + 2[M_2] + 2[X_1] \pmod{4}$. In terms of RSIs and TCMs, the bulk polarization for symmetry class A pertaining to spinless electrons can be expressed in three possible ways,

$$\begin{aligned}
\mathbf{P} &= \frac{e}{2} (\delta_{1b}^{(1)} + \delta_{1b}^{(2)} + \delta_{1b}^{(3)} + \delta_{2c}) (\mathbf{a}_1 + \mathbf{a}_2) \\
&= \frac{e}{8} (s_1 \langle c_2(\mathbf{x}_{1b}) \rangle_F + s_2 \langle c_2(\mathbf{x}_{1c}) \rangle_F) (\mathbf{a}_1 + \mathbf{a}_2) \pmod{e} \text{ for } s_{1,2} \in \{-1, 1\}
\end{aligned} \tag{75}$$

$$\mathbf{P} = \frac{e}{8} (s_1 \langle c_2(\mathbf{x}_{2c}) \rangle_F + 2s_2 \text{Re}[\langle c_4(\mathbf{x}_{1b}) \rangle_F] + 2s_3 \text{Im}[\langle c_4(\mathbf{x}_{1b}) \rangle_F]) (\mathbf{a}_1 + \mathbf{a}_2) \pmod{e} \text{ for } s_{1,2,3} \in \{-1, 1\} \tag{76}$$

$$\mathbf{P} = \frac{e}{8} (4s_1 \text{Re}[\langle c_4(\mathbf{x}_{1b}) \rangle_F] + s_2 \langle c_2(\mathbf{x}_{1b}) \rangle_F + s_3 \langle c_2(\mathbf{x}_{2c}) \rangle_F) (\mathbf{a}_1 + \mathbf{a}_2) \pmod{e} \text{ for } s_{1,2,3} \in \{-1, +1\}. \tag{77}$$

The sector charge for symmetry class A pertaining to spinless electrons can also be expressed in terms of the TCMs as,

$$Q_{\text{sector}} = \frac{e}{4} (\delta_{1b}^{(1)} + \delta_{1b}^{(2)} + \delta_{1b}^{(3)}) = \frac{e}{16} (-4 \text{Re}[\langle c_4(\mathbf{x}_{1b}) \rangle_F] - \langle c_2(\mathbf{x}_{1b}) \rangle_F) \pmod{e}. \tag{78}$$

It should be noted that the sector charge expression is *not unique* owing to the mod e constraint; as such, there are multiple other possible expressions for the sector charge which are all equivalent.

For symmetry class AI systems, time-reversal symmetry introduces the constraints $[M_3] = -([M_1] + 2[M_2])$ and $m(\Gamma_2) = m(\Gamma_4)$, implying $\nu = m(\Gamma_1) + 2m(\Gamma_2) + m(\Gamma_3)$. Additionally, time-reversal symmetry imposes the constraint $\delta_W^{(1)} = \delta_W^{(3)}$ and $\langle c_4(\mathbf{x}_W) \rangle_F = \langle (c_4(\mathbf{x}_W))^{-1} \rangle_F = (\langle c_4(\mathbf{x}_W) \rangle_F)^*$ for all $W \in \{1a, 1b\}$. Therefore, to evaluate the matrices for symmetry class AI, we must incorporate the additional constraints imposed by the symmetries and modify $\mathbf{v}_{\text{TCM}}^{(4)}$, $\mathbf{v}_{\text{MS}}^{(4)}$, and $\mathbf{v}_{\text{RSI}}^{(4)}$ to include only the independent set of quantities for each,

$$\begin{aligned}
\mathbf{v}_{\text{TCM}}^{(4)} &= (\nu, \langle c_4(\mathbf{x}_{1a}) \rangle_F, \langle c_4(\mathbf{x}_{1b}) \rangle_F, \langle c_2(\mathbf{x}_{1a}) \rangle_F, \langle c_2(\mathbf{x}_{1b}) \rangle_F, \langle c_2(\mathbf{x}_{2c}) \rangle_F)^T, \\
\mathbf{v}_{\text{MS}}^{(4)} &= (\nu, m(\Gamma_1), m(\Gamma_2), [X_1], [M_1], [M_2])^T, \\
\mathbf{v}_{\text{RSI}}^{(4)} &= (\nu, \delta_{1a}^{(1)}, \delta_{1a}^{(2)}, \delta_{1b}^{(1)}, \delta_{1b}^{(2)}, \delta_{2c})^T.
\end{aligned} \tag{79}$$

Thus, $M_{\text{TCM} \leftarrow \text{MS}}^{(4)}$ and $M_{\text{MS} \leftarrow \text{RSI}}^{(4)}$ for symmetry class AI are given as follows,

$$\begin{aligned}
& \begin{pmatrix} \nu \\ \langle c_4(\mathbf{x}_{1a}) \rangle_F \\ \langle c_4(\mathbf{x}_{1b}) \rangle_F \\ \langle c_2(\mathbf{x}_{1a}) \rangle_F \\ \langle c_2(\mathbf{x}_{1b}) \rangle_F \\ \langle c_2(\mathbf{x}_{2c}) \rangle_F \end{pmatrix} = \begin{pmatrix} 1 & 0 & 0 & 0 & 0 & 0 \\ -2 & 4 & 4 & 0 & 2 & 2 \\ 0 & 0 & 0 & 0 & -2 & -2 \\ 4 & 0 & -16 & 4 & 0 & -4 \\ 0 & 0 & 0 & -4 & 0 & -4 \\ 0 & 0 & 0 & 0 & 0 & 4 \end{pmatrix} \begin{pmatrix} \nu \\ m(\Gamma_1) \\ m(\Gamma_2) \\ [X_1] \\ [M_1] \\ [M_2] \end{pmatrix}, \\
& \begin{pmatrix} \nu \\ m(\Gamma_1) \\ m(\Gamma_2) \\ [X_1] \\ [M_1] \\ [M_2] \end{pmatrix} = \begin{pmatrix} 1 & 0 & 0 & 0 & 0 & 0 \\ 1/4 & -1/2 & -1/4 & -1/2 & -1/4 & -1/2 \\ 1/4 & 1/2 & -1/4 & 1/2 & -1/4 & 1/2 \\ 0 & 0 & 0 & 2 & -1 & 1 \\ 0 & 0 & 0 & 0 & 1 & 1 \\ 0 & 0 & 0 & 0 & 0 & -1 \end{pmatrix} \begin{pmatrix} \nu \\ \delta_{1a}^{(1)} \\ \delta_{1a}^{(2)} \\ \delta_{1b}^{(1)} \\ \delta_{1b}^{(2)} \\ \delta_{2c} \end{pmatrix}. \tag{80}
\end{aligned}$$

Computing $M_{\text{TCM} \leftarrow \text{RSI}}^{(4)}$ yields the following relations,

$$\begin{aligned}
\delta_W^{(2)} &= -\frac{1}{2} \langle c_4(\mathbf{x}_W) \rangle_F \text{ for } W \in \{1a, 1b\}, \\
2\delta_W^{(1)} - \delta_W^{(2)} &= -\frac{1}{4} \langle c_2(\mathbf{x}_W) \rangle_F \text{ for } W \in \{1a, 1b\}, \\
\delta_{2c} &= -\frac{1}{4} \langle c_2(\mathbf{x}_{2c}) \rangle_F, \tag{81}
\end{aligned}$$

which means the bulk polarization is the same as Eq. (75) or can be expressed as,

$$\mathbf{P} = \frac{e}{2} (2\delta_{1b}^{(1)} + \delta_{1b}^{(2)} + \delta_{2c}) (\mathbf{a}_1 + \mathbf{a}_2) = \frac{e}{8} (s_1 \langle c_2(\mathbf{x}_{2c}) \rangle_F + 2s_2 \langle c_4(\mathbf{x}_{1b}) \rangle_F) \pmod{e} \text{ for } s_{1,2} \in \{-1, 1\}, \tag{82}$$

for symmetry class AI. The sector charge for symmetry class AI can be expressed as,

$$Q_{\text{sector}} = \frac{e}{4} (2\delta_{1b}^{(1)} + \delta_{1b}^{(2)}) = -\frac{e}{16} (4 \langle c_4(\mathbf{x}_{1b}) \rangle_F + \langle c_2(\mathbf{x}_{1b}) \rangle_F) \pmod{e}. \tag{83}$$

Returning to the original definitions of $\mathbf{v}_{\text{TCM}}^{(4)}$, $\mathbf{v}_{\text{MS}}^{(4)}$, and $\mathbf{v}_{\text{RSI}}^{(4)}$ given by Eqs. (25), (26), and (30), one can construct the matrix $M_{\text{TCM} \leftarrow \text{MS}}^{(4)}$ once again using Eq. (20) and Table III for symmetry class A systems pertaining to spin-1/2

electrons,

$$\begin{pmatrix} \nu \\ \langle c_4(\mathbf{x}_{1a}) \rangle_F \\ \langle c_4(\mathbf{x}_{1b}) \rangle_F \\ \langle (c_4(\mathbf{x}_{1a}))^{-1} \rangle_F \\ \langle (c_4(\mathbf{x}_{1b}))^{-1} \rangle_F \\ \langle c_2(\mathbf{x}_{1a}) \rangle_F \\ \langle c_2(\mathbf{x}_{1b}) \rangle_F \\ \langle c_2(\mathbf{x}_{2c}) \rangle_F \end{pmatrix} = \begin{pmatrix} 1 & 0 & 0 & 0 & 0 & 0 & 0 & 0 \\ 2\bar{\eta} & 2(\eta - \bar{\eta}) & -4\bar{\eta} & -2(\eta + \bar{\eta}) & 0 & \eta - \bar{\eta} & -2\bar{\eta} & -(\eta + \bar{\eta}) \\ 0 & 0 & 0 & 0 & 0 & -(\eta - \bar{\eta}) & 2\bar{\eta} & \eta + \bar{\eta} \\ 2\eta & -2(\eta - \bar{\eta}) & -4\eta & -2(\eta + \bar{\eta}) & 0 & -(\eta - \bar{\eta}) & -2\eta & -(\eta + \bar{\eta}) \\ 0 & 0 & 0 & 0 & 0 & \eta - \bar{\eta} & 2\eta & \eta + \bar{\eta} \\ -4i & 8i & 0 & 8i & 4i & 2i & 0 & 2i \\ 0 & 0 & 0 & 0 & -4i & 2i & 0 & 2i \\ 0 & 0 & 0 & 0 & 0 & -2i & 0 & -2i \end{pmatrix} \begin{pmatrix} \nu \\ m(\Gamma_1) \\ m(\Gamma_2) \\ m(\Gamma_3) \\ [X_1] \\ [M_1] \\ [M_2] \\ [M_3] \end{pmatrix}, \quad (84)$$

where $\eta = e^{\pi i/4}$ and $\bar{\eta} = e^{-\pi i/4}$, and $M_{\text{MS} \leftarrow \text{RSI}}^{(4)}$ is identical to Eq. (70). From Eq. (84), the following relations can be determined,

$$\begin{aligned} \nu - 2m(\Gamma_2) - 2m(\Gamma_3) - ([M_2] + [M_3]) &= \frac{1}{\sqrt{2}} \text{Re}[\langle c_4(\mathbf{x}_{1a}) \rangle_F], \\ -\nu + 2m(\Gamma_1) + 2m(\Gamma_2) + [M_1] + [M_2] &= \frac{1}{\sqrt{2}} \text{Im}[\langle c_4(\mathbf{x}_{1a}) \rangle_F], \\ -2\nu + 4m(\Gamma_1) + 4m(\Gamma_3) + 2[X_1] + [M_1] + [M_3] &= \frac{1}{2i} \langle c_2(\mathbf{x}_{1a}) \rangle_F, \\ [M_2] + [M_3] &= \frac{1}{\sqrt{2}} \text{Re}[\langle c_4(\mathbf{x}_{1b}) \rangle_F], \\ -([M_1] + [M_2]) &= \frac{1}{\sqrt{2}} \text{Im}[\langle c_4(\mathbf{x}_{1b}) \rangle_F], \\ -2[X_1] + [M_1] + [M_3] &= \frac{1}{2i} \langle c_2(\mathbf{x}_{1b}) \rangle_F, \\ -([M_1] + [M_3]) &= \frac{1}{2i} \langle c_2(\mathbf{x}_{2c}) \rangle_F \end{aligned} \quad (85)$$

which implies the following *multiple* possible relations for the Chern number for symmetry class A pertaining to spin-1/2 electrons,

$$\mathcal{C} = [M_1] + 2[M_2] + 3[M_3] + 2[X_1] = \pm\sqrt{2} \text{Re}[\langle c_4(\mathbf{x}_W) \rangle_F] - \frac{i}{2} \langle c_2(\mathbf{x}_W) \rangle_F \pmod{4} \text{ for } W \in \{1a, 1b\}, \quad (86)$$

$$\mathcal{C} = [M_1] + 2[M_2] + 3[M_3] + 2[X_1] = \pm\sqrt{2} \text{Im}[\langle c_4(\mathbf{x}_W) \rangle_F] + \frac{i}{2} \langle c_2(\mathbf{x}_W) \rangle_F \pmod{4} \text{ for } W \in \{1a, 1b\}. \quad (87)$$

Computing the matrix $M_{\text{TCM} \leftarrow \text{RSI}}^{(4)}$ yields the following relations,

$$\begin{aligned} -\bar{\eta}\delta_W^{(1)} - \eta\delta_W^{(2)} + \bar{\eta}\delta_W^{(3)} &= \frac{1}{2} \langle c_4(\mathbf{x}_W) \rangle_F \text{ for } W \in \{1a, 1b\}, \\ i(\delta_W^{(1)} - \delta_W^{(2)} + \delta_W^{(3)}) &= -\frac{1}{4} \langle c_2(\mathbf{x}_W) \rangle_F \text{ for } W \in \{1a, 1b\}, \\ i\delta_{2c} &= -\frac{1}{4} \langle c_2(\mathbf{x}_{2c}) \rangle_F \end{aligned} \quad (88)$$

which means the bulk polarization can be expressed in four possible ways,

$$\begin{aligned} \mathbf{P} &= \frac{e}{2} (\delta_{1b}^{(1)} + \delta_{1b}^{(2)} + \delta_{1b}^{(3)} + \delta_{2c}) (\mathbf{a}_1 + \mathbf{a}_2) \\ &= \frac{ie}{8} (s_1 \langle c_2(\mathbf{x}_{1b}) \rangle_F + s_2 \langle c_2(\mathbf{x}_{2c}) \rangle_F) (\mathbf{a}_1 + \mathbf{a}_2) \pmod{e} \text{ for } s_{1,2} \in \{-1, 1\}, \end{aligned} \quad (89)$$

$$\mathbf{P} = \frac{e}{8}(is_1\langle c_2(\mathbf{x}_{2c})\rangle_F + 2\sqrt{2}s_2\text{Re}[\langle c_4(\mathbf{x}_{1b})\rangle_F])(\mathbf{a}_1 + \mathbf{a}_2) \pmod{e} \text{ for } s_{1,2} \in \{-1, 1\}, \quad (90)$$

$$\mathbf{P} = \frac{e}{8}(is_1\langle c_2(\mathbf{x}_{2c})\rangle_F + 2\sqrt{2}s_2\text{Im}[\langle c_4(\mathbf{x}_{1b})\rangle_F])(\mathbf{a}_1 + \mathbf{a}_2) \pmod{e} \text{ for } s_{1,2} \in \{-1, 1\}, \quad (91)$$

$$\mathbf{P} = \frac{e}{8}(4s_1\text{Re}[e^{-\frac{i\pi}{4}}\langle c_4(\mathbf{x}_{1b})\rangle_F] + i(s_2\langle c_2(\mathbf{x}_{1b})\rangle_F + s_3\langle c_2(\mathbf{x}_{2c})\rangle_F))(\mathbf{a}_1 + \mathbf{a}_2) \pmod{e} \text{ for } s_{1,2,3} \in \{-1, +1\}, \quad (92)$$

for symmetry class A pertaining to spin-1/2 electrons. The sector charge for symmetry class A pertaining to spin-1/2 electrons can be expressed as,

$$Q_{\text{sector}} = \frac{e}{4}(\delta_{1b}^{(1)} + \delta_{1b}^{(2)} + \delta_{1b}^{(3)}) = \frac{e}{16}(-4\text{Re}[e^{-\frac{i\pi}{4}}\langle c_4(\mathbf{x}_{1b})\rangle_F] + i\langle c_2(\mathbf{x}_{1b})\rangle_F) \pmod{e}. \quad (93)$$

Once again, we note that the above expression for the sector charge is *not unique* owing to the \pmod{e} constraint. Thus, there are several other expressions for the sector charge that are equivalent.

For symmetry class AII, time-reversal symmetry introduces the constraints $[M_1] = -[M_2] = -[M_3] = [M_4]$, $[X_1] = [X_2] = 0$, and $\nu = 2(m(\Gamma_1) + m(\Gamma_2))$. Furthermore, one also has $\delta_W^{(1)} = \delta_W^{(2)} \equiv \delta_W$, $\delta_W^{(3)} = 0$, and $\delta_{2c} = 0$. Additionally, time-reversal symmetry also enforces the constraints $\langle c_4(\mathbf{x}_W)\rangle_F = \langle (c_4(\mathbf{x}_W))^{-1}\rangle_F = (\langle c_4(\mathbf{x}_W)\rangle_F)^*$ for $W \in \{1a, 1b\}$ and $\langle c_2(\mathbf{x}_W)\rangle_F = 0$ for $W \in \{1a, 1b, 2c\}$. To evaluate the matrices for the symmetry class AII, we must incorporate the additional constraints imposed by the symmetries and modify $\mathbf{v}_{\text{TCM}}^{(4)}$, $\mathbf{v}_{\text{MS}}^{(4)}$, and $\mathbf{v}_{\text{RSI}}^{(4)}$ to include only the independent sets of quantities for each,

$$\begin{aligned} \mathbf{v}_{\text{TCM}}^{(4)} &= (\nu, \langle c_4(\mathbf{x}_{1a})\rangle_F, \langle c_4(\mathbf{x}_{1b})\rangle_F)^T, \\ \mathbf{v}_{\text{MS}}^{(4)} &= (\nu, m(\Gamma_1), [M_1])^T, \\ \mathbf{v}_{\text{RSI}}^{(4)} &= (\nu, \delta_{1a}, \delta_{1b})^T. \end{aligned} \quad (94)$$

Thus, $M_{\text{TCM} \leftarrow \text{MS}}^{(4)}$ and $M_{\text{MS} \leftarrow \text{RSI}}^{(4)}$ for symmetry class AII are given as follows,

$$\begin{aligned} \begin{pmatrix} \nu \\ \langle c_4(\mathbf{x}_{1a})\rangle_F \\ \langle c_4(\mathbf{x}_{1b})\rangle_F \end{pmatrix} &= \begin{pmatrix} 1 & 0 & 0 \\ (\eta + \bar{\eta}) & -4(\eta + \bar{\eta}) & 2(\eta + \bar{\eta}) \\ 0 & 0 & -2(\eta + \bar{\eta}) \end{pmatrix} \begin{pmatrix} \nu \\ m(\Gamma_1) \\ [M_1] \end{pmatrix}, \\ \begin{pmatrix} \nu \\ m(\Gamma_1) \\ [M_1] \end{pmatrix} &= \begin{pmatrix} 1 & 0 & 0 \\ 1/4 & -1/2 & -1/2 \\ 0 & 0 & 1 \end{pmatrix} \begin{pmatrix} \nu \\ \delta_{1a} \\ \delta_{1b} \end{pmatrix}. \end{aligned} \quad (95)$$

Computing $M_{\text{RSI} \leftarrow \text{MS}}^{(4)} = (M_{\text{MS} \leftarrow \text{RSI}}^{(4)})^{-1}$ yields the following relation,

$$\delta_W = -\frac{1}{2\sqrt{2}}\langle c_4(\mathbf{x}_W)\rangle_F \text{ for } W \in \{1a, 1b\}, \quad (96)$$

which means the bulk polarization for symmetry class AII is simply $\mathbf{P} = \mathbf{0} \pmod{e}$. Meanwhile, the sector charge for symmetry class AII can be expressed as,

$$Q_{\text{sector}} = \frac{e}{2}\delta_{1b} = -\frac{e}{4\sqrt{2}}\langle c_4(\mathbf{x}_{1b})\rangle_F \pmod{e}. \quad (97)$$

Finally, for symmetry class D systems, we consider both spinless and spin-1/2 electron systems. For spinless systems, particle-hole symmetry introduces the constraint on the rotation invariants $[M_2] = -[M_4]$ which implies $[M_1] = -[M_3]$. Furthermore, using Eq. (20), it follows that $\langle c(\mathbf{x}_{2c})\rangle_F = 0$. Therefore, similar to the approaches taken for symmetry classes AI and AII, for symmetry class D pertaining to spinless electrons, we modify $\mathbf{v}_{\text{TCM}}^{(4)}$ and $\mathbf{v}_{\text{MS}}^{(4)}$ (we do not consider $\mathbf{v}_{\text{RSI}}^{(4)}$ since atomic insulators do not exist in symmetry class D) to include only the independent set of quantities for each,

$$\mathbf{v}_{\text{TCM}}^{(4)} = (\nu, \langle c_4(\mathbf{x}_{1a})\rangle_F, \langle c_4(\mathbf{x}_{1b})\rangle_F, \langle (c_4(\mathbf{x}_{1a}))^{-1}\rangle_F, \langle (c_4(\mathbf{x}_{1b}))^{-1}\rangle_F, \langle c_2(\mathbf{x}_{1a})\rangle_F, \langle c_2(\mathbf{x}_{1b})\rangle_F)^T,$$

$$\mathbf{v}_{\text{MS}}^{(4)} = (\nu, m(\Gamma_1), m(\Gamma_2), m(\Gamma_3), [X_1], [M_1], [M_2])^T. \quad (98)$$

Thus, $M_{\text{TCM} \leftarrow \text{MS}}^{(4)}$ for symmetry class D for spinless electrons is given as follows,

$$\begin{pmatrix} \nu \\ \langle c_4(\mathbf{x}_{1a}) \rangle_F \\ \langle c_4(\mathbf{x}_{1b}) \rangle_F \\ \langle (c_4(\mathbf{x}_{1a}))^{-1} \rangle_F \\ \langle (c_4(\mathbf{x}_{1b}))^{-1} \rangle_F \\ \langle c_2(\mathbf{x}_{1a}) \rangle_F \\ \langle c_2(\mathbf{x}_{1b}) \rangle_F \end{pmatrix} = \begin{pmatrix} 1 & 0 & 0 & 0 & 0 & 0 & 0 \\ -2i & 2(1+i) & 4i & -2(1-i) & 0 & 2 & 2i \\ 0 & 0 & 0 & 0 & 0 & -2 & -2i \\ 2i & 2(1-i) & -4i & -2(1+i) & 0 & 2 & -2i \\ 0 & 0 & 0 & 0 & 0 & -2 & 2i \\ -4 & 8 & 0 & 8 & 4 & 0 & 0 \\ 0 & 0 & 0 & 0 & -4 & 0 & 0 \end{pmatrix} \begin{pmatrix} \nu \\ m(\Gamma_1) \\ m(\Gamma_2) \\ m(\Gamma_3) \\ [X_1] \\ [M_1] \\ [M_2] \end{pmatrix} \quad (99)$$

From Eq. (99), the same relations can be obtained as Eq. (71), but with the additional relations $[M_2] = -[M_4]$, $[M_1] = -[M_3]$, and $\langle c_2(\mathbf{x}_{2c}) \rangle_F = 0$. Therefore, this yields the same relations for the Chern number derived for symmetry class A for spinless electrons given by Eqs. (72)-(73). Similarly, for spin-1/2 systems, particle-hole symmetry introduces the constraints $[M_1] = -[M_4]$, $[M_2] = -[M_3]$. Additionally, particle-hole symmetry imposes the constraint $\langle c_4(\mathbf{x}_{1b}) \rangle_F = -\langle (c_4(\mathbf{x}_{1b}))^{-1} \rangle_F = -\langle (c_4(\mathbf{x}_{1b})) \rangle_F^*$. Hence, for symmetry class D pertaining to spin-1/2 electrons, we once again modify $\mathbf{v}_{\text{TCM}}^{(4)}$ and $\mathbf{v}_{\text{MS}}^{(4)}$ to include only the independent set of quantities for each,

$$\begin{aligned} \mathbf{v}_{\text{TCM}}^{(4)} &= (\nu, \langle c_4(\mathbf{x}_{1a}) \rangle_F, \langle c_4(\mathbf{x}_{1b}) \rangle_F, \langle (c_4(\mathbf{x}_{1a}))^{-1} \rangle_F, \langle c_2(\mathbf{x}_{1a}) \rangle_F, \langle c_2(\mathbf{x}_{1b}) \rangle_F, \langle c_2(\mathbf{x}_{2c}) \rangle_F)^T, \\ \mathbf{v}_{\text{MS}}^{(4)} &= (\nu, m(\Gamma_1), m(\Gamma_2), m(\Gamma_3), [X_1], [M_1], [M_2])^T. \end{aligned} \quad (100)$$

Thus, $M_{\text{TCM} \leftarrow \text{MS}}^{(4)}$ for symmetry class D for spin-1/2 electrons is given as follows,

$$\begin{pmatrix} \nu \\ \langle c_4(\mathbf{x}_{1a}) \rangle_F \\ \langle c_4(\mathbf{x}_{1b}) \rangle_F \\ \langle (c_4(\mathbf{x}_{1a}))^{-1} \rangle_F \\ \langle c_2(\mathbf{x}_{1a}) \rangle_F \\ \langle c_2(\mathbf{x}_{1b}) \rangle_F \\ \langle c_2(\mathbf{x}_{2c}) \rangle_F \end{pmatrix} = \begin{pmatrix} 1 & 0 & 0 & 0 & 0 & 0 & 0 \\ 2\bar{\eta} & 2(\eta - \bar{\eta}) & -4\bar{\eta} & -2(\eta + \bar{\eta}) & 0 & \eta - \bar{\eta} & \eta - \bar{\eta} \\ 0 & 0 & 0 & 0 & 0 & -(\eta - \bar{\eta}) & -(\eta - \bar{\eta}) \\ 2\eta & -2(\eta - \bar{\eta}) & -4\eta & -2(\eta + \bar{\eta}) & 0 & -(\eta - \bar{\eta}) & -(\eta - \bar{\eta}) \\ -4i & 8i & 0 & 8i & 4i & 2i & -2i \\ 0 & 0 & 0 & 0 & -4i & 2i & -2i \\ 0 & 0 & 0 & 0 & 0 & -2i & 2i \end{pmatrix} \begin{pmatrix} \nu \\ m(\Gamma_1) \\ m(\Gamma_2) \\ m(\Gamma_3) \\ [X_1] \\ [M_1] \\ [M_2] \end{pmatrix} \quad (101)$$

From Eq. (101), the same relations can be obtained as Eq. (85), but with the additional relations $[M_2] = -[M_3]$, $[M_1] = -[M_4]$, and $\langle c_4(\mathbf{x}_{1b}) \rangle_F = -\langle (c_4(\mathbf{x}_{1b}))^{-1} \rangle_F = -\langle (c_4(\mathbf{x}_{1b})) \rangle_F^*$. This yields the same relations for the Chern number derived for symmetry class A for spin-1/2 electrons given by Eqs. (86)-(87) (note that $\text{Re}[\langle c_4(\mathbf{x}_{1b}) \rangle_F] = 0$ so the Chern number can also be further simplified to $\mathcal{C} = -\frac{i}{2} \langle c_2(\mathbf{x}_W) \rangle_F \pmod{4}$ for $W \in \{1a, 1b\}$).

4. C_6 symmetry

For a C_6 -symmetric system, the filling ν constrains the rotation invariants, the $m(\Gamma_p)$ irrep multiplicities, and the Wannier orbital irrep multiplicities to satisfy the following equation,

$$\nu = \sum_{p=1}^6 m(\Gamma_p) = \sum_W \sum_{\ell} M_W n_W^{(\ell)} \rightarrow \sum_{p=1}^3 [K_p] = \sum_{p=1}^2 [M_p] = 0 \quad (102)$$

where $M_{1a} = 1$, $M_{2b} = 2$, and $M_{3c} = 3$ are the corresponding Wannier orbital multiplicities at WPs $1a$, $2b$, and $3c$ respectively. Using Eq. (20) and Table IV, we can determine the $M_{\text{TCM} \leftarrow \text{MS}}^{(6)}$ and $M_{\text{MS} \leftarrow \text{RSI}}^{(6)}$ matrices for symmetry class A pertaining to spinless electrons,

$$\begin{pmatrix} \nu \\ \langle c_6(\mathbf{x}_{1a}) \rangle_F \\ \langle (c_6(\mathbf{x}_{1a}))^{-1} \rangle_F \\ \langle c_3(\mathbf{x}_{1a}) \rangle_F \\ \langle c_3(\mathbf{x}_{2b}) \rangle_F \\ \langle (c_3(\mathbf{x}_{1a}))^{-1} \rangle_F \\ \langle (c_3(\mathbf{x}_{2b}))^{-1} \rangle_F \\ \langle c_2(\mathbf{x}_{1a}) \rangle_F \\ \langle c_2(\mathbf{x}_{3c}) \rangle_F \end{pmatrix} = \begin{pmatrix} 1 & 0 & 0 & 0 & 0 & 0 & 0 & 0 & 0 \\ \bar{\zeta} & 1 - \bar{\zeta} & \zeta - \bar{\zeta} & \omega - \bar{\zeta} & -(1 + \bar{\zeta}) & \bar{\omega} - \bar{\zeta} & 0 & 0 & 0 \\ \zeta & 1 - \zeta & -(\zeta - \bar{\zeta}) & \bar{\omega} - \zeta & -(1 + \zeta) & \omega - \zeta & 0 & 0 & 0 \\ 3\bar{\omega} & 3(1 - \bar{\omega}) & 3(\omega - \bar{\omega}) & 0 & 3(1 - \bar{\omega}) & 3(\omega - \bar{\omega}) & 2(1 - \bar{\omega}) & 2(\omega - \bar{\omega}) & 0 \\ 0 & 0 & 0 & 0 & 0 & 0 & -(1 - \bar{\omega}) & -(\omega - \bar{\omega}) & 0 \\ 3\omega & -3(\omega - 1) & -3(\omega - \bar{\omega}) & 0 & -3(\omega - 1) & -3(\omega - \bar{\omega}) & -2(\omega - 1) & -2(\omega - \bar{\omega}) & 0 \\ 0 & 0 & 0 & 0 & 0 & 0 & \omega - 1 & \omega - \bar{\omega} & 0 \\ -4 & 8 & 0 & 8 & 0 & 8 & 0 & 0 & 6 \\ 0 & 0 & 0 & 0 & 0 & 0 & 0 & 0 & -2 \end{pmatrix} \begin{pmatrix} \nu \\ m(\Gamma_1) \\ m(\Gamma_2) \\ m(\Gamma_3) \\ m(\Gamma_4) \\ m(\Gamma_5) \\ [K_1] \\ [K_2] \\ [M_1] \end{pmatrix},$$

$$\begin{pmatrix} \nu \\ m(\Gamma_1) \\ m(\Gamma_2) \\ m(\Gamma_3) \\ m(\Gamma_4) \\ m(\Gamma_5) \\ [K_1] \\ [K_2] \\ [M_1] \end{pmatrix} = \begin{pmatrix} 1 & 0 & 0 & 0 & 0 & 0 & 0 & 0 & 0 \\ 1/6 & -1/6 & -1/6 & -1/6 & -1/6 & -1/6 & -1/3 & -1/3 & -1/2 \\ 1/6 & 5/6 & -1/6 & -1/6 & -1/6 & -1/6 & 2/3 & -1/3 & 1/2 \\ 1/6 & -1/6 & 5/6 & -1/6 & -1/6 & -1/6 & -1/3 & 2/3 & -1/2 \\ 1/6 & -1/6 & -1/6 & 5/6 & -1/6 & -1/6 & -1/3 & -1/3 & 1/2 \\ 1/6 & -1/6 & -1/6 & -1/6 & 5/6 & -1/6 & 2/3 & -1/3 & -1/2 \\ 0 & 0 & 0 & 0 & 0 & 0 & 1 & 1 & 0 \\ 0 & 0 & 0 & 0 & 0 & 0 & -2 & 1 & 0 \\ 0 & 0 & 0 & 0 & 0 & 0 & 0 & 0 & 2 \end{pmatrix} \begin{pmatrix} \nu \\ \delta_{1a}^{(1)} \\ \delta_{1a}^{(2)} \\ \delta_{1a}^{(3)} \\ \delta_{1a}^{(4)} \\ \delta_{1a}^{(5)} \\ \delta_{2b}^{(1)} \\ \delta_{2b}^{(2)} \\ \delta_{3c} \end{pmatrix}. \quad (103)$$

where $\zeta = e^{\pi i/3}$, $\omega = e^{2\pi i/3}$, $\bar{\zeta} = e^{-\pi i/3}$, and $\bar{\omega} = e^{-2\pi i/3}$. Note that the entries of the rows of $M_{\text{TCM} \leftarrow \text{MS}}^{(6)}$ corresponding to $\langle (c_6(\mathbf{x}_{1a}))^{-1} \rangle_F$ are complex conjugates of the entries of the rows corresponding to $\langle c_6(\mathbf{x}_{1a}) \rangle_F$, and the same holds true for $\langle (c_3(\mathbf{x}_{1a}))^{-1} \rangle_F$ and $\langle (c_3(\mathbf{x}_{2b}))^{-1} \rangle_F$ with respect to $\langle c_3(\mathbf{x}_{1a}) \rangle_F$ and $\langle c_3(\mathbf{x}_{2b}) \rangle_F$ respectively (e.g., $\langle (c_6(\mathbf{x}_{1a})) \rangle_F^* = \langle (c_6(\mathbf{x}_{1a}))^{-1} \rangle_F$ and $\langle (c_3(\mathbf{x}_W)) \rangle_F^* = \langle (c_3(\mathbf{x}_W))^{-1} \rangle_F$ for $W \in \{1a, 2b\}$). From Eq. (103) and computing $M_{\text{MS} \leftarrow \text{TCM}}^{(6)} = (M_{\text{TCM} \leftarrow \text{MS}}^{(6)})^{-1}$, the following relations can be determined,

$$\begin{aligned} & 6(m(\Gamma_1) - 2m(\Gamma_2) + 2m(\Gamma_3) - m(\Gamma_4)) - 4[K_1] - 8[K_2] + 9[M_1] \\ &= \frac{2i}{\sqrt{3}} (\langle c_3(\mathbf{x}_{1a}) \rangle_F - \langle (c_3(\mathbf{x}_{1a}))^{-1} \rangle_F) + \frac{3}{2} \langle c_2(\mathbf{x}_{1a}) \rangle_F \end{aligned} \quad (104)$$

$$2[K_1] + 4[K_2] - 3[M_1] = \frac{2i}{\sqrt{3}} (\langle c_3(\mathbf{x}_{2b}) \rangle_F - \langle (c_3(\mathbf{x}_{2b}))^{-1} \rangle_F) + \frac{3}{2} \langle c_2(\mathbf{x}_{3c}) \rangle_F \quad (105)$$

which leads to the following *multiple* relations for the Chern number for spinless electron systems in symmetry class A,

$$\mathcal{C} = 2[K_1] - 2[K_2] + 3[M_1] = -\frac{4}{\sqrt{3}} \text{Im}[\langle c_3(\mathbf{x}_{1a}) \rangle_F] + \frac{3}{2} \langle c_2(\mathbf{x}_{1a}) \rangle_F \pmod{6}, \quad (106)$$

$$\mathcal{C} = 2[K_1] - 2[K_2] + 3[M_1] = -\frac{4}{\sqrt{3}}\text{Im}[\langle c_3(\mathbf{x}_{2b}) \rangle_F] + \frac{3}{2}\langle c_2(\mathbf{x}_{3c}) \rangle_F \pmod{6}, \quad (107)$$

Computing $M_{\text{TCM} \leftarrow \text{RSI}}^{(6)}$ yields the following relations,

$$\begin{aligned} \zeta\delta_{1a}^{(1)} + \omega\delta_{1a}^{(2)} - \delta_{1a}^{(3)} + \bar{\omega}\delta_{1a}^{(4)} + \bar{\zeta}\delta_{1a}^{(5)} &= \langle c_6(\mathbf{x}_{1a}) \rangle_F, \\ \omega\delta_{1a}^{(1)} + \bar{\omega}\delta_{1a}^{(2)} + \delta_{1a}^{(3)} + \omega\delta_{1a}^{(4)} + \bar{\omega}\delta_{1a}^{(5)} &= \frac{1}{3}\langle c_3(\mathbf{x}_{1a}) \rangle_F, \\ \omega\delta_{2b}^{(1)} + \bar{\omega}\delta_{2b}^{(2)} &= \frac{1}{3}\langle c_3(\mathbf{x}_{2b}) \rangle_F, \\ \delta_{1a}^{(1)} - \delta_{1a}^{(2)} + \delta_{1a}^{(3)} - \delta_{1a}^{(4)} + \delta_{1a}^{(5)} &= -\frac{1}{4}\langle c_2(\mathbf{x}_{1a}) \rangle_F, \\ \delta_{3c} &= -\frac{1}{4}\langle c_2(\mathbf{x}_{3c}) \rangle_F. \end{aligned} \quad (108)$$

Note that for atomic insulators, the Chern number must be zero, which enforces an additional constraint on the rotation invariants, $[K_2] = [K_1] + \frac{3}{2}[M_1] \pmod{6}$. The sector charge for symmetry class A systems pertaining to spinless electrons expressed in terms of RSIs and TCMs is given as,

$$Q_{\text{sector}} = \frac{e}{6} \sum_{\ell=1}^5 \delta_{1a}^{(\ell)} = -\frac{e}{72} (24\text{Re}[\langle c_6(\mathbf{x}_{1a}) \rangle_F] + 8\text{Re}\langle c_3(\mathbf{x}_{1a}) \rangle_F + 3\langle c_2(\mathbf{x}_{1a}) \rangle_F) \pmod{e}. \quad (109)$$

Owing to the \pmod{e} constraint on the sector charge, this expression is non-unique - there are multiple other possible ways of expressing the sector charge in terms of the TCMs that are also equivalent.

For symmetry class AI systems, time-reversal symmetry imposes the constraints $m(\Gamma_2) = m(\Gamma_6)$, $m(\Gamma_3) = m(\Gamma_5)$, and $[K_1] = -2[K_2]$ which implies $\nu = m(\Gamma_1) + 2(m(\Gamma_2) + m(\Gamma_3)) + m(\Gamma_4)$. Additionally, one also has $\delta_{1a}^{(1)} = \delta_{1a}^{(5)}$, $\delta_{1a}^{(2)} = \delta_{1a}^{(4)}$, $\delta_{2b}^{(1)} = \delta_{2b}^{(2)} \equiv \delta_{2b}$, $\langle c_6(\mathbf{x}_{1a}) \rangle_F = \langle (c_6(\mathbf{x}_{1a}))^{-1} \rangle_F = \langle (c_6(\mathbf{x}_{1a})) \rangle_F^*$, and $\langle c_3(\mathbf{x}_W) \rangle_F = \langle (c_3(\mathbf{x}_W))^{-1} \rangle_F = \langle (c_3(\mathbf{x}_W)) \rangle_F^*$ for $W \in \{1a, 2b\}$. Therefore, to evaluate the matrices for symmetry class AI, we must incorporate the additional constraints imposed by the symmetries and modify $\mathbf{v}_{\text{TCM}}^{(6)}$, $\mathbf{v}_{\text{MS}}^{(6)}$, and $\mathbf{v}_{\text{RSI}}^{(6)}$ to include only the independent set of quantities for each,

$$\begin{aligned} \mathbf{v}_{\text{TCM}}^{(6)} &= (\nu, \langle c_6(\mathbf{x}_{1a}) \rangle_F, \langle c_3(\mathbf{x}_{1a}) \rangle_F, \langle c_3(\mathbf{x}_{2b}) \rangle_F, \langle c_2(\mathbf{x}_{1a}) \rangle_F, \langle c_2(\mathbf{x}_{3c}) \rangle_F)^T, \\ \mathbf{v}_{\text{MS}}^{(6)} &= (\nu, m(\Gamma_1), m(\Gamma_2), m(\Gamma_3), [K_1], [M_1])^T, \\ \mathbf{v}_{\text{RSI}}^{(6)} &= (\nu, \delta_{1a}^{(1)}, \delta_{1a}^{(2)}, \delta_{1a}^{(3)}, \delta_{2b}, \delta_{3c})^T \end{aligned} \quad (110)$$

Thus, $M_{\text{TCM} \leftarrow \text{MS}}^{(6)}$ and $M_{\text{MS} \leftarrow \text{RSI}}^{(6)}$ for symmetry class AI are given as follows,

$$\begin{pmatrix} \nu \\ \langle c_6(\mathbf{x}_{1a}) \rangle_F \\ \langle c_3(\mathbf{x}_{1a}) \rangle_F \\ \langle c_3(\mathbf{x}_{2b}) \rangle_F \\ \langle c_2(\mathbf{x}_{1a}) \rangle_F \\ \langle c_2(\mathbf{x}_{3c}) \rangle_F \end{pmatrix} = \begin{pmatrix} 1 & 0 & 0 & 0 & 0 & 0 \\ -1 & 2 & 3 & 1 & 0 & 0 \\ 3 & 0 & -9 & -9 & 3 & 0 \\ 0 & 0 & 0 & 0 & -3/2 & 0 \\ -4 & 8 & 0 & 16 & 0 & 6 \\ 0 & 0 & 0 & 0 & 0 & -2 \end{pmatrix} \begin{pmatrix} \nu \\ m(\Gamma_1) \\ m(\Gamma_2) \\ m(\Gamma_3) \\ [K_1] \\ [M_1] \end{pmatrix},$$

$$\begin{pmatrix} \nu \\ m(\Gamma_1) \\ m(\Gamma_2) \\ m(\Gamma_3) \\ [K_1] \\ [M_1] \end{pmatrix} \begin{pmatrix} 1 & 0 & 0 & 0 & 0 & 0 \\ 1/6 & -1/3 & -1/3 & -1/6 & -2/3 & -1/2 \\ 1/6 & 2/3 & -1/3 & -1/6 & 1/3 & 1/2 \\ 1/6 & -1/3 & 2/3 & -1/6 & 1/3 & -1/2 \\ 0 & 0 & 0 & 0 & 2 & 0 \\ 0 & 0 & 0 & 0 & 0 & 2 \end{pmatrix} \begin{pmatrix} \nu \\ \delta_{1a}^{(1)} \\ \delta_{1a}^{(2)} \\ \delta_{1a}^{(3)} \\ \delta_{2b} \\ \delta_{3c} \end{pmatrix} \quad (111)$$

Computing $M_{\text{TCM} \leftarrow \text{RSI}}^{(6)}$ yields the following relations,

$$\begin{aligned}
\delta_{1a}^{(1)} - \delta_{1a}^{(2)} - \delta_{1a}^{(3)} &= \langle c_6(\mathbf{x}_{1a}) \rangle_F, \\
-\delta_{1a}^{(1)} - \delta_{1a}^{(2)} + \delta_{1a}^{(3)} &= \frac{1}{3} \langle c_3(\mathbf{x}_{1a}) \rangle_F, \\
\delta_{2b} &= -\frac{1}{3} \langle c_3(\mathbf{x}_{2b}) \rangle_F, \\
2\delta_{1a}^{(1)} - 2\delta_{1a}^{(2)} + \delta_{1a}^{(3)} &= -\frac{1}{4} \langle c_2(\mathbf{x}_{1a}) \rangle_F, \\
\delta_{3c} &= -\frac{1}{4} \langle c_2(\mathbf{x}_{3c}) \rangle_F.
\end{aligned} \quad (112)$$

The sector charge for symmetry class AI is therefore given as,

$$Q_{\text{sector}} = \frac{e}{6} (2\delta_{1a}^{(1)} + 2\delta_{1a}^{(2)} + \delta_{1a}^{(3)}) = -\frac{e}{72} (24 \langle c_6(\mathbf{x}_{1a}) \rangle_F + 8 \langle c_3(\mathbf{x}_{1a}) \rangle_F + 3 \langle c_2(\mathbf{x}_{1a}) \rangle_F) \pmod{e}. \quad (113)$$

Returning to the original definition of $\mathbf{v}_{\text{TCM}}^{(6)}$, $\mathbf{v}_{\text{MS}}^{(6)}$, and $\mathbf{v}_{\text{RSI}}^{(6)}$ given by Eqs. (25), (26), and (30), one can construct the matrix $M_{\text{TCM} \leftarrow \text{MS}}^{(6)}$ once again using Eq. (20) and Table IV for symmetry class A systems pertaining to spin-1/2 electrons,

$$\begin{pmatrix} \nu \\ \langle c_6(\mathbf{x}_{1a}) \rangle_F \\ \langle (c_6(\mathbf{x}_{1a}))^{-1} \rangle_F \\ \langle c_3(\mathbf{x}_{1a}) \rangle_F \\ \langle c_3(\mathbf{x}_{2b}) \rangle_F \\ \langle (c_3(\mathbf{x}_{1a}))^{-1} \rangle_F \\ \langle (c_3(\mathbf{x}_{2b}))^{-1} \rangle_F \\ \langle c_2(\mathbf{x}_{1a}) \rangle_F \\ \langle c_2(\mathbf{x}_{3c}) \rangle_F \end{pmatrix} = \begin{pmatrix} 1 & 0 & 0 & 0 & 0 & 0 & 0 & 0 & 0 \\ \bar{\gamma} & \gamma - \bar{\gamma} & i - \bar{\gamma} & -2\bar{\gamma} & -(\gamma + \bar{\gamma}) & -(i + \bar{\gamma}) & 0 & 0 & 0 \\ \gamma & -(\gamma - \bar{\gamma}) & -(i + \gamma) & -2\gamma & -(\gamma + \bar{\gamma}) & i - \gamma & 0 & 0 & 0 \\ 3\bar{\zeta} & 3(\zeta - \bar{\zeta}) & -3(1 + \bar{\zeta}) & 0 & 3(\zeta - \bar{\zeta}) & -3(1 + \bar{\zeta}) & 2(\zeta - \bar{\zeta}) & -2(1 + \bar{\zeta}) & 0 \\ 0 & 0 & 0 & 0 & 0 & 0 & -(\zeta - \bar{\zeta}) & 1 + \bar{\zeta} & 0 \\ 3\zeta & -3(\zeta - \bar{\zeta}) & -3(1 + \zeta) & 0 & -3(\zeta - \bar{\zeta}) & -3(1 + \zeta) & -2(\zeta - \bar{\zeta}) & -2(1 + \zeta) & 0 \\ 0 & 0 & 0 & 0 & 0 & 0 & \zeta - \bar{\zeta} & 1 + \zeta & 0 \\ -4i & 8i & 0 & 8i & 0 & 8i & 0 & 0 & 6i \\ 0 & 0 & 0 & 0 & 0 & 0 & 0 & 0 & -2i \end{pmatrix} \begin{pmatrix} \nu \\ m(\Gamma_1) \\ m(\Gamma_2) \\ m(\Gamma_3) \\ m(\Gamma_4) \\ m(\Gamma_5) \\ [K_1] \\ [K_2] \\ [M_1] \end{pmatrix} \quad (114)$$

where $\gamma = e^{\pi i/6}$, $\zeta = e^{\pi i/3}$, $\bar{\gamma} = e^{-\pi i/6}$, and $\bar{\zeta} = e^{-\pi i/3}$, and $M_{\text{MS} \leftarrow \text{RSI}}^{(6)}$ is identical to Eq. (103). From Eq. (114), the following relations can be determined,

$$\begin{aligned}
&6(m(\Gamma_2) - 2m(\Gamma_3) + 2m(\Gamma_4) - m(\Gamma_5)) + 8[K_1] + 4[K_2] - 9[M_1] \\
&= -\frac{2i}{\sqrt{3}} (\langle c_3(\mathbf{x}_{1a}) \rangle_F - \langle (c_3(\mathbf{x}_{1a}))^{-1} \rangle_F) + \frac{3i}{2} \langle c_2(\mathbf{x}_{1a}) \rangle,
\end{aligned}$$

$$-4[K_1] - 2[K_2] + 3[M_1] = -\frac{2i}{\sqrt{3}}(\langle c_3(\mathbf{x}_{2b}) \rangle_F - \langle (c_3(\mathbf{x}_{2b}))^{-1} \rangle_F) + \frac{3i}{2} \langle c_2(\mathbf{x}_{3c}) \rangle_F, \quad (115)$$

which leads to the following *multiple* relations for the Chern number for spin-1/2 electron systems in symmetry class A,

$$C = 2[K_1] - 2[K_2] + 3[M_1] = \frac{4}{\sqrt{3}} \text{Im}[\langle c_3(\mathbf{x}_{1a}) \rangle_F] + \frac{3i}{2} \langle c_2(\mathbf{x}_{1a}) \rangle_F \pmod{6}, \quad (116)$$

$$C = 2[K_1] - 2[K_2] + 3[M_1] = \frac{4}{\sqrt{3}} \text{Im}[\langle c_3(\mathbf{x}_{2b}) \rangle_F] + \frac{3i}{2} \langle c_2(\mathbf{x}_{3c}) \rangle_F \pmod{6}, \quad (117)$$

Computing $M_{\text{TCM} \leftarrow \text{RSI}}^{(6)}$ yields the following relations,

$$\begin{aligned} i\delta_{1a}^{(1)} - \bar{\gamma}\delta_{1a}^{(2)} - \gamma\delta_{1a}^{(3)} - i\delta_{1a}^{(4)} + \bar{\gamma}\delta_{1a}^{(5)} &= \langle c_6(\mathbf{x}_{1a}) \rangle_F, \\ -\delta_{1a}^{(1)} + \bar{\zeta}\delta_{1a}^{(2)} + \zeta\delta_{1a}^{(3)} - \delta_{1a}^{(4)} + \bar{\zeta}\delta_{1a}^{(5)} &= \frac{1}{3} \langle c_3(\mathbf{x}_{1a}) \rangle_F, \\ -\delta_{2b}^{(1)} + \bar{\zeta}\delta_{2b}^{(2)} &= \frac{1}{3} \langle c_3(\mathbf{x}_{2b}) \rangle_F, \\ \delta_{1a}^{(1)} - \delta_{1a}^{(2)} + \delta_{1a}^{(3)} - \delta_{1a}^{(4)} + \delta_{1a}^{(5)} &= \frac{i}{4} \langle c_2(\mathbf{x}_{1a}) \rangle_F, \\ \delta_{3c} &= \frac{i}{4} \langle c_2(\mathbf{x}_{3c}) \rangle_F \end{aligned} \quad (118)$$

The sector charge for symmetry class A pertaining to spin-half electrons is therefore given as,

$$\begin{aligned} Q_{\text{sector}} &= \frac{e}{6} \sum_{\ell=1}^5 \delta_{1a}^{(\ell)} = \frac{e}{6} \left(-5\delta_{1a}^{(1)} + \sum_{\ell=2}^5 \delta_{1a}^{(\ell)} \right) \\ &= \frac{e}{72} (-24 \text{Im}[\langle c_6(\mathbf{x}_{1a}) \rangle_F] + 8 \text{Re}[\langle c_3(\mathbf{x}_{1a}) \rangle_F] - 3i \langle c_2(\mathbf{x}_{1a}) \rangle_F) \pmod{e}. \end{aligned} \quad (119)$$

Once again, we note that the expression for the sector charge is not unique owing to the $(\text{mod } e)$ constraint, so there are other equivalent expressions for the sector charge.

For symmetry class AII systems, time-reversal symmetry imposes the constraints $m(\Gamma_1) = m(\Gamma_6)$, $m(\Gamma_2) = m(\Gamma_5)$, $m(\Gamma_3) = m(\Gamma_4)$, which implies $\nu = 2(m(\Gamma_1) + m(\Gamma_2) + m(\Gamma_3))$, in addition to $[K_2] = -2[K_1]$, and $[M_1] = [M_2] = 0$. Furthermore, this also imposes the constraints $\delta_{1a}^{(1)} = \delta_{1a}^{(4)}$, $\delta_{1a}^{(2)} = \delta_{1a}^{(3)}$, $\delta_{1a}^{(5)} = 0$, $\delta_{2b}^{(1)} \equiv \delta_{2b}$, and $\delta_{2b}^{(2)} = \delta_{3c} = 0$, in addition to $\langle c_6(\mathbf{x}_{1a}) \rangle_F = \langle (c_6(\mathbf{x}_{1a}))^{-1} \rangle_F = (\langle c_6(\mathbf{x}_{1a}) \rangle_F)^*$, $\langle c_3(\mathbf{x}_W) \rangle_F = \langle (c_3(\mathbf{x}_W))^{-1} \rangle_F = (\langle c_3(\mathbf{x}_W) \rangle_F)^*$ for $W \in \{1a, 2b\}$, and $\langle c_2(\mathbf{x}_W) \rangle_F = 0$ for $W \in \{1a, 2b, 3c\}$. To evaluate the matrices for symmetry class AII, we must incorporate the additional constraints imposed by the symmetries and modify $\mathbf{v}_{\text{TCM}}^{(6)}$, $\mathbf{v}_{\text{MS}}^{(6)}$, and $\mathbf{v}_{\text{RSI}}^{(6)}$ to include only the independent sets of quantities for each,

$$\begin{aligned} \mathbf{v}_{\text{TCM}}^{(6)} &= (\nu, \langle c_6(\mathbf{x}_{1a}) \rangle_F, \langle c_3(\mathbf{x}_{1a}) \rangle_F, \langle c_3(\mathbf{x}_{2b}) \rangle_F)^T, \\ \mathbf{v}_{\text{MS}}^{(6)} &= (\nu, m(\Gamma_1), m(\Gamma_2), [K_1])^T, \\ \mathbf{v}_{\text{RSI}}^{(6)} &= (\nu, \delta_{1a}^{(1)}, \delta_{1a}^{(2)}, \delta_{2b})^T. \end{aligned} \quad (120)$$

Thus, $M_{\text{TCM} \leftarrow \text{MS}}^{(6)}$ and $M_{\text{MS} \leftarrow \text{RSI}}^{(6)}$ for symmetry class AII are given as follows,

$$\begin{pmatrix} \nu \\ \langle c_6(\mathbf{x}_{1a}) \rangle_F \\ \langle c_3(\mathbf{x}_{1a}) \rangle_F \\ \langle c_3(\mathbf{x}_{2b}) \rangle_F \end{pmatrix} = \begin{pmatrix} 1 & 0 & 0 & 0 \\ -\frac{1}{2}(\gamma + \bar{\gamma}) & 2(\gamma + \bar{\gamma}) & \gamma + \bar{\gamma} & 0 \\ \frac{3}{2}(\zeta + \bar{\zeta}) & 0 & -9 & 6 \\ 0 & 0 & 0 & -3 \end{pmatrix} \begin{pmatrix} \nu \\ m(\Gamma_1) \\ m(\Gamma_2) \\ [K_1] \end{pmatrix},$$

$$\begin{pmatrix} \nu \\ m(\Gamma_1) \\ m(\Gamma_2) \\ [K_1] \end{pmatrix} = \begin{pmatrix} 1 & 0 & 0 & 0 \\ 1/6 & -1/3 & -1/3 & -1/3 \\ 1/6 & 2/3 & -1/3 & 2/3 \\ 0 & 0 & 0 & 1 \end{pmatrix} \begin{pmatrix} \nu \\ \delta_{1a}^{(1)} \\ \delta_{1a}^{(2)} \\ \delta_{2b} \end{pmatrix}. \quad (121)$$

Computing $M_{\text{TCM} \leftarrow \text{RSI}}^{(6)}$ yields the following relations,

$$\begin{aligned} \delta_{1a}^{(2)} &= -\frac{1}{\sqrt{3}} \langle c_6(\mathbf{x}_{1a}) \rangle_F, \\ 2\delta_{1a}^{(1)} - \delta_{1a}^{(2)} &= -\frac{1}{3} \langle c_3(\mathbf{x}_{1a}) \rangle_F, \\ \delta_{2b} &= -\frac{1}{3} \langle c_3(\mathbf{x}_{2b}) \rangle_F. \end{aligned} \quad (122)$$

The sector charge for symmetry class AII systems is therefore given by,

$$Q_{\text{sector}} = \frac{e}{3} (\delta_{1a}^{(1)} + \delta_{1a}^{(2)}) = \frac{e}{3} (-2\delta_{1a}^{(1)} + \delta_{1a}^{(2)}) = \frac{e}{9} \langle c_3(\mathbf{x}_{1a}) \rangle_F \pmod{e}. \quad (123)$$

Finally, for symmetry class D systems, we consider both spinless and spin-1/2 electron systems. For spinless systems, particle-hole symmetry introduces the constraint on the rotation invariants $[K_1] = 0$ in addition to $\langle c_3(\mathbf{x}_{2b}) \rangle_F = -\langle (c_3(\mathbf{x}_{2b}))^{-1} \rangle_F = -\langle c_3(\mathbf{x}_{2b}) \rangle_F^*$. Therefore, similar to approaches for the taken for symmetry classes AI and AII, for symmetry class D pertaining to spinless electrons, we modify $\mathbf{v}_{\text{TCM}}^{(6)}$ and $\mathbf{v}_{\text{MS}}^{(6)}$ (we do not consider $\mathbf{v}_{\text{RSI}}^{(6)}$ since atomic insulators do not exist in symmetry class D) to include only the independent quantities for each,

$$\begin{aligned} \mathbf{v}_{\text{TCM}}^{(6)} &= (\nu, \langle c_6(\mathbf{x}_{1a}) \rangle_F, \langle (c_6(\mathbf{x}_{1a}))^{-1} \rangle_F, \langle c_3(\mathbf{x}_{1a}) \rangle_F, \langle c_3(\mathbf{x}_{2b}) \rangle_F, \langle (c_3(\mathbf{x}_{1a}))^{-1} \rangle_F, \langle c_2(\mathbf{x}_{1a}) \rangle_F, \langle c_2(\mathbf{x}_{3c}) \rangle_F)^T, \\ \mathbf{v}_{\text{MS}}^{(6)} &= (\nu, m(\Gamma_1), m(\Gamma_2), m(\Gamma_3), m(\Gamma_4), m(\Gamma_5), [K_2], [M_1])^T, \end{aligned} \quad (124)$$

Therefore, $M_{\text{TCM} \leftarrow \text{MS}}^{(6)}$ for symmetry class D pertaining to spinless electrons is,

$$\begin{pmatrix} \nu \\ \langle c_6(\mathbf{x}_{1a}) \rangle_F \\ \langle (c_6(\mathbf{x}_{1a}))^{-1} \rangle_F \\ \langle c_3(\mathbf{x}_{1a}) \rangle_F \\ \langle c_3(\mathbf{x}_{2b}) \rangle_F \\ \langle (c_3(\mathbf{x}_{1a}))^{-1} \rangle_F \\ \langle c_2(\mathbf{x}_{1a}) \rangle_F \\ \langle c_2(\mathbf{x}_{3c}) \rangle_F \end{pmatrix} = \begin{pmatrix} 1 & 0 & 0 & 0 & 0 & 0 & 0 & 0 \\ \bar{\zeta} & 1 - \bar{\zeta} & \zeta - \bar{\zeta} & \omega - \bar{\zeta} & -(1 + \bar{\zeta}) & \bar{\omega} - \bar{\zeta} & 0 & 0 \\ \zeta & 1 - \zeta & -(\zeta - \bar{\zeta}) & \bar{\omega} - \zeta & -(1 + \zeta) & \omega - \zeta & 0 & 0 \\ 3\bar{\omega} & 3(1 - \bar{\omega}) & 3(\omega - \bar{\omega}) & 0 & 3(1 - \bar{\omega}) & 3(\omega - \bar{\omega}) & 2(\omega - \bar{\omega}) & 0 \\ 0 & 0 & 0 & 0 & 0 & 0 & -(\omega - \bar{\omega}) & 0 \\ 3\omega & -3(\omega - 1) & -3(\omega - \bar{\omega}) & 0 & -3(\omega - 1) & -3(\omega - \bar{\omega}) & -2(\omega - \bar{\omega}) & 0 \\ -4 & 8 & 0 & 8 & 0 & 8 & 0 & 6 \\ 0 & 0 & 0 & 0 & 0 & 0 & 0 & -2 \end{pmatrix} \begin{pmatrix} \nu \\ m(\Gamma_1) \\ m(\Gamma_2) \\ m(\Gamma_3) \\ m(\Gamma_4) \\ m(\Gamma_5) \\ [K_2] \\ [M_1] \end{pmatrix}, \quad (125)$$

From Eq. (125), it follows that the same relations as Eqs. (105) and (107) can be obtained with $[K_1] = 0$ and $\langle c_3(\mathbf{x}_{2b}) \rangle_F = -\langle (c_3(\mathbf{x}_{2b}))^{-1} \rangle_F = -\langle c_3(\mathbf{x}_{2b}) \rangle_F^*$. This means the Chern number for symmetry class D is equivalent to the Chern number for symmetry class A for spinless electrons. Similarly, for spin-1/2 systems, particle-hole symmetry imposes the constraints $[K_2] = 0$ and the same constraint $\langle c_3(\mathbf{x}_{2b}) \rangle_F = -\langle (c_3(\mathbf{x}_{2b}))^{-1} \rangle_F = -\langle c_3(\mathbf{x}_{2b}) \rangle_F^*$. Once again, we modify $\mathbf{v}_{\text{MS}}^{(6)}$ to incorporate the constraint imposed by the symmetry, but retain the definition of $\mathbf{v}_{\text{TCM}}^{(6)}$ given by Eq. (124),

$$\mathbf{v}_{\text{MS}}^{(6)} = (\nu, m(\Gamma_1), m(\Gamma_2), m(\Gamma_3), m(\Gamma_4), m(\Gamma_5), [K_1], [M_1])^T, \quad (126)$$

which means $M_{\text{TCM} \leftarrow \text{MS}}^{(6)}$ for symmetry class D pertaining to spin-1/2 electrons is,

$$\begin{pmatrix} \nu \\ \langle c_6(\mathbf{x}_{1a}) \rangle_F \\ \langle (c_6(\mathbf{x}_{1a}))^{-1} \rangle_F \\ \langle c_3(\mathbf{x}_{1a}) \rangle_F \\ \langle c_3(\mathbf{x}_{2b}) \rangle_F \\ \langle (c_3(\mathbf{x}_{1a}))^{-1} \rangle_F \\ \langle c_2(\mathbf{x}_{1a}) \rangle_F \\ \langle c_2(\mathbf{x}_{3c}) \rangle_F \end{pmatrix} = \begin{pmatrix} 1 & 0 & 0 & 0 & 0 & 0 & 0 & 0 \\ \bar{\gamma} & \gamma - \bar{\gamma} & i - \bar{\gamma} & -2\bar{\gamma} & -(\gamma + \bar{\gamma}) & -(i + \bar{\gamma}) & 0 & 0 \\ \gamma & -(\gamma - \bar{\gamma}) & -(i + \gamma) & -2\gamma & -(\gamma + \bar{\gamma}) & i - \gamma & 0 & 0 \\ 3\bar{\zeta} & 3(\zeta - \bar{\zeta}) & -3(1 + \bar{\zeta}) & 0 & 3(\zeta - \bar{\zeta}) & -3(1 + \bar{\zeta}) & 2(\zeta - \bar{\zeta}) & 0 \\ 0 & 0 & 0 & 0 & 0 & 0 & -(\zeta - \bar{\zeta}) & 0 \\ 3\zeta & -3(\zeta - \bar{\zeta}) & -3(1 + \zeta) & 0 & -3(\zeta - \bar{\zeta}) & -3(1 + \zeta) & -2(\zeta - \bar{\zeta}) & 0 \\ -4i & 8i & 0 & 8i & 0 & 8i & 0 & 6i \\ 0 & 0 & 0 & 0 & 0 & 0 & 0 & -2i \end{pmatrix} \begin{pmatrix} \nu \\ m(\Gamma_1) \\ m(\Gamma_2) \\ m(\Gamma_3) \\ m(\Gamma_4) \\ m(\Gamma_5) \\ [K_1] \\ [M_1] \end{pmatrix}. \quad (127)$$

From Eq. (127), one can obtain the same relations as Eq. (115), but with $[K_2] = 0$. It follows that the Chern number for symmetry class D is equivalent to the Chern number for symmetry class A for spin-1/2 electrons.

VII. DERIVATION OF MOMENTUM QUANTIZATION CONDITION UNDER TWISTED BOUNDARY CONDITIONS

In this section, we derive the momentum quantization condition presented in the main text,

$$\mathbf{k} = \left(\frac{n_1}{N_1} - \frac{\theta_1}{2\pi N_1} \right) \mathbf{b}_1 + \left(\frac{n_2}{N_2} - \frac{\theta_2}{2\pi N_2} \right) \mathbf{b}_2. \quad (128)$$

where $n_i \in \{0, \dots, N_i - 1\}$ for $i \in \{1, 2\}$ (in this section, we are working with the convention $\mathbf{b}_i \cdot \mathbf{a}_j = 2\pi\delta_{ij}$). This applies to a lattice with dimensions $N_1 \times N_2$ and twisted boundary conditions parameterized by (θ_1, θ_2) , which can be understood as two fluxes introduced along two distinct co-cycles of the torus in the \mathbf{a}_1 and \mathbf{a}_2 directions respectively. The twisted boundary conditions are defined as follows,

$$|\mathbf{R} + N_i \mathbf{a}_i, \alpha\rangle = e^{-i\theta_i} |\mathbf{R}, \alpha\rangle \text{ for } i \in \{1, 2\} \quad (129)$$

Let us extend n_1, n_2 to be any integer, i.e., $n_1, n_2 \in \mathbb{Z}$, introduce $l_1, l_2 \in \mathbb{Z}$, and denote C as the normalization constant for the Fourier transform. The Fourier transform in the periodic basis is given as,

$$|\mathbf{k}, \alpha\rangle \equiv \frac{1}{\sqrt{N}} \sum_{\mathbf{R}} e^{2\pi i \mathbf{k} \cdot \mathbf{R}} |\mathbf{R}, \alpha\rangle. \quad (130)$$

Re-expressing Eq. (130) in the following manner,

$$\begin{aligned} |\mathbf{k}, \alpha\rangle &= C \sum_{\mathbf{R}, l_1, l_2} e^{2\pi i \mathbf{k} \cdot (\mathbf{R} + l_1 N_1 \mathbf{a}_1 + l_2 N_2 \mathbf{a}_2)} |\mathbf{R} + l_1 N_1 \mathbf{a}_1 + l_2 N_2 \mathbf{a}_2, \alpha\rangle, \\ &= C \sum_{\mathbf{R}, l_1, l_2} e^{2\pi i \mathbf{k} \cdot (\mathbf{R} + l_1 N_1 \mathbf{a}_1 + l_2 N_2 \mathbf{a}_2) - i(l_1 \theta_1 + l_2 \theta_2)} |\mathbf{R}, \alpha\rangle, \\ &= C \left(\sum_{\mathbf{R}} e^{2\pi i \mathbf{k} \cdot \mathbf{R}} |\mathbf{R}, \alpha\rangle \right) \left(\sum_{l_1, l_2} e^{2\pi i \left(\mathbf{k} - \frac{\theta_1}{2\pi N_1} \mathbf{b}_1 - \frac{\theta_2}{2\pi N_2} \mathbf{b}_2 \right) \cdot (l_1 N_1 \mathbf{a}_1 + l_2 N_2 \mathbf{a}_2)} \right), \\ &= C \left(\sum_{\mathbf{R}} e^{2\pi i \mathbf{k} \cdot \mathbf{R}} |\mathbf{R}, \alpha\rangle \right) \left(\sum_{l_1, l_2} e^{2\pi i \left(\left(\frac{n_1}{N_1} - \frac{\theta_1}{2\pi N_1} \right) \mathbf{b}_1 + \left(\frac{n_2}{N_2} - \frac{\theta_2}{2\pi N_2} \right) \mathbf{b}_2 \right) \cdot (l_1 N_1 \mathbf{a}_1 + l_2 N_2 \mathbf{a}_2)} \right), \\ &= C \left(\sum_{l_1, l_2} e^{i(l_1(2\pi n_1 - \theta_1) + l_2(2\pi n_2 - \theta_2))} \right) \sum_{\mathbf{R}} e^{2\pi i \mathbf{k} \cdot \mathbf{R}} |\mathbf{R}, \alpha\rangle. \end{aligned} \quad (131)$$

In order for the equality to remain true, the quantity in the parentheses must be equal to 1. To do so, we impose $2\pi n_i - \theta_i \in 2\pi\mathbb{Z}$ for $i \in \{1, 2\}$. Equivalently, we redefine $n_i \rightarrow n_i - \frac{\theta_i}{2\pi}$ in $\mathbf{k} = \frac{n_1}{N_1}\mathbf{b}_1 + \frac{n_2}{N_2}\mathbf{b}_2$. This means,

$$\mathbf{k} = \frac{1}{N_1} \left(n_1 - \frac{\theta_1}{2\pi} \right) \mathbf{b}_1 + \frac{1}{N_2} \left(n_2 - \frac{\theta_2}{2\pi} \right) \mathbf{b}_2 \quad (132)$$

which yields Eq. (128).

VIII. FULLY TRACED TCMS FOR ARBITRARY FINITE-SIZE C_n -SYMMETRIC LATTICE UTILIZING TWISTED BOUNDARY CONDITIONS

Here, we review the implementation of fully traced TCMS for any C_n -symmetric lattice with finite dimensions $N_1 \times N_2$ that *do not* satisfy the constraint

$$\begin{aligned} C_2 : (N_1, N_2) &= (0, 0) \pmod{2}, \\ C_4 : N &= 0 \pmod{2}, \\ C_{n=3,6} : N &= 0 \pmod{n}, \end{aligned} \quad (133)$$

using twisted boundary conditions. Any lattice with dimensions $N_1 \times N_2$ that satisfies Eq. (133) will support a BZ with the complete set of high symmetry momenta. This is a necessary condition to be able to express the Chern number, bulk polarization, and sector charge in terms of momentum-space rotation invariants, but limits the applicability to lattices of other dimensions. When (N_1, N_2) do not satisfy Eq. (133), the BZ supports a reduced set of high symmetry momenta when only periodic boundary conditions are considered. Twisting the boundary conditions by introducing θ_1 and θ_2 adjusts the momentum quantization as shown in Eq. (128). By choosing appropriate θ_1 and θ_2 , different sets of high symmetry momenta can be accessed. Thus, when a C_n -symmetric lattice with dimensions $N_1 \times N_2$ does not satisfy Eq. (133), it is still possible to evaluate the Chern number, bulk polarization, and sector charge for such lattices by *jointly* considering lattices with different sets of boundary conditions. In this section, we will state the mapping of the fully traced TCMS corresponding to the lattice that satisfy Eq. (133) to the fully traced TCMS corresponding to the C_n -symmetric lattices that do not satisfy Eq. (133) by adding over the appropriate twisted boundary conditions. Using this mapping, it is possible to extend the Chern number, bulk polarization, and sector charge for C_n -symmetric lattices with dimensions $N_1 \times N_2$ that satisfy Eq. (133), to any C_n -symmetric lattice. The fully traced TCM for a lattice with twisted boundary conditions is given by $\langle c_n(\mathbf{r}_o) \rangle_F^{(\theta_1, \theta_2)}$. When $\theta_1 = \theta_2 = 0$, which corresponds to periodic boundary conditions, this superscript will usually be suppressed, i.e., $\langle c_n(\mathbf{r}_o) \rangle_F^{(0,0)} \equiv \langle c_n(\mathbf{r}_o) \rangle_F$.

1. C_2 symmetry

A C_2 -symmetric lattice with dimensions $N_1 \times N_2$ can support either $(N_1, N_2) = (0, 0) \pmod{2}$, $(N_1, N_2) = (1, 0) \pmod{2}$, $(N_1, N_2) = (0, 1) \pmod{2}$, or $(N_1, N_2) = (1, 1) \pmod{2}$. For each of these dimensions, these are the corresponding set of invariant WPs in $\mathcal{X}[c_2(\mathbf{r}_o)]$,

$$\begin{aligned} (N_1, N_2) = (0, 0) \pmod{2} : \mathbf{r}_o &\in \{\mathbf{x}_{1a}, \mathbf{x}_{1b}, \mathbf{x}_{1c}, \mathbf{x}_{1d}\}, \\ (N_1, N_2) = (1, 0) \pmod{2} : \mathbf{r}_o &\in \{\mathbf{x}_{1a}, \mathbf{x}_{1c}\}, \\ (N_1, N_2) = (0, 1) \pmod{2} : \mathbf{r}_o &\in \{\mathbf{x}_{1a}, \mathbf{x}_{1b}\}, \\ (N_1, N_2) = (1, 1) \pmod{2} : \mathbf{r}_o &\in \{\mathbf{x}_{1a}\}. \end{aligned} \quad (134)$$

Hence, we can map the fully traced TCMS for the $(N_1, N_2) = (0, 0) \pmod{2}$ lattice to the fully traced TCMS corresponding to the other lattice dimensions. We will use the convention that the *left-hand side* corresponds to $(N_1, N_2) = (0, 0) \pmod{2}$ and the *right-hand side* corresponds to $(N_1, N_2) \neq (0, 0) \pmod{2}$. For $(N_1, N_2) = (1, 0) \pmod{2}$, this mapping is given as follows,

$$\begin{aligned} \langle c_2(\mathbf{x}_{1a}) \rangle_F &\leftrightarrow \sum_{\theta \in \{0, \pi\}} \langle c_2(\mathbf{x}_{1a}) \rangle_F^{(\theta, 0)}, \\ \langle c_2(\mathbf{x}_{1b}) \rangle_F &\leftrightarrow \sum_{\theta \in \{0, \pi\}} e^{i\theta} \langle c_2(\mathbf{x}_{1a}) \rangle_F^{(\theta, 0)}, \end{aligned}$$

$$\begin{aligned}
\langle c_2(\mathbf{x}_{1c}) \rangle_F &\leftrightarrow \sum_{\theta \in \{0, \pi\}} \langle c_2(\mathbf{x}_{1c}) \rangle_F^{(\theta, 0)}, \\
\langle c_2(\mathbf{x}_{1d}) \rangle_F &\leftrightarrow \sum_{\theta \in \{0, \pi\}} e^{i\theta} \langle c_2(\mathbf{x}_{1c}) \rangle_F^{(\theta, 0)},
\end{aligned} \tag{135}$$

and for $(N_1, N_2) = (0, 1) \pmod{2}$,

$$\begin{aligned}
\langle c_2(\mathbf{x}_{1a}) \rangle_F &\leftrightarrow \sum_{\theta \in \{0, \pi\}} \langle c_2(\mathbf{x}_{1a}) \rangle_F^{(0, \theta)}, \\
\langle c_2(\mathbf{x}_{1b}) \rangle_F &\leftrightarrow \sum_{\theta \in \{0, \pi\}} \langle c_2(\mathbf{x}_{1b}) \rangle_F^{(0, \theta)}, \\
\langle c_2(\mathbf{x}_{1c}) \rangle_F &\leftrightarrow \sum_{\theta \in \{0, \pi\}} e^{i\theta} \langle c_2(\mathbf{x}_{1a}) \rangle_F^{(0, \theta)}, \\
\langle c_2(\mathbf{x}_{1d}) \rangle_F &\leftrightarrow \sum_{\theta \in \{0, \pi\}} e^{i\theta} \langle c_2(\mathbf{x}_{1b}) \rangle_F^{(0, \theta)},
\end{aligned} \tag{136}$$

and finally, for $(N_1, N_2) = (1, 1) \pmod{2}$,

$$\begin{aligned}
\langle c_2(\mathbf{x}_{1a}) \rangle_F &\leftrightarrow \sum_{\theta_1 \in \{0, \pi\}} \sum_{\theta_2 \in \{0, \pi\}} \langle c_2(\mathbf{x}_{1a}) \rangle_F^{(\theta_1, \theta_2)}, \\
\langle c_2(\mathbf{x}_{1b}) \rangle_F &\leftrightarrow \sum_{\theta_1 \in \{0, \pi\}} \sum_{\theta_2 \in \{0, \pi\}} e^{i\theta_1} \langle c_2(\mathbf{x}_{1a}) \rangle_F^{(\theta_1, \theta_2)}, \\
\langle c_2(\mathbf{x}_{1c}) \rangle_F &\leftrightarrow \sum_{\theta_1 \in \{0, \pi\}} \sum_{\theta_2 \in \{0, \pi\}} e^{i\theta_2} \langle c_2(\mathbf{x}_{1a}) \rangle_F^{(\theta_1, \theta_2)}, \\
\langle c_2(\mathbf{x}_{1d}) \rangle_F &\leftrightarrow \sum_{\theta_1 \in \{0, \pi\}} \sum_{\theta_2 \in \{0, \pi\}} e^{i(\theta_1 + \theta_2)} \langle c_2(\mathbf{x}_{1a}) \rangle_F^{(\theta_1, \theta_2)}.
\end{aligned} \tag{137}$$

2. C_3 symmetry

A C_3 -symmetric lattice with dimensions $N \times N$ can support either $N = 0 \pmod{3}$ or $N = \pm 1 \pmod{3}$. For each of these dimensions, these are the corresponding set of invariant WPs in $\mathcal{X}[c_3(\mathbf{r}_o)]$,

$$\begin{aligned}
N = 0 \pmod{3} : \mathbf{r}_o &\in \{\mathbf{x}_{1a}, \mathbf{x}_{1b}, \mathbf{x}_{1c}\}, \\
N = \pm 1 \pmod{3} : \mathbf{r}_o &\in \{\mathbf{x}_{1a}\}.
\end{aligned} \tag{138}$$

Hence, we can map the fully traced TCMs for the $N = 0 \pmod{3}$ lattice to the fully traced TCMs corresponding to the other lattice dimensions. We will use the convention that the *left-hand side* corresponds to $N = 0 \pmod{3}$ and the *right-hand side* corresponds to $N = \pm 1 \pmod{3}$. For $N = 1 \pmod{3}$, this mapping is given as follows,

$$\begin{aligned}
\langle c_3(\mathbf{x}_{1a}) \rangle_F &\leftrightarrow \sum_{\theta \in \{0, \pm \frac{2\pi}{3}\}} \langle c_3(\mathbf{x}_{1a}) \rangle_F^{(\theta, -\theta)}, \\
\langle c_3(\mathbf{x}_{1b}) \rangle_F &\leftrightarrow \sum_{\theta \in \{0, \pm \frac{2\pi}{3}\}} e^{-i\theta} \langle c_3(\mathbf{x}_{1a}) \rangle_F^{(\theta, -\theta)}, \\
\langle c_3(\mathbf{x}_{1c}) \rangle_F &\leftrightarrow \sum_{\theta \in \{0, \pm \frac{2\pi}{3}\}} e^{i\theta} \langle c_3(\mathbf{x}_{1a}) \rangle_F^{(\theta, -\theta)},
\end{aligned} \tag{139}$$

and for $N = -1 \pmod{3}$,

$$\begin{aligned}
\langle c_3(\mathbf{x}_{1a}) \rangle_F &\leftrightarrow \sum_{\theta \in \{0, \pm \frac{2\pi}{3}\}} \langle c_3(\mathbf{x}_{1a}) \rangle_F^{(\theta, -\theta)}, \\
\langle c_3(\mathbf{x}_{1b}) \rangle_F &\leftrightarrow \sum_{\theta \in \{0, \pm \frac{2\pi}{3}\}} e^{i\theta} \langle c_3(\mathbf{x}_{1a}) \rangle_F^{(\theta, -\theta)},
\end{aligned}$$

$$\langle c_3(\mathbf{x}_{1c}) \rangle_F \leftrightarrow \sum_{\theta \in \{0, \pm \frac{2\pi}{3}\}} e^{-i\theta} \langle c_3(\mathbf{x}_{1a}) \rangle_F^{(\theta, -\theta)}, \quad (140)$$

3. C_4 symmetry

A C_4 -symmetric lattice with dimensions $N \times N$ can support either $N = 0 \pmod{2}$ or $N = 1 \pmod{2}$. For each of these dimensions, these are the corresponding set of WPs in $\mathcal{X}[c_4(\mathbf{r}_o)]$,

$$\begin{aligned} N = 0 \pmod{2} : \mathbf{r}_o &\in \{\mathbf{x}_{1a}, \mathbf{x}_{1b}\}, \\ N = 1 \pmod{2} : \mathbf{r}_o &\in \{\mathbf{x}_{1a}\}, \end{aligned} \quad (141)$$

and the corresponding set of WPs in $\mathcal{X}[c_2(\mathbf{r}_o)]$,

$$\begin{aligned} N = 0 \pmod{2} : \mathbf{r}_o &\in \{\mathbf{x}_{1a}, \mathbf{x}_{1b}, \mathbf{x}_{2c}^{(1)}, \mathbf{x}_{2c}^{(2)}\}, \\ N = 1 \pmod{2} : \mathbf{r}_o &\in \{\mathbf{x}_{1a}\}. \end{aligned} \quad (142)$$

where $\mathbf{x}_{2c}^{(1)} = \frac{1}{2}\mathbf{a}_1$ and $\mathbf{x}_{2c}^{(2)} = \frac{1}{2}\mathbf{a}_2$. Hence, we can map the fully traced TCMs for the $N = 0 \pmod{2}$ lattice to the fully traced TCMs corresponding to the other lattice dimensions. We will use the convention that the *left-hand side* corresponds to $N = 0 \pmod{2}$ and the *right-hand side* corresponds to $N = 1 \pmod{2}$. Therefore, the mapping is given as follows,

$$\begin{aligned} \langle c_4(\mathbf{x}_{1a}) \rangle_F &\leftrightarrow \sum_{\theta \in \{0, \pi\}} \langle c_4(\mathbf{x}_{1a}) \rangle_F^{(\theta, \theta)}, \\ \langle c_4(\mathbf{x}_{1b}) \rangle_F &\leftrightarrow \sum_{\theta \in \{0, \pi\}} e^{i\theta} \langle c_4(\mathbf{x}_{1a}) \rangle_F^{(\theta, \theta)}, \\ \langle c_2(\mathbf{x}_{1a}) \rangle_F &\leftrightarrow \sum_{\theta_1 \in \{0, \pi\}} \sum_{\theta_2 \in \{0, \pi\}} \langle c_2(\mathbf{x}_{1a}) \rangle_F^{(\theta_1, \theta_2)}, \\ \langle c_2(\mathbf{x}_{1b}) \rangle_F &\leftrightarrow \sum_{\theta_1 \in \{0, \pi\}} \sum_{\theta_2 \in \{0, \pi\}} e^{i(\theta_1 + \theta_2)} \langle c_2(\mathbf{x}_{1a}) \rangle_F^{(\theta_1, \theta_2)}, \\ \langle c_2(\mathbf{x}_{2b}^{(1)}) \rangle_F &\leftrightarrow \sum_{\theta_1 \in \{0, \pi\}} \sum_{\theta_2 \in \{0, \pi\}} e^{i\theta_1} \langle c_2(\mathbf{x}_{1a}) \rangle_F^{(\theta_1, \theta_2)}, \\ \langle c_2(\mathbf{x}_{2b}^{(2)}) \rangle_F &\leftrightarrow \sum_{\theta_1 \in \{0, \pi\}} \sum_{\theta_2 \in \{0, \pi\}} e^{i\theta_2} \langle c_2(\mathbf{x}_{1a}) \rangle_F^{(\theta_1, \theta_2)}. \end{aligned} \quad (143)$$

4. C_6 symmetry

A C_6 -symmetric lattice with dimensions $N \times N$ can support either $N = 0 \pmod{6}$, $N = \pm 1 \pmod{6}$, $N = \pm 2 \pmod{6}$, or $N = \pm 3 \pmod{6}$. For each of these dimensions, it is always true that the only WP in $\mathcal{X}[c_6(\mathbf{r}_o)]$ is $\mathbf{r}_o = \mathbf{x}_{1a}$. The corresponding set of WPs in $\mathcal{X}[c_3(\mathbf{r}_o)]$ for each set of lattice dimensions is given as follows,

$$\begin{aligned} N = 0, \pm 2 \pmod{6} : \mathbf{r}_o &\in \{\mathbf{x}_{1a}, \mathbf{x}_{2b}^{(1)}, \mathbf{x}_{2b}^{(2)}\}, \\ N = \pm 1, \pm 3 \pmod{6} : \mathbf{r}_o &\in \{\mathbf{x}_{1a}\}, \end{aligned} \quad (144)$$

and the corresponding set of WPs in $\mathcal{X}[c_2(\mathbf{r}_o)]$ for each set of lattice dimensions is given as follows,

$$\begin{aligned} N = 0, \pm 3 \pmod{6} : \mathbf{r}_o &\in \{\mathbf{x}_{1a}, \mathbf{x}_{3c}^{(1)}, \mathbf{x}_{3c}^{(2)}, \mathbf{x}_{3c}^{(3)}\}, \\ N = \pm 1, \pm 2 \pmod{6} : \mathbf{r}_o &\in \{\mathbf{x}_{1a}\}, \end{aligned} \quad (145)$$

where $\mathbf{x}_{2b}^{(1)} = \frac{1}{3}(\mathbf{a}_1 + \mathbf{a}_2)$, $\mathbf{x}_{2b}^{(2)} = \frac{1}{3}(-\mathbf{a}_1 + 2\mathbf{a}_2)$, $\mathbf{x}_{3c}^{(1)} = \frac{1}{2}\mathbf{a}_1$, $\mathbf{x}_{3c}^{(2)} = \frac{1}{2}\mathbf{a}_2$, and $\mathbf{x}_{3c}^{(3)} = \frac{1}{2}(\mathbf{a}_2 - \mathbf{a}_1)$. Hence, we can map the fully traced TCMs for the $N = 0 \pmod{6}$ lattice to the fully traced TCMs corresponding to the other lattice dimensions. We will use the convention that the *left-hand side* corresponds to $N = 0 \pmod{6}$ and the *right-hand side* corresponds to $N \neq 0 \pmod{6}$. For $N = 1 \pmod{6}$, this mapping is given as follows,

$$\langle c_6(\mathbf{x}_{1a}) \rangle_F \leftrightarrow \langle c_6(\mathbf{x}_{1a}) \rangle_F,$$

$$\begin{aligned}
\langle c_3(\mathbf{x}_{1a}) \rangle_F &\leftrightarrow \sum_{\theta \in \{0, \pm \frac{2\pi}{3}\}} \langle c_3(\mathbf{x}_{1a}) \rangle_F^{(\theta, -\theta)}, \\
\langle c_3(\mathbf{x}_{2b}^{(1)}) \rangle_F &\leftrightarrow \sum_{\theta \in \{0, \pm \frac{2\pi}{3}\}} e^{-i\theta} \langle c_3(\mathbf{x}_{1a}) \rangle_F^{(\theta, -\theta)}, \\
\langle c_3(\mathbf{x}_{2b}^{(2)}) \rangle_F &\leftrightarrow \sum_{\theta \in \{0, \pm \frac{2\pi}{3}\}} e^{i\theta} \langle c_3(\mathbf{x}_{1a}) \rangle_F^{(\theta, -\theta)}, \\
\langle c_2(\mathbf{x}_{3c}^{(1)}) \rangle_F &\leftrightarrow \sum_{\theta_1 \in \{0, \pi\}} \sum_{\theta_2 \in \{0, \pi\}} e^{i\theta_1} \langle c_2(\mathbf{x}_{1a}) \rangle_F^{(\theta_1, \theta_2)}, \\
\langle c_2(\mathbf{x}_{3c}^{(2)}) \rangle_F &\leftrightarrow \sum_{\theta_1 \in \{0, \pi\}} \sum_{\theta_2 \in \{0, \pi\}} e^{i\theta_2} \langle c_2(\mathbf{x}_{1a}) \rangle_F^{(\theta_1, \theta_2)}, \\
\langle c_2(\mathbf{x}_{3c}^{(3)}) \rangle_F &\leftrightarrow \sum_{\theta_1 \in \{0, \pi\}} \sum_{\theta_2 \in \{0, \pi\}} e^{i(\theta_1 + \theta_2)} \langle c_2(\mathbf{x}_{1a}) \rangle_F^{(\theta_1, \theta_2)}. \tag{146}
\end{aligned}$$

and for $N = -1 \pmod{6}$, the mappings are identical to Eq. (146) with the exception that the mappings for $\langle c_3(\mathbf{x}_{2b}^{(1)}) \rangle_F$ and $\langle c_3(\mathbf{x}_{2b}^{(2)}) \rangle_F$ are interchanged. For $N = 2 \pmod{6}$, the mapping is given by,

$$\begin{aligned}
\langle c_6(\mathbf{x}_{1a}) \rangle_F &\leftrightarrow \langle c_6(\mathbf{x}_{1a}) \rangle_F, \\
\langle c_3(\mathbf{x}_{1a}) \rangle_F &\leftrightarrow \sum_{\theta \in \{0, \pm \frac{2\pi}{3}\}} \langle c_3(\mathbf{x}_{1a}) \rangle_F, \\
\langle c_3(\mathbf{x}_{2b}^{(1)}) \rangle_F &\leftrightarrow \sum_{\theta \in \{0, \pm \frac{2\pi}{3}\}} e^{-i\theta} \langle c_3(\mathbf{x}_{1a}) \rangle_F^{(\theta, -\theta)}, \\
\langle c_3(\mathbf{x}_{2b}^{(2)}) \rangle_F &\leftrightarrow \sum_{\theta \in \{0, \pm \frac{2\pi}{3}\}} e^{i\theta} \langle c_3(\mathbf{x}_{1a}) \rangle_F^{(\theta, -\theta)}, \\
\langle c_2(\mathbf{x}_{3c}) \rangle_F &\leftrightarrow \langle c_2(\mathbf{x}_{3c}) \rangle_F. \tag{147}
\end{aligned}$$

For $N = -2 \pmod{6}$, the mapping are identical to Eq. (147) with the exception that the mappings for $\langle c_3(\mathbf{x}_{2b}^{(1)}) \rangle_F$ and $\langle c_3(\mathbf{x}_{2b}^{(2)}) \rangle_F$ are interchanged. Finally, for $N = \pm 3 \pmod{6}$,

$$\begin{aligned}
\langle c_6(\mathbf{x}_{1a}) \rangle_F &\leftrightarrow \langle c_6(\mathbf{x}_{1a}) \rangle_F, \\
\langle c_3(\mathbf{x}_{1a}) \rangle_F &\leftrightarrow \langle c_3(\mathbf{x}_{1a}) \rangle_F, \\
\langle c_3(\mathbf{x}_{2b}) \rangle_F &\leftrightarrow \langle c_3(\mathbf{x}_{2b}) \rangle_F, \\
\langle c_2(\mathbf{x}_{3c}^{(1)}) \rangle_F &\leftrightarrow \sum_{\theta_1 \in \{0, \pi\}} \sum_{\theta_2 \in \{0, \pi\}} e^{i\theta_1} \langle c_2(\mathbf{x}_{1a}) \rangle_F^{(\theta_1, \theta_2)}, \\
\langle c_2(\mathbf{x}_{3c}^{(2)}) \rangle_F &\leftrightarrow \sum_{\theta_1 \in \{0, \pi\}} \sum_{\theta_2 \in \{0, \pi\}} e^{i\theta_2} \langle c_2(\mathbf{x}_{1a}) \rangle_F^{(\theta_1, \theta_2)}, \\
\langle c_2(\mathbf{x}_{3c}^{(3)}) \rangle_F &\leftrightarrow \sum_{\theta_1 \in \{0, \pi\}} \sum_{\theta_2 \in \{0, \pi\}} e^{i(\theta_1 + \theta_2)} \langle c_2(\mathbf{x}_{1a}) \rangle_F^{(\theta_1, \theta_2)}. \tag{148}
\end{aligned}$$

-
- [1] Zhi-Da Song, Luis Elcoro, and B. Andrei Bernevig, ‘‘Twisted bulk-boundary correspondence of fragile topology,’’ *Science* **367**, 794–797 (2020).
 - [2] Jennifer Cano and Barry Bradlyn, ‘‘Band Representations and Topological Quantum Chemistry,’’ *Annual Review of Condensed Matter Physics* **12**, 225–246 (2021).
 - [3] Tianhe Li, Penghao Zhu, Wladimir A. Benalcazar, and Taylor L. Hughes, ‘‘Fractional disclination charge in two-dimensional C_n -symmetric topological crystalline insulators,’’ *Phys. Rev. B* **101**, 115115 (2020).
 - [4] Ryo Takahashi, Tiantian Zhang, and Shuichi Murakami, ‘‘General corner charge formula in two-dimensional C_n -symmetric higher-order topological insulators,’’ *Phys. Rev. B* **103**, 205123 (2021).
 - [5] Max Geier, Piet W. Brouwer, and Luka Trifunovic, ‘‘Symmetry-based indicators for topological Bogoliubov–de Gennes Hamiltonians,’’ *Phys. Rev. B* **101**, 245128 (2020).

- [6] Seishiro Ono, Hoi Chun Po, and Haruki Watanabe, “Refined symmetry indicators for topological superconductors in all space groups,” *Science Advances* **6**, eaaz8367 (2020).
- [7] Bingrui Peng, Hongming Weng, and Chen Fang, “Wire construction of class DIII topological crystalline superconductors in two dimensions,” *Phys. Rev. B* **106**, 174512 (2022).